DEVELOPMENT OF PORTABLE ELECTROCHEMICAL SENSORS FOR DETERMINATION OF HEAVY METALS, NITROGEN OXIDES AND THIOCYANATE ION

Miss Kingkan Pungjunun

A Dissertation Submitted in Partial Fulfillment of the Requirements

for the Degree of Doctor of Philosophy in Chemistry

Department of Chemistry

FACULTY OF SCIENCE

Chulalongkorn University

Academic Year 2019

การพัฒนาเซ็นเซอร์เชิงเคมีไฟฟ้าแบบพกพาสำหรับการตรวจวัดโลหะหนัก สารประกอบไนโตรเจน
ออกไซด์ และไทโอไซยาเนตไอออน

น.ส.กิ่งกาญจน์ พังจุนันท์

Thesis Title	DEVELOPMENT OF PORTABLE ELECTROCHEMICAL SENSORS FOR DETERMINATION OF HEAVY METALS, NITROGEN OXIDES AND THIOCYANATE ION
By	Miss Kingkan Pungjunun
Field of Study	Chemistry
Thesis Advisor	Professor Dr. ORAWON CHAILAPAKUL
Thesis Co Advisor	Associate Professor Dr. Weena Siangproh
	Associate Professor Dr. NARONG PRAPHAIRAKSIT

Accepted by the FACULTY OF SCIENCE, Chulalongkorn University in Partial Fulfillment of the Requirement for the Doctor of Philosophy

.... Dean of the FACULTY OF SCIENCE

(Professor Dr. POLKIT SANGVANICH)

DISSERTATION COMMITTEE

.... Chairman

(Associate Professor Dr. VUDHICHAI PARASUK)

.... Thesis Advisor

(Professor Dr. ORAWON CHAILAPAKUL)

.... Thesis Co-Advisor

(Associate Professor Dr. Weena Siangproh)

.... Thesis Co-Advisor

(Associate Professor Dr. NARONG PRAPHAIRAKSIT)

.... Examiner

(Dr. JANJIRA PANCHOMPOO)

.... Examiner

(Associate Professor Dr. NATTAYA NGAMROJANAVANICH)

.... External Examiner

(Assistant Professor Dr. Amara Apilux)

กิ่งกาญจน์ พังจุนันท์ : การพัฒนาเซ็นเซอร์เชิงเคมีไฟฟ้าแบบพกพาสำหรับการตรวจวัดโลหะ
หนัก สารประกอบไนโตรเจนออกไซด์ และไทโอไซยาเนตไอออน. (DEVELOPMENT OF PORTABLE
ELECTROCHEMICAL SENSORS FOR DETERMINATION OF HEAVY METALS, NITROGEN OXIDES
AND THIOCYANATE ION) อ.ที่ปรึกษาหลัก : ศ. ดร.อรวรรณ ชัยลภากุล, อ.ที่ปรึกษาร่วม : รศ. ดร.วีณา
เสียงเพราะ,รศ. ดร.ณรงค์ ประไพรักษ์สิทธิ์

วิทยานิพนธ์ฉบับนี้มุ่งเน้นการพัฒนาเซ็นเซอร์เคมีไฟฟ้าแบบพกพาบนอุปกรณ์วิเคราะห์ฐานกระดาษสำหรับ
การตรวจวัดสารประกอบสำคัญ / สารบ่งชี้ทางชีวภาพในการใช้งานที่หลากหลาย โดยการพิจารณาถึงการใช้งานของสาร
เป้าหมายทำให้วิทยานิพนธ์นี้สามารถแบ่งออกเป็นสามส่วนหลักประกอบด้วย การประยุกต์ใช้ด้านการตรวจวิเคราะห์ความ
ปลอดภัยของอาหาร การวิเคราะห์ในสิ่งแวดล้อม และการประยุกต์ทางคลินิก ตามลำดับ ในส่วนแรกจะมีสองส่วนย่อยที่
อธิบายเกี่ยวกับการตรวจวัดโลหะหนักที่ปนเปื้อนในอาหาร การรวมอุปกรณ์วิเคราะห์ฐานกระดาษและขั้วไฟฟ้าเพชรเจือ
โบรอนถูกพัฒนาสำหรับการวิเคราะห์หาปริมาณสารหนูทั้งหมดในส่วนย่อยแรก อุปกรณ์ดังกล่าวดำเนินการโดยใช้วิธีการ
พับอุปกรณ์กระดาษสำหรับการเตรียมอนุภาคทองคำระดับนาโนดัดแปรบนขั้วไฟฟ้าเพชรเจือโบรอน และการวัดสารหนู
(III) ด้วยเทคนิคแอโนดิกสตริปปิงโวลต์แทมเมทรีบนอุปกรณ์ชิ้นเดียวกัน การเชื่อมต่ออุปกรณ์วิเคราะห์ฐานกระดาษกับโพ
เทน-ชิโอมิเตอร์แบบพกพาถูกเสนอสำหรับการตรวจวัดดีบุกและตะกั่วในเวลาเดียวกันโดยใช้ขั้วไฟฟ้าอนุภาคบิสมัทระดับ
นาโนที่ดัดแปรบนขั้วไฟฟ้าพิมพ์สกรีนแกรฟีนเป็นขั้วไฟฟ้าทำงานในส่วนย่อยที่สอง ในส่วนที่สองเสนออุปกรณ์วิเคราะห์
ฐานกระดาษที่ถูกออกแบบมาเพื่อตรวจวัดแก๊สไนโตรเจนออกไซด์เป็นสารเป้าหมายต้นแบบเพื่อการวิเคราะห์ใน
สิ่งแวดล้อม การใช้งานของรูปแบบอุปกรณ์ที่พัฒนานั้นถูกปรับปรุงโดยการรวมกันของตัวดูดซับแก๊สและขั้วไฟฟ้าทองแดง
อนุภาคนาโนดัดแปรบนขั้วไฟฟ้าพิมพ์สกรีนแกรฟีนภายในอุปกรณ์เดียวกันสำหรับการจับแก๊สที่จำเพาะ การพัฒนาตัว
ตรวจจับแก๊สสามารถนำไปใช้เพื่อตรวจสอบแก๊สไนโตรเจนออกไซด์ในตัวอย่างแก๊สที่หลายหลาย เช่นอากาศและแก๊สไอ
เสียจากรถยนต์ที่มีความแม่นยำและความน่าเชื่อถือสูง ในส่วนสุดท้ายนี้อุปกรณ์ฐานกระดาษเชิงเคมีไฟฟ้าร่วมกับการ
ตรวจวัดเชิงสีถูกเสนอสำหรับการตรวจวัดสารชีวโมเลกุลของไทโอไซยาเนตในน้ำลาย ในงานนี้มีการประดิษฐ์ร่องไมโคร
แคปิลลารีบนอุปกรณ์วิเคราะห์ฐานกระดาษที่ทำหน้าที่เป็นไมโครแคปิลลารีปั๊มเพื่อช่วยการเคลื่อนที่ของน้ำลายหนืดตาม
ช่องโดยไม่ต้องใช้ขั้นตอนการปรับสภาพตัวอย่าง / อุปกรณ์วัดขนาดใหญ่ โดยรวมแล้วรูปแบบอุปกรณ์วิเคราะห์ฐาน
กระดาษเชิงเคมีไฟฟ้าเหล่านี้มีประสิทธิภาพสูงสำหรับการวิเคราะห์เชิงปฏิบัติและได้รับการพัฒนารูปแบบขั้นสูงต่อไปไป

สาขาวิชา	เคมี	ลายมือชื่อนิสิต ....
ปีการศึกษา	2562	ลายมือชื่อ อ.ที่ปรึกษาหลัก ....
		ลายมือชื่อ อ.ที่ปรึกษาร่วม ....
		ลายมือชื่อ อ.ที่ปรึกษาร่วม ....

5872804223 : MAJOR CHEMISTRY

KEYWORD: ELECTROCHEMICAL DETECTION, METAL NANOPARTICLES, PAPER-BASED ANALYTICAL DEVICE, VOLTAMMETRIC DETECTION

Kingkan Pungjunun : DEVELOPMENT OF PORTABLE ELECTROCHEMICAL SENSORS FOR DETERMINATION OF HEAVY METALS, NITROGEN OXIDES AND THIOCYANATE ION . Advisor: Prof. Dr. ORAWON CHAILAPAKUL Co-advisor: Assoc. Prof. Dr. Weena Siangproh,Assoc. Prof. Dr. NARONG PRAPHAIRAKSIT

This dissertation focused on the development of portable electrochemical sensors using the paper-based analytical device (ePAD) for the determination of the important compounds/biomarkers in various applications. Considering the target applications, this dissertation can be divided into three main parts including food safety application, environmental analysis and clinical application, respectively. In the first part, two sub-sections relating to the detection of heavy metals contaminated in food will be discussed. For the first sub-section, an ePAD coupled with a boron-doped diamond electrode was developed for the determination of total arsenic. The device was performed using the origami paper device for the preparation of gold nanoparticle-modified boron-doped diamond electrodes and the measurement of arsenic (III) using anodic stripping voltammetry on a single device. For the second sub-section, an ePAD coupled with a portable potentiostat was demonstrated for the simultaneous determination of tin and lead using a bismuth nanoparticle-modified screen-printed graphene electrode as working electrode. In the second part, an ePAD was engineered for NOx gas determination as a model for environmental analysis. The functionality of the developed platform was enhanced by integrating the gas absorber and copper nanoparticle-modified screen-printed graphene electrode within the same device for selective capturing. This novel gas sensing device could be applied to determine NOx gas in various gaseous samples, such as air and exhaust gases from cars with high accuracy and reliability. Lastly, an ePAD coupled with colorimetric detection was demonstrated for the biological sensing of salivary thiocyanate. Here, the microcapillary grooves fabricated on a paper device functioned as a microcapillary pump to facilitate the viscous salivary transportation along the microfluidic channel without requiring for sample pretreatment steps/bulky instrumentations. All in all, these ePAD formats exhibited good performances for the practical analysis and allowed for further development of an advanced platform.

Field of Study:	Chemistry	Student's Signature ....
Academic Year:	2019	Advisor's Signature ....
		Co-advisor's Signature ....
		Co-advisor's Signature ....

ACKNOWLEDGEMENTS

TABLE OF CONTENTS

LIST OF TABLES

จุฬาลงกรณ์มหาวิทยาลัย

CHULALONGKORN UNIVERSITY

LIST OF FIGURES

LIST OF ABBREVIATIONS

ΔE_p	Peak separation
Δi	Current difference
μPADs	Microfluidic paper-based analytical devices
μpumpPAD	Micropump on the paper-based analytical device
A	Electrode area (in cm^2)
AAS	Atomic absorption spectrometry
AgNPs	Silver nanoparticles
AuNP/BDDE	Gold nanoparticle-modified boron-doped diamond electrode
AuNPs	Gold nanoparticles
BDDE	Boron-doped diamond electrode
BiNP/SPGE	Bismuth nanoparticle-modified screen-printed graphene electrode
BiNPs	Bismuth nanoparticles
C	Concentration (in $mol\ mL^{-1}$)
CE	Counter electrode
cPAD	Colorimetric PAD
CuNP/SPGE	Copper nanoparticle-modified screen-printed graphene electrode
CuPc/SPGE	Copper (II) phthalocyanine modified screen-printed graphene electrode
CV	Cyclic voltammetry
D	Diffusion coefficient (in $cm^2\ s^{-1}$)
DPV	Differential pulse voltammetry
DPVs	Differential pulse voltammograms
E°	Standard reduction potential
EDS	Energy dispersive x-ray spectra
E_p	Potential
$E_{p,a}$	Anodic peak potential

$E_{p,c}$	Cathodic peak potential
ePAD	Paper-based analytical device
FAO	Food and Agriculture Organization
GCE	Glassy carbon electrode
gPAD	Gas-sensing paper-based analytical device
HMDE	Hanging mercury drop electrode
i_1	Before application of potential pulse
i_2	End of potential pulse
ICP-MS	Inductively coupled plasma mass spectrometry
ICP-OES	Inductively coupled plasma optical emission spectrometry
i_f	Forward pulse
i_r	End of reverse pulse
LIF	Laser-induced fluorescence
LOD	Limit of detection
mPAD	Multiplestep paper-based analytical device
n	Number of electrons
NOx	Nitrogen oxides
PAD	Paper-based analytical device
POC	Point-of-care
R^2	Correlation coefficient
RE	Reference electrode
RSD	Relative standard deviation
SEM	Scanning electron spectroscopy
SPCE	Screen-printed carbon electrode
SPGE	Screen-printed graphene electrode
SWASV	Square wave anodic stripping voltammetry
SWASVs	Square wave anodic stripping voltammograms
SWV	Square wave voltammetry
SWVs	Square wave voltammograms
WE	Working electrode
WHO	World health organization

v	Scan rate (in V s^{-1})
α	Transfer coefficient

CHAPTER 1

INTRODUCTION

1.1 Introduction

Recently, the development of sensors with high sensitivity and selectivity has been the main challenge for the determination of target analyte. The key requirements for the developed sensor include the portability (for on-field testing), fast analysis, ease of use, low-cost and low sample volume consumption. Hence, the microfluidic paper-based analytical devices (µPADs) have been recognized as an ideal platform because of its economical perspective, biodegradability, inherent resource renewability, and broad applicability [1]. Besides, µPADs can be fabricated by high-speed coating and printing techniques that are fast and simple for creating hydrophilic and hydrophobic zones on the paper [2]. As a consequence of such benefits, µPADs have been utilized in a broad range of applications including food regulation, environmental analysis and point-of-care applications [3-5]. Moreover, the paper itself is known to be an excellent material for controlling the fluid flow without requiring any external power source. Unfortunately, several platforms of the previously designed paper-based devices were only limited to a direct contact, single analyte determination and not suitable for a complex analytical procedure. Hence, additional functionalities of the µPADs should ideally be integrated to obtain a better detection performance and allow a multiplex procedure within a single paper device.

With that goal in mind along with the innovative design, multiple sensing devices for certain purposes/applications will be developed in this work.

Among a variety of detection methods on μPADs, electrochemical detection is one of the most common methods employed on μPADs due to their easy integration on paper material. The electrochemical detection on the paper-based analytical device (ePAD), in particular, offers a sensitive and selective response yet maintaining a simple procedure and allowing portability [6]. In some circumstances, electrode modification is required to gain an enhanced sensing capability. Therefore, broad ranges of modifying agents including metal nanoparticles, carbon-based nanomaterials and nanocomposites are often utilized [7, 8]. These modifying agents usually share excellent electrical properties; increasing the effective surface area of the electrode, increasing the electron transfer kinetic or enabling the electrocatalytic properties [9, 10]. By selecting an appropriate agent, a superior sensing performance toward the analyte of interest is achieved.

Here, in this research, novel electrochemical detection paper-based analytical devices (ePAD) are developed for various applications. This includes food safety application, environmental analysis and clinical application.

For food safety application, we concentrated on the electroanalytical detection of heavy metals since they are mainly concerned as major contaminants in food and known for their potential toxicity. The metals can be presented in both organometallic and inorganic forms with a wide range of hazards. The toxicity of

heavy metals strongly depends on their oxidative states and chemical forms [11]. Herein, heavy metals such as arsenic (As), lead (Pb) and tin (Sn) are of concern because of their predominant contamination in foods [12, 13]. These metals are considered highly toxic to humans and potential causes of several illness (such as diabetes, hepatotoxicity, and nephrotoxicity) [14]. Moreover, some heavy metals (As, for instance) has been classified as mutagenic and carcinogenic leading to serious diseases [15]. For these reasons, several techniques have been continually developed for the determination of heavy metals such as atomic absorption spectrometry (AAS) [16, 17], inductively coupled plasma optical emission spectrometry (ICP-OES) [18], and inductively coupled plasma mass spectrometry (ICP-MS) [19]. However, limitations such as their bulky instruments, high-cost and non-portability are a bottleneck which still requires a major development presuming that it will be further used for on-field analysis.

Furthermore, environmental monitoring is also another concern nowadays. Air pollution, in particular, poses a major threat to health and climate. It has been estimated by the World Health Organization (WHO) that 9 out of 10 people breathe air containing high levels of pollutants [20]. The pollutant in the air is an important factor that affects the health of humans, especially, on the respiration system [21]. Moreover, some pollutant compounds contribute to suffering the environment such as acid rain and the greenhouse effect [22]. In this research, nitrogen oxides (NOx) were represented as a model analyte. The conventional methods for NOx detection

comprise spectrophotometry [23], chemiluminescence [24], laser-induced fluorescence (LIF) [25], and resistive sensors [26]. Nevertheless, the complexed requirements (such as a high-temperature operation) of these techniques convinced the manufacturer's interest towards a portable miniaturized setup. Therefore, a compact electrochemical sensor for gas sensing is still a major challenge among electrochemists.

Lastly, the advantages of ePAD can also be extended to the point-of-care (POC) application. The POC device is an important tool to promptly diagnose and follow-up on the disease. Currently, the trends towards non-invasive detection are desirable. The intrusive test from blood, for instance, is generally inconvenient and causes negative perception among patients. Alternatively, saliva, commonly considered as the 'mirror of the body', is a very attractive biofluid for clinical diagnosis since it contains plentiful disease biomarkers [27]. Here, Salivary thiocyanate (SCN$^-$), a vital metabolite in living organisms, was chosen as a representative biomarker to prove the concept of ePAD for POC application.

In this research, different ePAD platforms will be developed for particular purposes; i.e. food safety, environmental monitoring and clinical application. Complex functionalities of the paper device were also designed to simplify the tedious analytical procedure and open new possibilities in ePAD. To further prove the potential applicability of the developed platform, real samples were tested, and the results were validated against the traditional methods.

1.2 Research objective

This research strives towards 2 main objectives as below;

1. To develop a novel electrochemical sensor for determination of heavy metals, pollutants and biomarkers of certain diseases.

2. To integrate and simplify the multiple analytical procedures within a single paper-based analytical device.

1.3 Scope of the research

To achieve the above mentioned objectives, the scopes of the research have been set as below;

1. A novel multistep paper-based analytical device (mPAD) integrating the AuNPs/BDD electrode preparation step and the detection step in a single paper device was demonstrated for total arsenic determination. The mPAD was applied to detect the total arsenic in rice samples.

2. A bismuth nanoparticle-modified screen-printed graphene electrode (BiNP/SPGE) using CTAB and oxalic acid on paper-based sensor coupling with portable potentiostat was demonstrated for the simultaneous determination of tin and lead. The BiNP/SPGE was applied to determine tin and lead in canned food samples.

3. A disposable gas-sensing paper-based analytical device (gPAD) for electrochemical detection of NOx gas was developed. The sensor was designed to

integrate the gas adsorber and the electrochemical detection (using copper nanoparticle-modified screen-printed graphene electrode (CuNP/SPGE) as a working electrode) into a one-shot sensor. The gPAD was used to detect three types of gas samples; ambient indoor air, outdoor air, and exhaust gases from a diesel engine automobile.

4. A novel capillary micropump on the paper-based analytical device (μpumpPAD) for dual-mode (colorimetric and electrochemical) sensing of thiocyanate was demonstrated. Saliva samples from healthy and smoker volunteers were tested with the proposed platform.

There are six chapters in this dissertation. Chapter I is the introduction. Chapter II describes the theory for the paper-based analytical device fabrication and detection methods (including electrochemical and colorimetric detection). Next, chapter III demonstrates the development of ePAD for food safety application while chapter IV exemplifies the development of ePAD for environmental monitoring application. Chapter V reports on the development of ePAD for clinical application. Lastly, chapter VI is the conclusion and future perspectives for this dissertation.

CHAPTER 2

THEORY

2.1 Paper-based analytical device

Since the first report of the paper-based analytical device (PAD) published by Whiteside group, various sensing applications using such device have been broadly explored. The PAD is an alternative analytical platform using paper as a substrate. A superior sensing performance has been achieved in paper material because of its microporous structure which allows a power-free fluid transport. In addition, the extensive cellulosic network of paper represents the desired storage capacity for the reagent loading. The flexible design of PAD could also be patterned for specific applications using a wide range of fabrication techniques.

2.2 Fabrication of paper-based analytical device

2.2.1 Wax-printing

PAD could be fabricated using various methods, for example, photolithography, wax-printing, cutting, etc. Among the fabrication methods available on PAD, wax-printing is the most employed fabrication method because it offers a high performance in terms of high throughput, speed, cost efficiency, and simplicity, with no template required. The fabricated procedure using the wax-printing method consists of 2 steps. First, a desirable pattern of hydrophobic wax barrier is printed

onto a paper surface by a commercially available printer. Next, the printed-patterned

paper is placed on a hot plate at 175 °C for 40 s so that the wax penetrated through

the porous layer and formed the three-dimensional hydrophobic barrier as shown in

Figure 2.1. Hence, this straightforward fabrication has led to a broad development of

PAD which could be elaborately designed for certain applications.
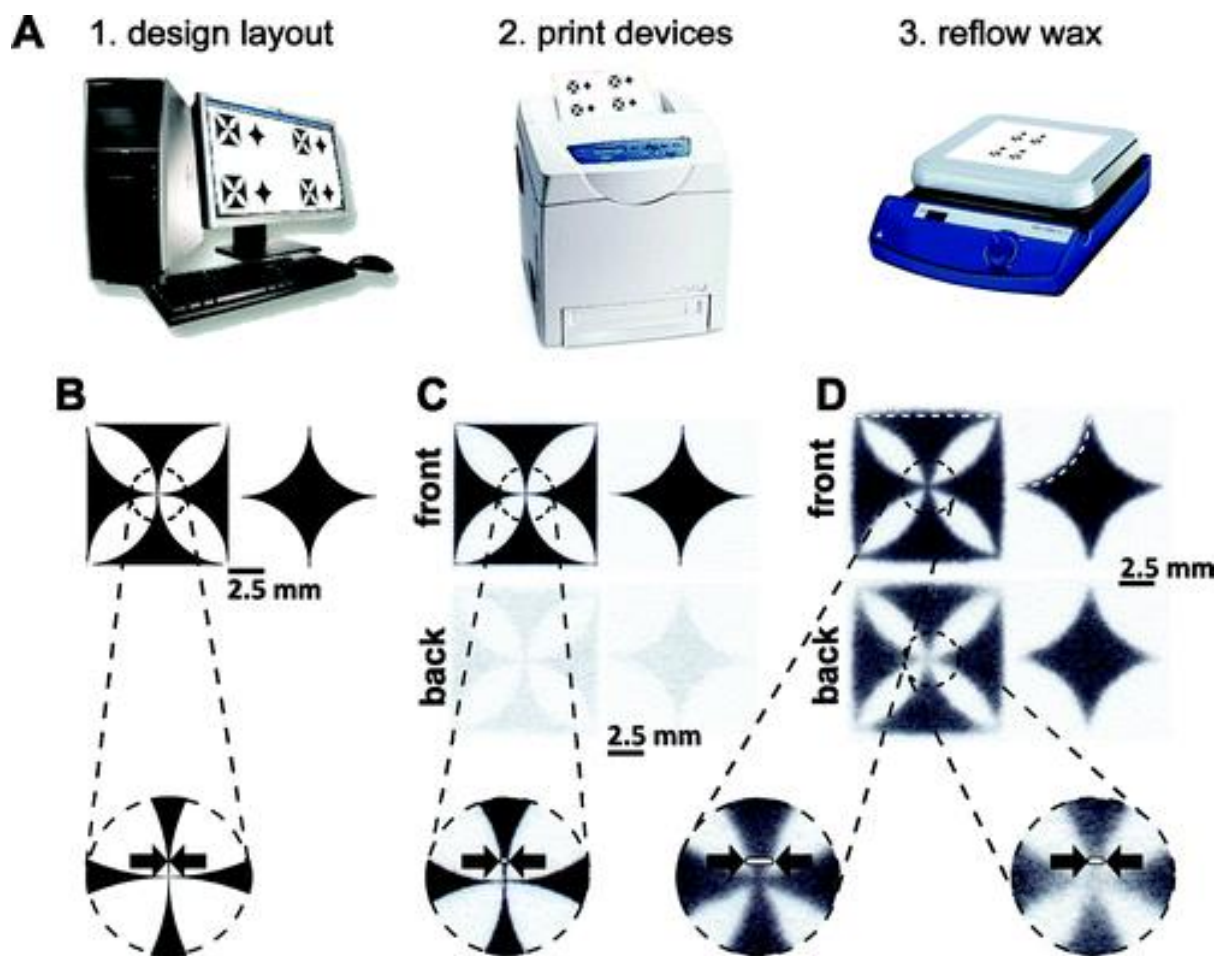
Figure 2.1 Schematic representation of the basic steps of wax printing method [28]

2.3 Detection method on PAD

The detection method is a key process for the response identification and further conversion to a measureable signal. The detection methods have been extensively developed for the application of PAD. So far, a number of detection methods including electrochemical detection, colorimetric detection, fluorescence, and so on, have been reported. Among these, electrochemical detection and

colorimetric detection coupling with PAD have been advantageously developed due to its smaller instrumentation and low-cost, allowing for on-field analysis. Therefore, these two detection methods will be selected and further described.

2.3.1 Electrochemical detection

Electrochemical detection has been broadly used and miniaturized on PAD for the determination of certain target analytes. The principle of electrochemical detection is to study the chemical process which causes electrons transfer. The electron exchange phenomenon produces a form of electrical change, for example, current, potential and charge, which could be generated by such process between the electrode and electrolyte known as oxidation-reduction (redox) reaction.

2.3.1.1 Faradaic and non-faradaic processes

There are 2 processes which occur at the interface between electrode and solution, called, faradaic and non-faradaic processes [29]. For the Faradaic process, the electrons or charges are transferred across the metal-solution interface, resulting in oxidation or reduction reaction of electroactive species complying with Faraday's law. The faradaic process is initialed by applying the potential which is higher/lower than the potential of electroactive species. This can cause the reduction/oxidation to occur at the electrode surface. Consequently, the product of reduction/oxidation

reaction diffuses from the electrode surface to the bulk solution. Meanwhile, the diffusion of electroactive species from bulk solution to the electrode surface arises as shown in Figure 2.2.
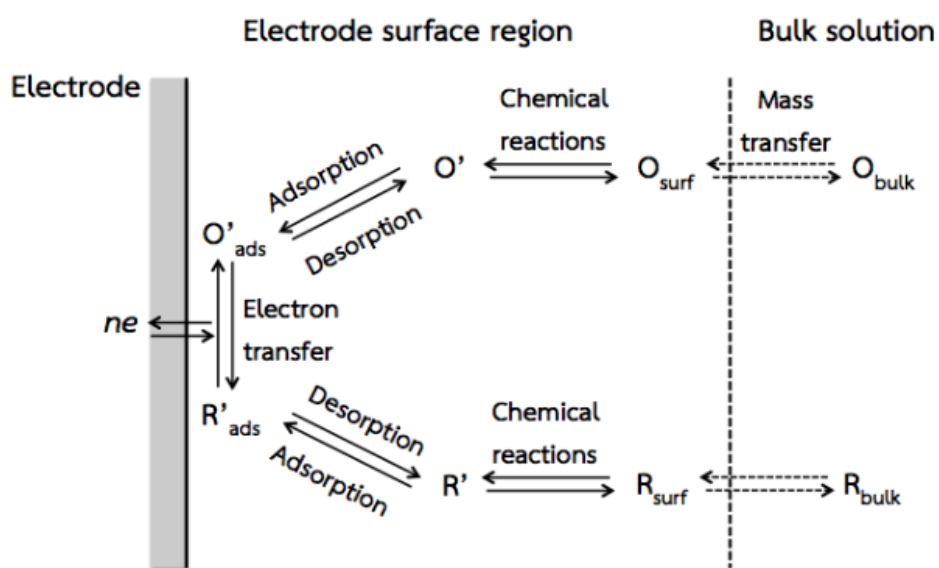
Figure 2.2 Pathway of electrode process. [30]

The non-faradaic process, on the other hand, is not related to the electron or charge transfer at the metal-solution interface. Under some conditions, adsorption or desorption could occur at electrode surfaces without charge involvement. As a result of adsorption or desorption at electrode surface, the potential or electrode area would be changed.

2.3.1.2 Mass transfer

Mass transfer is the sum movement of particles from one location to another such as different phases, streams, fractions, and so on. The movement of elements in a solution arises either from the differences in concentration or charge regions [29]. There are 3 different modes of mass transfer in an electrochemical cell as follows;

1. Diffusion is a transport phenomenon caused by a gradient of chemical potential. In other words, ions would transport from the higher concentration region to the lower concentration region.

2. Migration is the mobility of charged particles in response to location of electric field. The negatively charged ions would migrate toward the positive charge electrode, while, the positively charged ions would migrate to the opposite side.

3. Convection is the hydrodynamic transport phenomena from external force convection and natural convection (from density gradients).

Mass transfer to a working electrode is described by the Nerst-Planck equation as

$$J_i(x) = -D_i \frac{\partial C_i(x)}{\partial x} - \frac{z_i F}{RT} D_i C_i \frac{\partial \phi(x)}{\partial x} + C_i V(x)$$

for one-dimensional mass transfer along the x-axis, where $J_i(x)$ is the flux of species I (mol s^{-1} cm^{-2}) at distance x from the surface, D_i is the diffusion coefficient (cm^2 s^{-1}), $\frac{\partial C_i(x)}{\partial x}$ is the concentration gradient at distance x, $\frac{\partial \phi(x)}{\partial x}$ is the potential gradient, z_i is the charge of species i (dimensionless), C_i is the concentration (mol cm$^-$

^{3}) of species i, and V(x) is the velocity (cm s^{-1}) in which a volume element in solution moves along the axis. The three terms on the right-hand side represent the contributions of diffusion, migration, and convection, respectively, to the flux.

2.3.1.3 Electrochemical techniques

Electrochemistry is a type of analytical technique that is used for determination of target analyte concentration by the measurement of electrical quantities; the current, potential, or charge. Electrochemical techniques are classified into 4 main categories consisting of potentiometry, coulometry, amperometry, and voltammetry as shown in Figure 2.3. The voltammetric method was utilized as the model analytical tool in this research, therefore, only this technique will be discussed in this section.
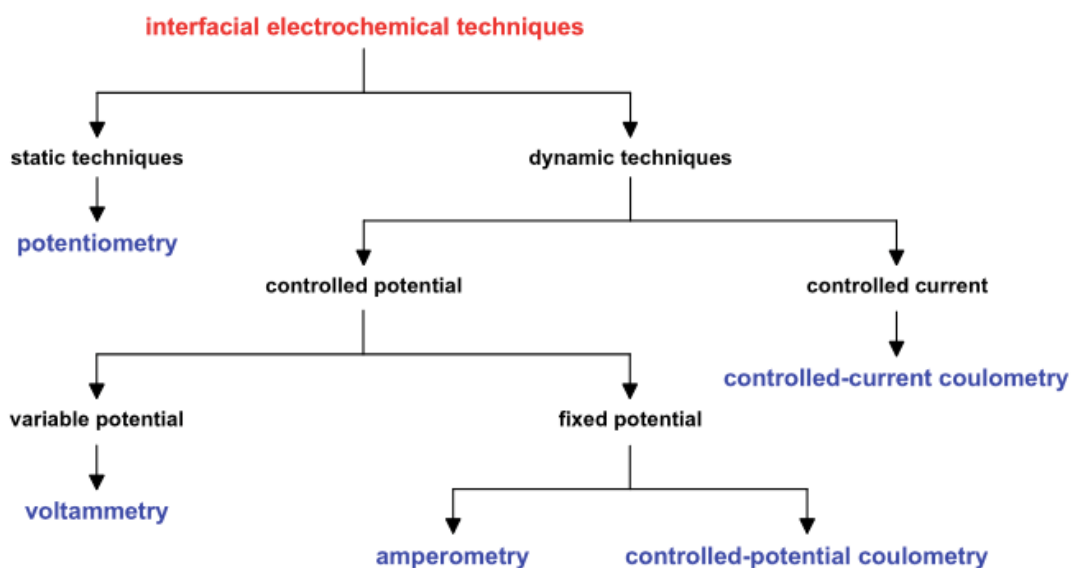
Figure 2.3 the diagram of electrochemical techniques [31]

2.3.1.3.1 Voltammetry

The controlled-potential techniques are based on the study of charge-transfer processes at the electrode-solution interface. The electrode is supplied with a constant and/or varying potential to derive an electron-transfer reaction while the resultant current is measured. Voltammetry investigates the half-cell reactivity of the target analyte. The desired potential is controlled in such a way that it facilitates the transfer of charge to/from the analyte. In brief, the target analyte could be reduced when a potential is applied to a more negative direction. In contrast, the oxidation reaction occurs when potential is applied to a more positive direction [29]. Voltammetric techniques are classified in accordance with their voltage-time functions (waveform) (Figure 2.4) into various types such as cyclic voltammetry, differential pulse voltammetry, square wave voltammetry, anodic stripping voltammetry, which were used in this dissertation.
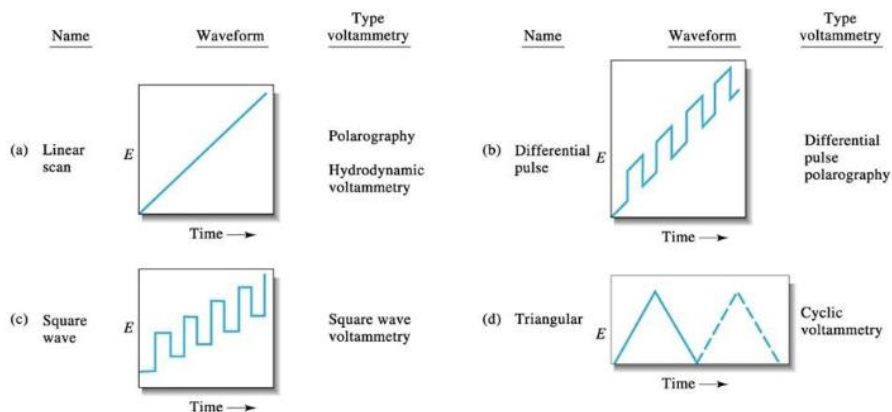
Figure 2.4 The voltage-time functions (waveform) of (a) linear scan, (b) differential pulse voltammetry, (c) square-wave voltammetry, and (d) cyclic votammetry [32].

2.3.1.3.1.1 Cyclic voltammetry (CV)

Cyclic voltammetry (CV) is an electrochemical technique that has been commonly used for the initial electrochemical characterization of a developed electrochemical sensing. The result from CV is obtained from the information of electrochemical processes on the electrode surface. CV is performed by scanning the potential linearly versus time conforming to a triangular potential waveform. In brief, the potential is initially scanned toward the negative direction, resulting in the reduction of electroactive species. The cathodic current begins to increase and reach a peak. After the potential reached the switching point, the WE potential is swept back in the positive direction resulting in the oxidation reaction on working electrode

surface, and the anodic current is measured using a potentiostat. The resulting plot

between current and potential is called cyclic voltammogram as shown in Figure 2.5.
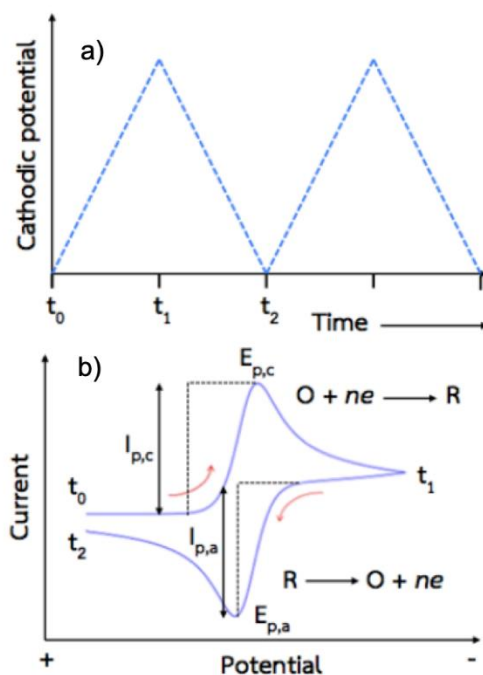
Figure 2.5 Voltage-time excitation functions (waveform) in cyclic voltammetry

(a) and a typical cyclic voltammogram for a reversible electrochemical process (b) [33].

In a Nernstian method (reversible systems) [29], at 25 °C, the peak current (I_p) is

proportional to the concentration of analyte, which can be described by Randles-

Sevick equation.

$$I_p = (2.69 \times 10^5)n^{\frac{3}{2}} A\ F\ C\ D^{\frac{1}{2}}\ v^{\frac{1}{2}}$$

where n is the number of electrons, A is the electrode area (in cm^2), C is the

concentration (in mol mL^{-1}), D is the diffusion coefficient (in cm^2 s^{-1}), and v is the

scan rate (in V s^{-1}). The peaks position on the potential axis (Ep) is related to the

formal potential of the redox process. For a reversible system, the formal potential is centered between $E_{p,a}$ and $E_{p,c}$.

$$E^0 = \frac{E_{p,c} + E_{p,a}}{2}$$

The peak separation (ΔE_p, mV) between the peak potential is provided by

$$\Delta E_p = E_{p,a} - E_{p,c} = \frac{59}{n}$$

Meanwhile, in totally irreversible systems, the peak current is found to be

$$I_p = (2.99 \times 10^5)\alpha^{\frac{1}{2}} A\ C\ D^{\frac{1}{2}}\ v^{\frac{1}{2}}$$

Where α is the transfer coefficient

2.3.1.3.1.2 Differential pulse voltammetry (DPV)

Differential pulse voltammetry (DPV) is a voltammetric method which is used for the trace analysis of target analyte. DPV is commonly used for both quantitative analysis and the investigation of chemical reaction mechanism. The potential waveform of DPV is a sequence of pulses increasing along a linear baseline as shown in Figure 2.6 a. The current is firstly sampled before the application of the potential pulse (i_1). The step of the potential pulse is small and the current is sampled at the end of the potential pulse (i_2). The current difference ($\Delta i = i_1 - i_2$) at these points in each potential pulse is measured and plotted with the potential that is designed to minimize background charging current (Figure 2.6 b) [29]. This could lead to an

enhanced sensitivity in this technique. Besides, the differential pulse voltammogram could be used as a means to determine the concentration of target analyte which is proportional to the peak height (current).
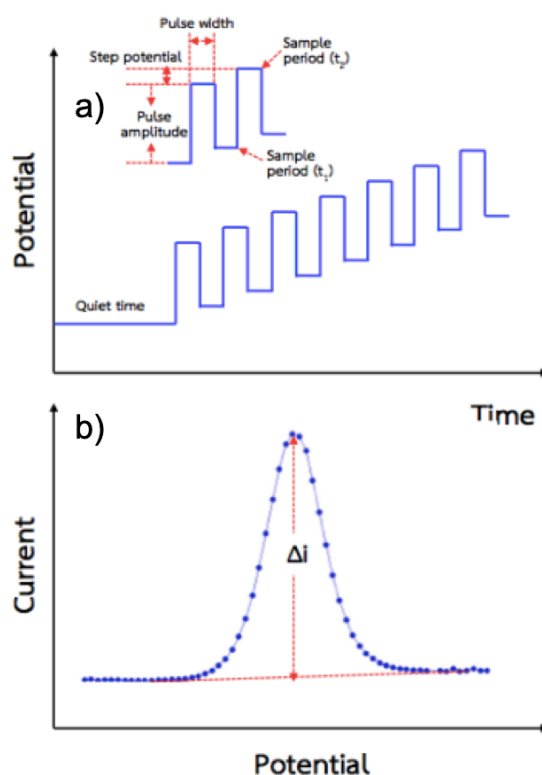
Figure 2.6 Excit*ation* signal of differential pulse voltammetry (a) and differential pulse voltammogram (b) [33].

2.3.1.3.1.3 Square wave voltammetry (SWV)

Square wave voltammetry (SWV) represents one of the most promising voltammetric techniques for determination of trace heavy metals or inorganic compounds. The potential waveform of SWV involves the application of symmetrical

square-shaped potential pulses superimposed on a base staircase potential sweep as shown in Figure 2.7. The current is sampled at two positions on the square-wave pulse; the end of the forward pulse (i_f), and the end of reverse pulse (i_r). The difference between these currents ($\Delta i = i_f - (-i_r)$) is a net square-wave voltammogram as shown in Figure 2.8 [29]. Based on such measurement, a larger peak height and an improved signal-to-noise ratio are achieved in SWV making it the most sensitive electrochemical technique and enabling trace level determination of metal ions and inorganic compounds.
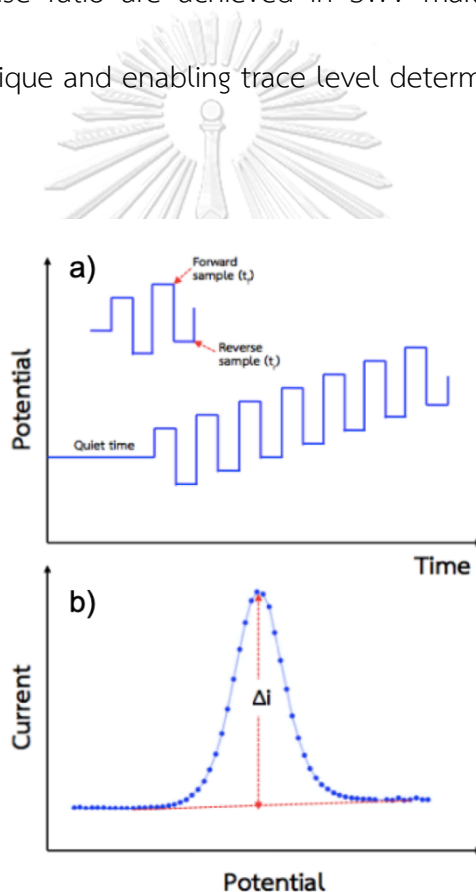
Figure 2.7 Excitation signal of square wave voltammetry (a), and differential pulse voltammogram (b) [33].
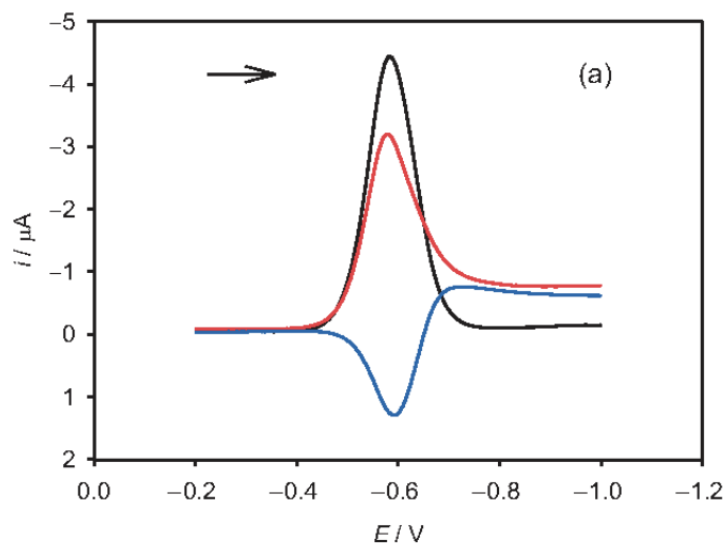
Figure 2.8 The forward pulse for the reduction reaction (i_f) (red line), and the end of reverse pulse for the oxidation reaction (I_r) (blue line). The difference between these currents ($\Delta i = i_f - (-i_r)$) is presented in a black line [34].

2.3.1.3.1.4 Square wave anodic stripping voltammetry (SWASV)

Square wave anodic stripping voltammetry (SWASV) is a voltammetric coupling between SWV and anodic stripping technique. Square wave anodic stripping voltammetry comprises 2 procedures of the deposition process and stripping process as shown in Figure 2.9. First, the deposition step is performed by applying the constant cathodic potential in order to accumulate of target analyte onto the electrode surface by reduction reaction. After the deposition process has been completed, the potential is applied as an exciting waveform for SWV on the working electrode in a positive direction, the target analyte on the electrode surface is

oxidized to bulk solution again. The resulting current from diffusion is then measured and related to the concentration of target analyte.
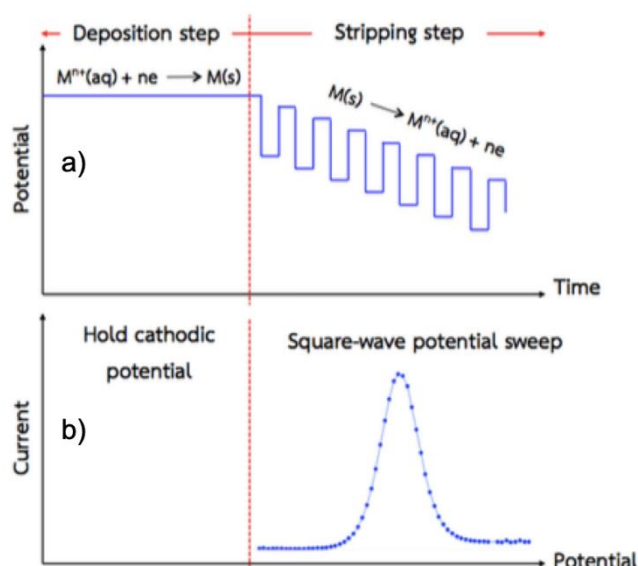
Figure 2.9 Potential waveform of square wave anodic stripping voltammetry (a), and the resultant voltammogram (b) [33].

2.3.1.4 Electrochemical cell

The voltammetric technique is operated using the three electrodes system in an electrochemical cell including a working electrode (WE), counter electrode (CE), and reference electrode (RE). These electrodes are immersed in a supporting electrolyte solution of an aqueous solution or non-aqueous solution containing ionic species for reducing the migration effect. Besides, the supporting electrolyte solution should have adequately low resistance and inert nature to the target analytes as well as electrodes. The potentiostat is an electronic instrument required to control the potential difference between the working electrode and reference electrode

(having a stable reference potential). For electrochemical measurement, a current pass from the working electrode to counter electrode is measured.

2.3.1.4.1 Working electrode

Working electrode (WE) is an electrode where the reaction and electron transfer of target analytes occur on its the surface in an electrochemical cell. Generally, WE should be made of inert materials for long-term stability and robustness. The types of WE material, size, and shape of WE vary and depend on the application. In this research, three types of WE which are boron-doped diamond electrode (BDDE), screen-printed carbon electrode (SPCE), and screen-printed graphene electrode (SPGE), were used to enhance the performance of PAD.

2.3.1.4.1.1 Boron-doped diamond electrode (BDDE)

Boron-doped diamond electrode (BDDE) is a relatively new working electrode employed in electrochemical cell. BDDE is a carbon-based material with an sp^3 hybridization structure in a diamond crystal lattice incorporated with an admixture of boron atom in a small portion (approximately 0.1%). Carbon atoms in the diamond crystal lattice are replaced by a small portion of boron atoms introduced into the crystal lattice p-acceptor atoms and enable conductivity. Because of sp^3 hybridization structure of BDDE surface, the significantly improved performance of

BDDE is achieved in terms of non-fouling electrode, low background current, chemical robustness, and broad potential window [3].

2.3.1.4.1.2 Screen-printed carbon electrode (SPCE)

Screen-printed carbon electrode (SPCE) is a carbon-based conductive ink which is screen-printed to create a miniaturized electrochemical cell on various substrates such as polymer plate, ceramic, and paper. Nowadays, SPCEs have widely been used as a working electrode in the electrochemical measurement because of its easy fabrication and mass production [35].

2.3.1.4.1.3 Screen-printed graphene electrode (SPGE)

Screen-printed graphene electrode (SPGE) is a carbon-based conductive ink that has graphene sheet forming a main component. Generally, graphene electrode is a planar sheet of sp^2 hybridization structure as a honeycomb crystal lattice. Graphene conductive ink has recently attracted great interest as a material for screen-printed electrode owing to its superior electrical properties. Besides, the SPGE also exhibits outstanding properties such as good mechanical strength, high carrier mobility, and large surface area [36].

2.3.1.4.2 Reference electrode

Reference electrode (RE) is an electrode which has a constant and well-known potential. The potential of RE is used as referent point for controlling potential in an electrochemical cell. RE should be durable with electrolyte species in the electrochemical cell. Ag/AgCl, in particular, is employed as a common primary RE consisting of Ag in saturated AgCl and KCl solution [30].

2.3.1.4.3 Counter electrode

Counter electrode (CE) is an electrode in which another half of redox reaction occurs. Moreover, CE is used to complete the current circuit of electrochemical cell. Therefore, CE does not relate with target analyte reaction. Typically, CE surface area should be higher than that of WE because CE takes part as a source/sink of electrons in electrochemical circuit [30].

2.3.1.5 Screen printing method

The electrochemical cell on PAD could be miniaturized and created on paper substrate using various fabrication technique. Screen printing method is the most common technique for electrode fabrication on PAD. Typically, three electrodes system consisting of a working electrode, reference electrode, and counter electrode is often employed (Figure 2.10). Here, to miniaturize electrochemical cells on the

paper, the three electrodes can be directly screen-printed onto a filter paper substrate through the silk screen mask. After printing the conductive paste or ink onto the paper, the printed electrode is placed in the oven at 55 °c for 1 hr for drying.
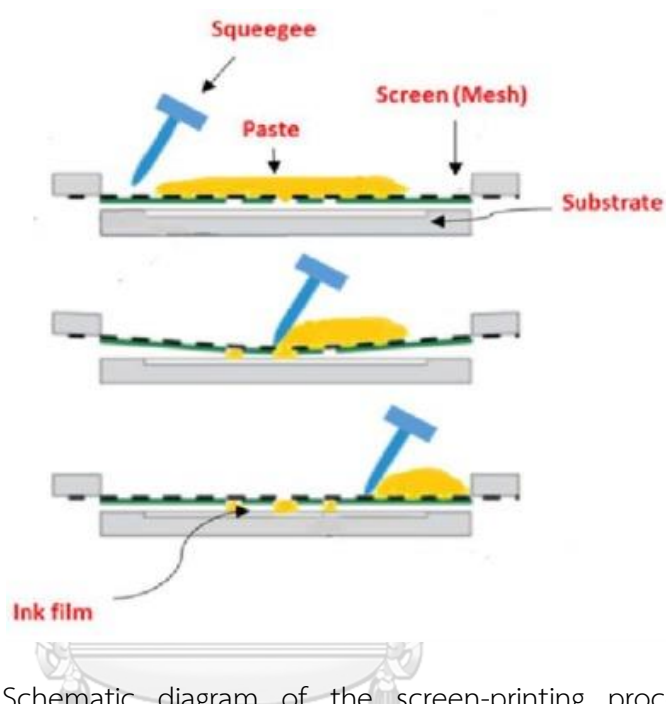
Figure 2.10 Schematic diagram of the screen-printing process for the electrode manufacture [37]

2.3.3 Optical detection

Optical method has been broadly employed with PAD because of its simple detection and interpretation. Till now, there is a variety of optical detections on PAD, for example, colorimetry, fluorescence, chemiluminescence, etc. However, the colorimetric detection was chosen herein in this research due to its simplicity in terms of operation and data analysis by available softwares on smartphones.

2.3.3.1 Colorimetric detection

Colorimetric detection is a common method to determine the concentration of the colored compound(s) derived from the target analyte(s). Colorimetric method is widely used in various applications, namely, point-of-care testing, industries and environment. Currently, colorimetric detection method could be developed to perform on PAD for the measurement of selected target analyte(s). The colored system could be miniaturized onto a piece of paper leading to simplicity to operation, low-cost, disposability, portability, minimal instrument, and required power. The principle of colorimetric method is the change of color induced by the reaction between the target analyte and its complementary reagent. This color change can be further monitored through a smartphone, camera, or scanner for simplicity and convenience.

CHAPTER 3

THE DEVELOPMENT OF ePAD FOR FOOD SAFETY APPLICATION

This chapter comprises of two parts. The former (Part I; section 3.1) describes the anodic stripping voltammetric determination of total arsenic using a gold nanoparticle-modified boron-doped diamond electrode on a paper-based device. The latter (Part II; section 3.2) reports the enhanced sensitivity and separation for simultaneous determination of tin and lead using paper-based sensors combined with a portable potentiostat.

Part I

3.1 Anodic Stripping Voltammetric Determination of Total Arsenic Using a

Gold Nanoparticle-modified Boron-doped Diamond Electrode on a

Paper-based Device

(Microchimica Acta)

Kingkan Pungjunun[a], Sudkate Chaiyo[a], Issarapong Jantrahong[a], Siriwan Nantaphol[a],

Weena Siangproh[b,**], Orawon Chailapakul[a, c,*]

[a] Electrochemistry and Optical Spectroscopy Center of Excellence, Department of Chemistry, Faculty of Science, Chulalongkorn University, 254 Phayathai Road, Pathumwan, Bangkok 10330, Thailand

[b] Department of Chemistry, Faculty of Science, Srinakharinwirot University, Sukhumvit 23, Wattana, Bangkok 10110, Thailand

[c] Center of Excellence on Petrochemical and Materials Technology, Chulalongkorn University, Patumwan, Bangkok 10330, Thailand

Corresponding author: Prof. Dr. Orawon Chailapakul

E-mail addresses: corawon@chula.ac.th Tel.: +66 2 218 7615; Fax: +66 2 218 7615

*** Co-corresponding author:* Associate Prof. Dr. Weena Siangproh

E-mail addresses: weena@g.swu.ac.th, weenasi@hotmail.com Tel.: +662 640 5000 ext 18208; Fax: +66 2 259 209

Abstract

A multistep paper-based analytical device (mPAD) was first designed and applied to the voltammetric determination of total inorganic arsenic. The electrodeposition of gold nanoparticles on a boron-doped diamond (AuNP/BDD) electrode and the determination of total inorganic arsenic can be achieved in a single device. Total inorganic arsenic can be determined by first reducing As(V) to As(III) using thiosulfate in 1.0 mol L^{-1} HCl. As(III) is then deposited on the electrode surface, and total inorganic arsenic is quantified as As(III) by square-wave anodic stripping voltammetry between potential range of -0.25 V and 0.35 V vs. Ag/AgCl. Under optimal conditions, the voltammetric response for As(III) detection is linear in the range from 0.1 to 1.5 µg mL^{-1} and the limit of detection (3SD/slope) is 20 ng mL^{-1}. The relative standard deviation at 0.3, 0.7 and 1.0 µg mL^{-1} of As(III) are 3.6, 4.3 and 3.3, respectively (10 different electrodes). The results show that the assay has high precision and excellent sensor-to-sensor reproducibility. The method was employed to the determination of total inorganic arsenic in rice samples. Results agreed well with those obtained by inductively coupled plasma-optical emission spectroscopy (ICP-OES).

Keywords: paper-based device, portable sensor, metal nanoparticles, arsenic detection, thiosulfate, electrochemical detection, rice sample

3.1.1 Introduction

Generally, inorganic arsenic substances, such as arsenite (As(III)) and arsenate (As(V)), are highly toxic to humans and can cause cancer of the lung, skin and urinary bladder [38]. The intake of arsenic by humans occurs through contaminated water and food. Rice is the main food in many areas, especially in Asia and is considered an agricultural commodity. Rice has been reported that contains a relatively high amount of arsenic compared to other foods. The maximum arsenic concentration limit in rice at 1.0 mg kg^{-1} has been established by the Food and Agriculture Organization/World Health Organization (FAO/WHO) [39]. Therefore, analytical methods to monitor and control the inorganic arsenic species in rice are important.

Previously, several techniques have been developed for the determination of arsenic such as atomic absorption spectrometry (AAS) [40], inductively coupled plasma with mass spectrometry (ICP-MS) [41], atomic fluorescence spectrometry (AFS) [42] and the Arsenator sold by Palintest (https://www.palintest.com). However, these techniques have some limitations including non-portable, expensive, and time-consuming for analysis. Hence, the development of a sensor for the determination of arsenic is an interesting approach. Electrochemical methods for determination of trace heavy metals has gained considerable attention because of its ease of operation, inexpensiveness, and portability for routine analysis [43]. Anodic stripping voltammetry (ASV) is the most promising electroanalytical technique for the determination of trace heavy metals due to its ability to provide high sensitivity and

a low detection limit with short analysis times [44, 45]. The determination of arsenic using ASV has been accomplished at various electrodes, especially mercury-, platinum-, and gold-based electrodes [46-48]. Compared to mercury and platinum, gold is a more sensitive and compatible electrode for measuring arsenic. Stable inter-metallic of Au–As compounds can be formed during the deposition step, which can improve the capability for the cathodic preconcentration of As(0) [49, 50]. In addition, modification of an electrode with gold nanoparticles (AuNPs) has been considered an effective strategy to enhance the sensitivity due to the increase in active surface area and the intrinsic properties of gold at the nanometer scale [51]. Previously, the use of AuNP-modified electrodes has been successfully developed for the determination of As(III) [52, 53].

Electrochemical detection on paper-based analytical de- vices (ePADs) is quite frequently preferred for designing the detection platform. ePADs can exhibit high sensitivity and selectivity. These devices are easily miniaturized and have low costs [54, 55]. Our research group is interested in developing the use of nanoparticle-modified boron-doped diamond electrode coupled with PADs to create a low-cost and high-performance electrochemical biosensor [56]. Due to the unique properties of the BDD electrode, such as of chemical inertness, high stability, low background current and wide potential window, this sensing platform can increase the reproducibility and detection sensitivity. However, using this platform, the modified

electrode need to be ex-situ prepared before applying as a working electrode in ePADs leading to complicated steps.

To simplify this process, a multistep paper-based analytical device (mPAD) has been developed as a novel, alternative tool for the determination of total inorganic arsenic into one sensor. Figure 3.1 shows that electrodeposition and analytical measurements can be performed with the same device. The mPAD was incorporated into the origami method [57] for the preparation of gold nanoparticle-modified boron-doped diamond (AuNP/BDD) electrodes and measurement of As(III) by ASV on a single device. In addition, the detection of total arsenic was proposed using thiosulfate as a reducing agent to reduce As(V) to As(III). To the best of our knowledge, there is no report of PADs for the successive electrode preparation and electro- chemical detection. Moreover, the capability of the device was evaluated by applying it for the determination of total inorganic arsenic in rice samples.

3.1.2 Experimental

3.1.2.1 Materials and reagents

Whatman #1 filter paper and a gold chloride solution ($AuCl_3$) were obtained from Sigma-Aldrich (St. Louis, USA, www. sigmaaldrich.com). Sodium arsenite ($NaAsO_2$), sodium hydrogen arsenate heptahydrate ($Na_2HAsO_4.7H_2O$), sodium thiosulfate ($Na_2S_2O_3$), cadmium nitrate ($Cd(NO_3)_2$) and nickel sulfate ($NiSO_4$) were

acquired from Carlo Erba Reagenti-SDS (Val de Reuil, France, https://www. carloerbareagents.com). Magnesium chloride ($MgCl_2$), 37% fuming hydrochloric acid (HCl), 65% nitric acid (HNO_3), and methanol were purchased from Merck (Darmstadt, Germany, http://www.merckmillipore.com). Calcium chloride ($CaCl_2$) and manganese chloride ($MnCl_2$) were obtained from M&B (Dangenham, England, http://www. may-baker.com). Potassium ferrocyanide ($K_4[Fe(CN)_6]$), lead nitrate ($Pb(NO_3)_2$) and zinc nitrate ($Zn(NO_3)_2$) were purchased from Ajax Finechemical (NSW, Australia, http://www.ajaxfinechem.com). Copper sulfate ($CuSO_4$) was purchased from BDH Middle East, LLC (BDH, England, http://www.bdhme.com). Silver/silver chloride ink was purchased from the Gwent group (Gwent Electronic Materials, Ltd., UK, http://www.gwent.org). Carbon ink was purchased from Acheson (California, USA, http://www.henkel- adhesives.com). All solutions were prepared with deionized water (18.2 MΩ.cm) from a Milli-Q system (Millipore, UK). Stock solution of As(III) and As(V) was prepared by dissolving in 1.0 mol L^{-1} HCl.

3.1.2.2 Instrumentation

The electrochemical measurements were performed using an Autolab potentiostat (PGSTAT101) (Metrohm Autolab B.V., The Netherlands, http://www.metrohm-autolab.com) controlled by a personal computer via NOVA 1.6 software. A boron-doped diamond electrode (1.3 × 1. 3 cm) was used as the working

electrode; a screen- printed carbon electrode and a screen-printed Ag/AgCl electrode were used as the counter electrode and the reference electrode, respectively. A Xerox Color Qube 8570 series (Xerox, Japan, http://www.office.xerox.com) wax printer was used to fabricate the PAD devices. The morphology of the AuNP/BDD electrode was investigated using a JSM-6400 field emission scanning electron microscope (Japan Electron Optics Laboratory Co., Ltd., Japan, https://www.jeol.co.jp). The accuracy of the method was tested by comparing the results obtained from this present method with those obtained from inductively coupled plasma-optical emission spectroscopy (iCAP 6000 series, Thermo Scientific, USA, https://www.thermofisher.com).

3.1.2.3 Design and fabrication of mPAD

First, the patterned paper device was designed by Adobe Illustrator CS6. Next, the design pattern was printed onto filter paper (Whatman #1, A4 size) using the wax printer model Color Qube 8570. On each wax-patterned paper, there were three parts, namely, the modification zone (for electrodeposition of AuNPs: 1.5 × 1.5 cm, circle: 8.0 mm in diameter), the working electrode zone (for BDD electrode: 1.5 × 1.5 cm) and the detection zone (for determination of As(III): 1.5 × 1.5 cm, circle: 8.0 mm in diameter) (Figure 3.1.2a). The wax-patterned paper was placed over a hot plate at 175 °C for 40 s to melt the printed wax so that wax penetrated through the paper to

form a hydro- phobic barrier. Then, the wax-patterned paper was used as a substrate

for the screen-printed electrodes. As seen in the circle of the modification zone and

the detection zone, carbon ink and Ag/AgCl ink were used for screen-printing the

counter electrode and the reference electrode, respectively (Figure 3.2b). Then, the

prepared paper was cut, as shown in Figure 3.1a.
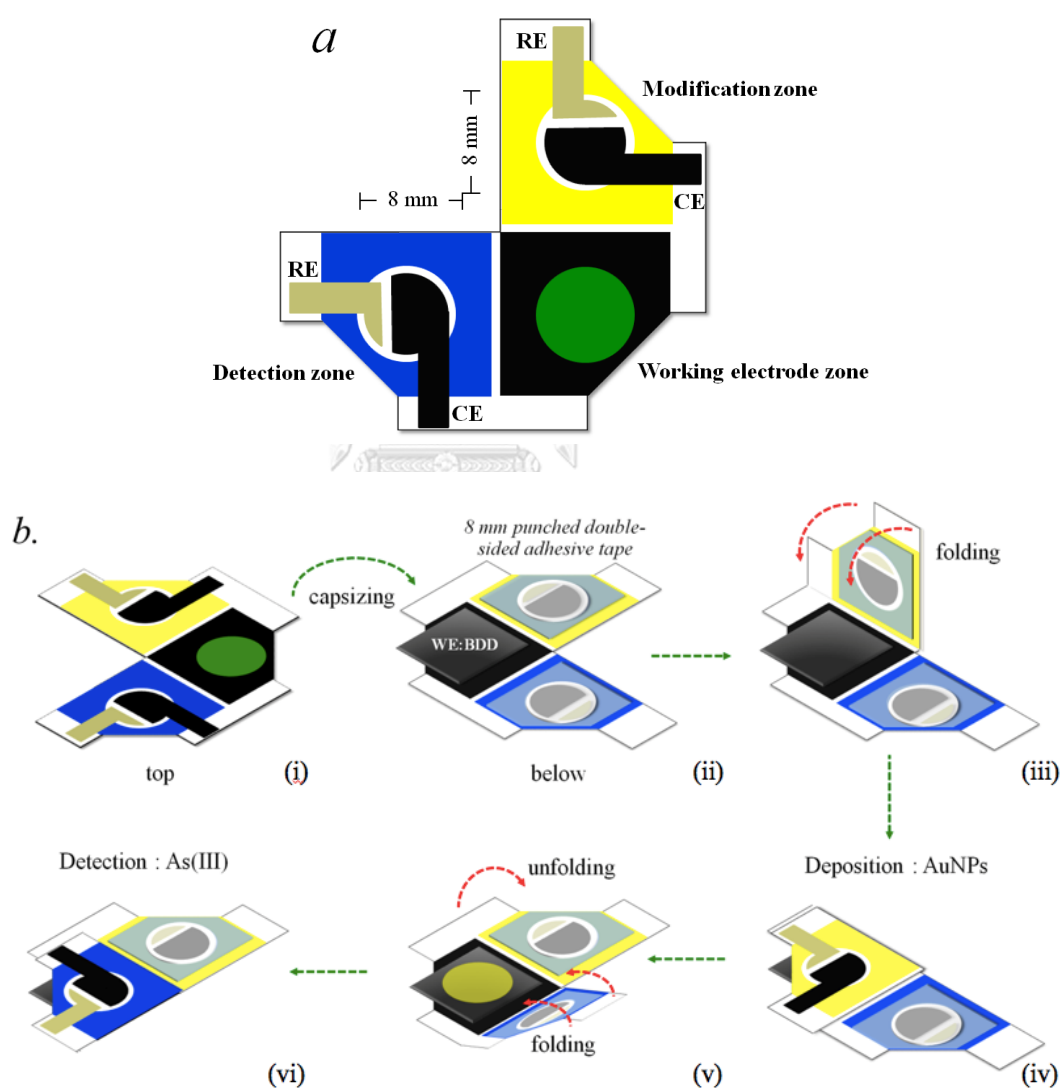
Figure 3.1 The pieces of mPAD (a). Schematic representation of the

fabrication and assay procedure of mPAD (b).
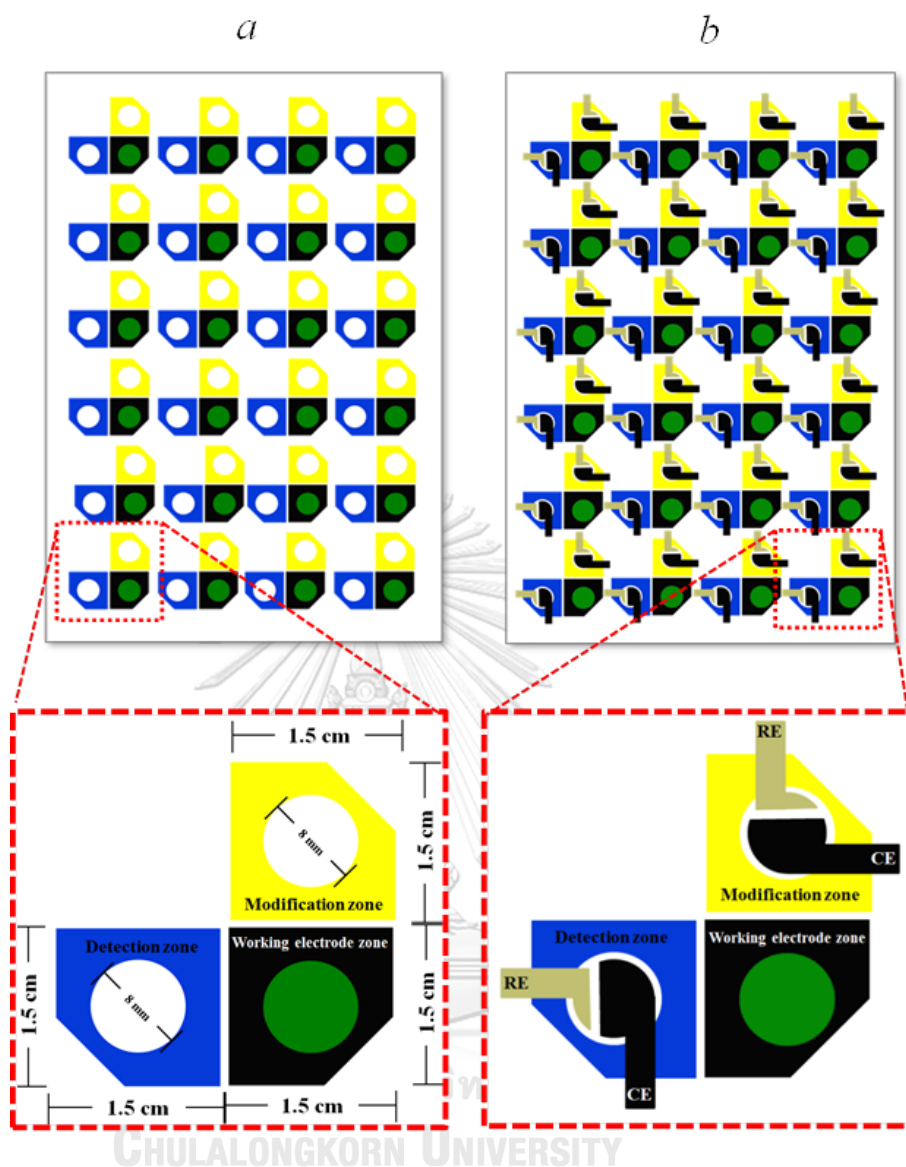
Figure 3.2 Paper sheets were first patterned in bulk using a wax printer (a). After baking, two electrodes were screen-printed on the wax-patterned sheet in bulk (b).

3.1.2.4 Modification of electrode and electrochemical detection

The modification and analytical procedures are shown in Figure 3.1b. First, on the mPAD, the BDD electrode was attached to the working electrode zone on the

back of the paper using double- sided adhesive tape (i). In addition, 8-mm-punched double-sided adhesive tape was attached to the modification zone and the detection zone (ii). Next, the modification paper zone was folded onto the bare BDD electrode (iii). Electrodeposition of AuNPs on BDD electrode surface was performed by dropping 100 μL of a 0.1% w/w Au(III) solution containing 1.0 mol L^{-1} HCl as supporting electrolyte into the modification paper zone. The constant potential of −0.3 V vs. Ag/AgCl was applied for 60 s to reduce Au(III) to Au(0) (iv). After the modification, the paper zone was peeled from the BDD electrode, and AuNPs were grown on the BDD electrode surface to form the so-called gold nanoparticle-modified BDD (AuNP/BDD) electrode. Next, the AuNP/BDD electrode was carefully rinsed with ultra-pure water (v). For the measurement step, the detection paper zone was assembled onto the AuNP/ BDD electrode by folding it together, leading to the completion of the three-electrode system, and the paper hole served as an electrochemical cell (vi). Before analysis, As(V) is reduced to As(III) which then can be quantified to give total inorganic arsenic. Consequently, sodium thiosulfate (Na$_2$S$_2$O$_3$) was selected to reduce As(V) to As(III) [58]. First, 60 mmol L^{-1} Na$_2$S$_2$O$_3$ was added to a solution 1 μg mL^{-1} As(V) containing 1.0 mol L^{-1} HCl as supporting electrolyte. Then, the solution was mixed and stirred for 30 min to convert As(V) to As(III). To detect As(III), square-wave anodic stripping voltammetry (SWASV) was employed. The sample or standard solution (100 μL) was dropped into the detection paper zone. Then, a deposition potential of −0.3 V vs. Ag/AgCl was applied for 120 s. After 5 s of

equilibration time, the SWV was recorded from −0.25 V to 0.35 V vs. Ag/AgCl with a step potential of 5 mV, a pulse amplitude of 50 mV and a frequency of 5 Hz.

3.1.2.5 Preparation of rice sample

Commercial rice samples were purchased from a local market (Bangkok, Thailand). The treatment process was performed according to the published literature [59]. Briefly, the rice samples were ground by a mortar and pestle into a fine powder. A portion (1 g) of rice flour was dissolved into 10 mL methanol-water (1:1) mixture containing 1% HNO_3. The mixture was placed in an ultrasonic bath for 30 min and centrifuged at 6000 rpm (8552 rcf) for 5 min. Then, the supernatant was loaded through a 30 μm anion exchanger (Oasis Max cartridge, USA). Before analysis, 1 mL of sample solution was transferred to a volumetric flask and diluted to 10 mL with 1.0 mol L^{-1} HCl as supporting electrolyte.

3.1.3 Results and discussion

3.1.3.1 Choice of materials

Various materials such as polypyrrole (PPy), polyaniline (PANI), reduced graphene oxide (rGO), AgNPs and AuNPs have been used to modify electrode for determination of As(III) owing to their high surface area to volume ratio and high conductivity. Among these, AuNPs offer the most suitable material due to a stable

intermetallic of Au–As compounds during deposition step [49, 50]. Therefore, AuNPs were chosen as modifier.

AuNPs have been used as modifier on various electrode substrates such as glassy carbon electrode (GCE) [60], screen-printed carbon electrodes (SPCEs) [61] and BDD electrode [62]. Compared to other electrode, BDD electrode provides wider electrochemical potential, lower background current, and higher resistance to surface fouling [56]. Therefore, AuNPs was modified on BDD electrode surface and applied as working electrode for measurement of As(III) using ASV on this present sensor.

3.1.3.2 Electrochemical response of As(III) on a AuNP/BDD electrode using mPAD

As mentioned above, gold is the most appropriate electrode to detect As(III) through the formation of As-Au compounds during the deposition process [63]. Hence, we used a gold nanoparticle-modified BDD (AuNP/BDD) electrode for the determination of As(III). The square-wave anodic stripping voltammograms (SWASVs) of As(III) obtained from bare BDD and AuNP/BDD are shown in Figure 3.3. Figure 3.3a shows the SWASVs of the supporting electrolyte (1.0 mol L^{-1} HCl), which does not exhibit any electrochemical signal. Figure 3.3b shows a small anodic peak of 1.0 μg mL^{-1} As(III) at the bare BDD at +0.01 V vs. Ag/ AgCl. Interestingly, in Figure 3.1.3c, which shows the SWASVs of 1.0 μg mL^{-1} As(III) at the AuNP/BDD, a sharp and very

large well-defined peak appeared at an approximate potential of +0.08 V vs. Ag/AgCl. As expected, the current signal of As(III) increased due to the formation of the As-Au compound, which can be easily oxidized. Moreover, the AuNPs provided a high surface area and increased the rate of electron transfer [64]. Therefore, this result illustrated that the use of AuNP/BDD coupled to mPAD can present a favorable performance towards the detection of As(III). It also suggests that this device is an excellent sensor for the field determination of As(III).
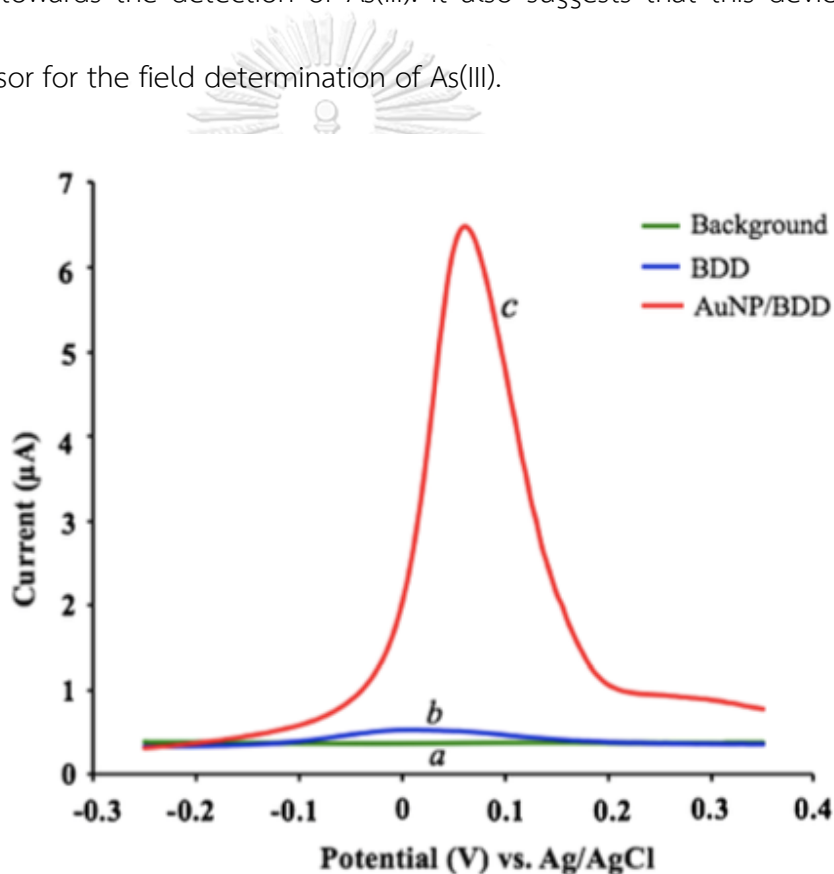
Figure 3.3 Comparison of SWASVs of a solution containing 1.0 µg mL^{-1} As(III) in 1.0 mol L^{-1} HCl (Background = 1.0 mol L^{-1} HCl (a)) at the bare BDD (b) and AuNP/BDD (c). Conditions: deposition potential -0.3 V vs. Ag/AgCl and deposition time 120 s.

3.1.3.3 Characterization of the AuNP/BDD electrode

A gold nanoparticle-modified BDD electrode was obtained by electrodeposition. To obtain a good electrochemical response for the determination of As(III), the important parameters for the modification of the electrode, including the deposition potential and electrodeposition time, were studied. Respective data and figures are given in Figure 3.4. The optimal condition was found at deposition potential of −0.3 V vs. Ag/ AgCl for 60 s.
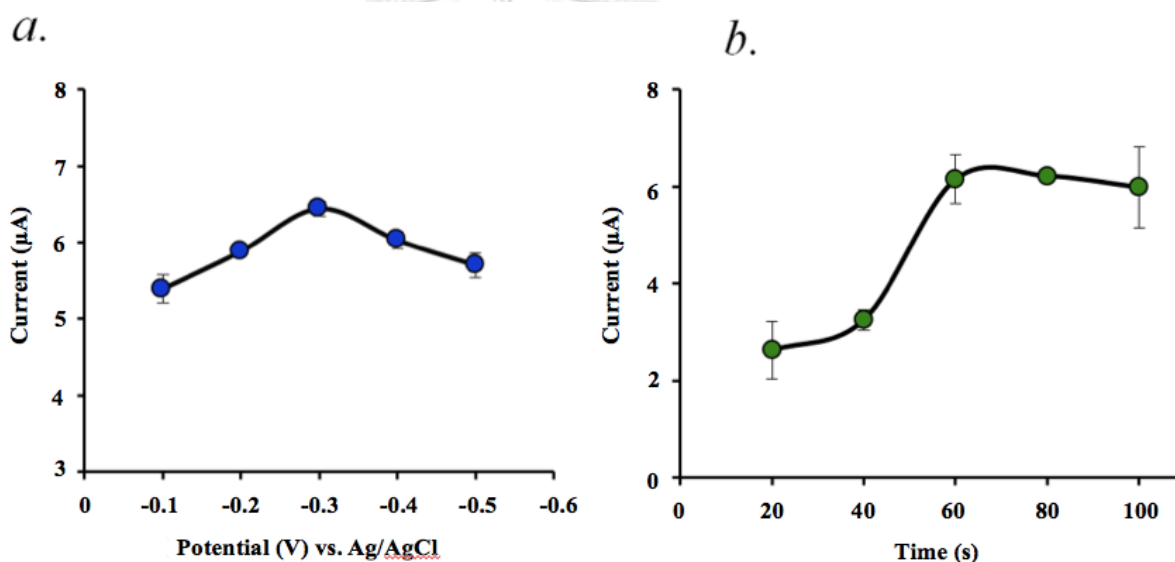
Figure 3.4 Effect of the electrodeposition potential (a) and the electrodeposition time (b) of 1.0 μg mL^{-1} As(III) at the AuNP/BDD electrode. Conditions: deposition potential -0.3 V vs. Ag/AgCl and deposition time 120 s.

After optimization, the surface morphology of AuNP/BDD electrode was investigated using scanning electron microscopy (SEM). Figure 3.5a-c shows SEM images of the bare BDD electrode (a), the AuNP/BDD electrode (b) and the BDD electrode at 40,000X magnification (c). Clearly, there are significant differences in the

surface structure be- tween the two electrodes. The bare BDD electrode has a rough

surface, while the SEM image of AuNP/BDD shows that the spherical gold

nanoparticles were uniformly dispersed onto the BDD electrode surface. The

diameter of the gold nanoparticles is approximately 70–90 nm. The distribution of

the nanoparticles observed in the SEM image can lead to a high surface area of the

modified electrode, which can enhance the electrochemical sensitivity of detection.
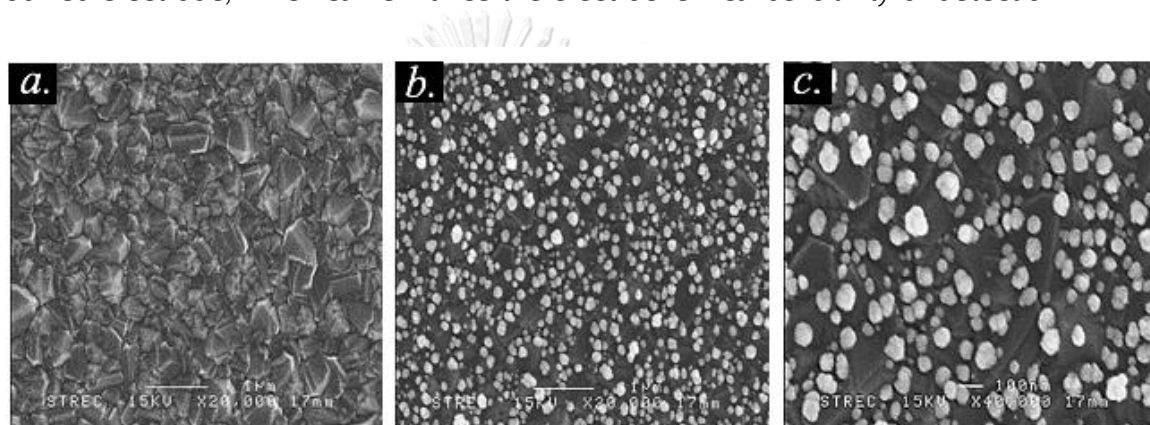
Figure 3.5 The scanning electron microscope image for the bare BDD

electrode (a), AuNP/BDD electrode (b) and AuNP/BDD electrode was magnified

40,000X (c). Conditions: deposition potential -0.3 V vs. Ag/AgCl and deposition time

60 s.

3.1.3.4 Analysis of total inorganic arsenic using mPAD

Generally, As(III) can directly detect using ASV. However, in case of As(V), it

requires high negative potential for reduction of As(V) to As(0). However, this

potential will generate hydrogen gas by the reduction process and hinder the

accumulation of As(0) at the electrode surface. Therefore, it is necessary to convert

As(V) to As(III), and the determination was recorded as the total inorganic arsenic. The reducing agent plays an important role in the determination of total inorganic arsenic. In present work, sodium thiosulfate ($Na_2S_2O_3$) was selected to reduce As(V) to As(III). The effects of the concentration of the reducing agent and reduction time were investigated. In summary, the optimal conditions for reducing As(V) to As(III) are 60 mmol L^{-1} reducing agent and 40 min reduction time (as show in Figure 3.6a-b).

To confirm the completeness of the conversion of As(V) to As(III), SWASVs of As(III) and As(V) in the absence and presence of $Na_2S_2O_3$ were examined under the optimal conditions. SWASVs of 3 different testing solutions were performed including (i) 1.0 μg mL^{-1} As(III) in the absence of $Na_2S_2O_3$, (ii) 1.0 μg mL^{-1} As(V) in the presence of $Na_2S_2O_3$ and (iii) a mixture of 0.5 μg mL^{-1} As(III) and 0.5 μg mL^{-1} As(V) in the presence of $Na_2S_2O_3$. As shown in Figure 3.6c-e, the results indicate that the SWASVs responses obtained from 3 different conditions had no significant difference. This result can confirm that these optimal conditions can be used to completely convert As(V) to As(III). Therefore, it was applied as a pretreatment step before the determination of total inorganic arsenic.
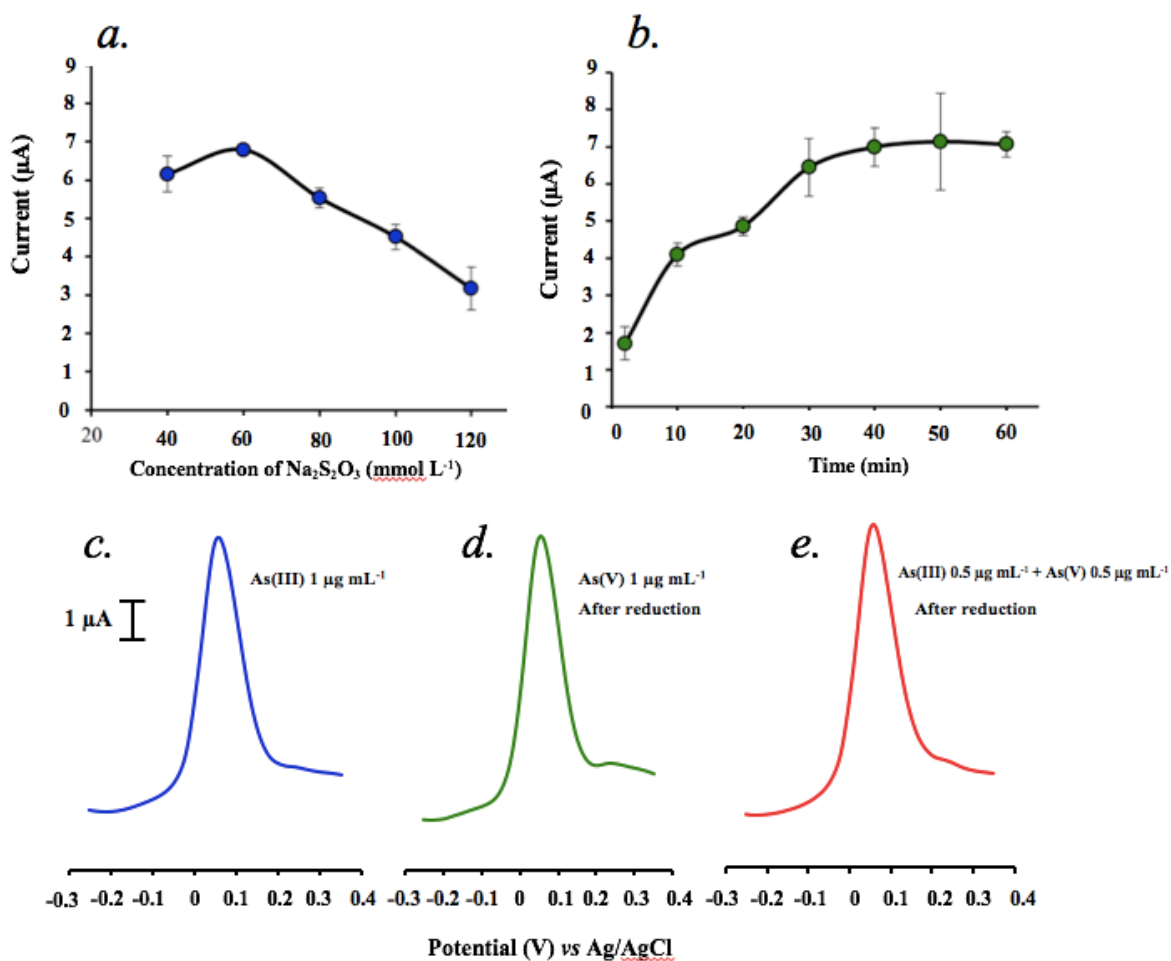
Figure 3.6 Effect of the reducing agent concentration (a) and the reduction time (b) at the AuNPs/BDD electrode on mPAD. SWASVs of 3 different testing solutions, 1.0 μg mL^{-1} As(III) in the absence of Na$_2$S$_2$O$_3$ (c), 1.0 μg mL^{-1} As(V) in the presence of Na$_2$S$_2$O$_3$ (d) and a mixture of 0.5 μg mL^{-1} As(III) and 0.5 μg mL^{-1} As(V) in the presence of Na$_2$S$_2$O$_3$ (e). Conditions: deposition potential -0.3 V vs. Ag/AgCl and deposition time 120 s.

For the detection of total inorganic arsenic after pretreatment using SWASV, the deposition potential and deposition time of SWASV were studied in order to

obtain the highest sensitivity. The optimal detection conditions were: (a) deposition

potential of −0.3 V vs Ag/AgCl (b) deposition time of 120 s as shown in Figure 3.7.
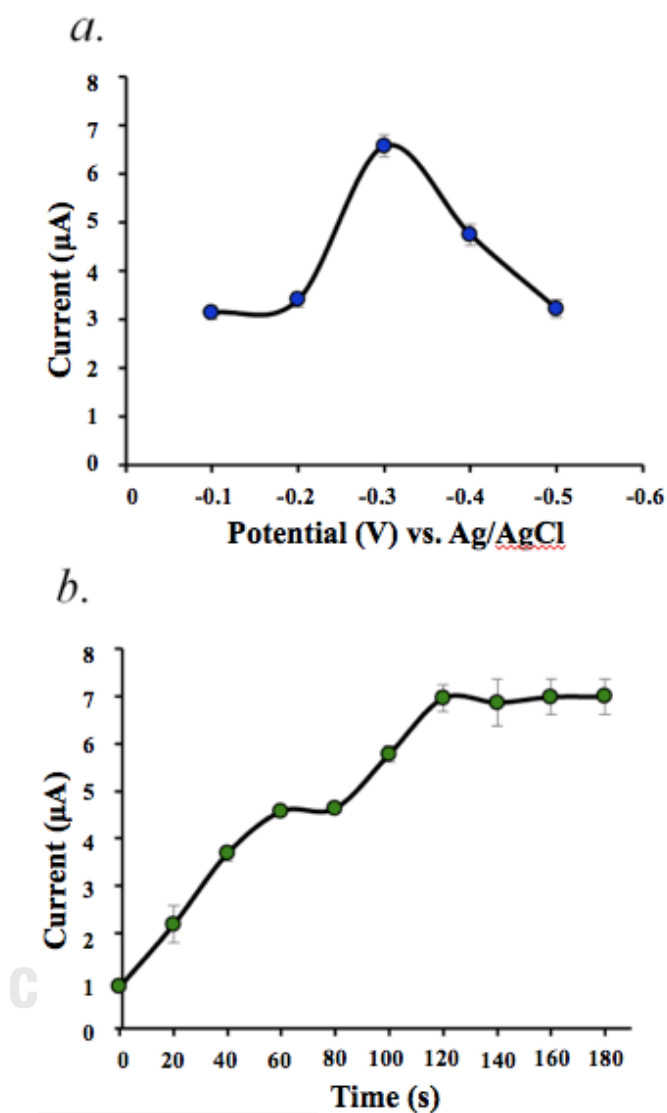
Figure 3.7 Effect of the deposition potential (a) and the deposition time (b) of

1.0 µg mL^{-1} As(III) at AuNP/BDD electrode on mPAD.

3.1.3.5 Analytical performance of mPAD

Under the optimal experimental conditions, the mPAD was used to modify the AuNPs and detect As(III). It can be seen from Figure 3.8 that well-defined SWASVs responses from As(III) were observed, and the responses increased proportionally to the As(III) concentration. A good linear relationship between the stripping current and As(III) concentration was obtained from 0.1 to 1.5 µg mL^{-1} with a regression equation of I (µA) = 4.5175C As(III) (µg mL^{-1}) +1.1527 (R^2 = 0.9972) (inset). The limit of detection (LOD = 3SD/σ) was calculated to be 0.02 µg mL^{-1} [65]. This mentioned limit of detection is in line with the range of concentrations of arsenic required to be measured for most contaminated rice according to Food Standards Australia New Zealand (1.0 µg mL^{-1}) [39] and the Food and Drug Administration of Thailand (2.0 µg mL^{-1}) [66] guidelines for arsenic. This information confirms that the device can be applied for the determination of total arsenic in rice samples. The repeatability of the mPAD was evaluated by the determination of As(III) at each of the following three concentrations: 0.3, 0.7 and 1.0 µg mL^{-1}. Ten sensors were prepared under the same conditions. The relative standard deviations were 3.64, 4.30 and 3.25%, respectively, indicating a high sensor-to-sensor reproducibility.
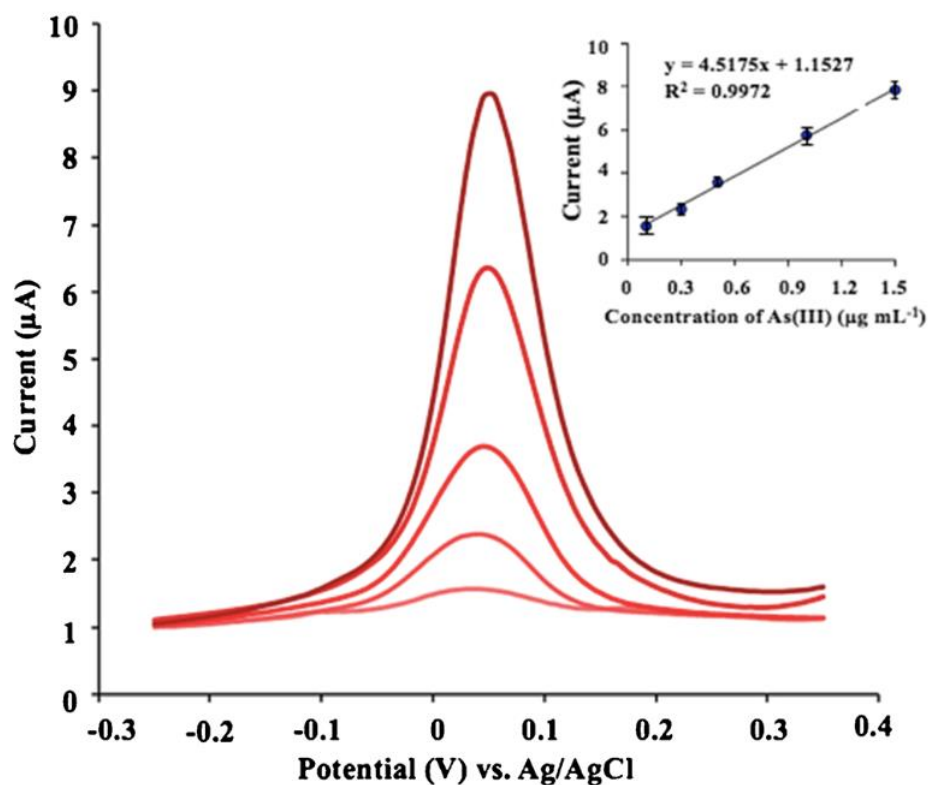
Figure 3.8 SWASVs of As(III) at a AuNPs/BDD electrode on mPAD in 1.0 mol L^{-1}

HCl at the concentrations of 0.1-1.5 µg mL^{-1} between potential range of -0.25 V and

0.35 V vs. Ag/AgCl. Inset of a: linear relationship of stripping currents versus As(III)

concentration. Conditions: deposition potential -0.3 V vs. Ag/AgCl and deposition

time 120 s.

The analytical performance was compared to those the previous reports

(Table 3.1). Those techniques provided lower LOD and wider linear range. However,

the LOD is acceptable or the detection of total arsenic in rice sample. Moreover, the

mPAD exhibits the advantages of disposability, portability, simplicity, and less

amount of sample volume and reagent consumption.

Table 3.1 Comparison between analytical methods for determination of arsenic compounds

Main nanomaterial modifier	Modification method	Oxidizing/reducing agent	Analyte	Detection method	Detection limit (ng mL⁻¹)			Ref
					As(III)	As(V)	Total As	
M-PMA	In situ chemical oxidative polymerization	-	As(III)/As(V)	MP-AES	0.0003	0.010	-	67
Al₂O₃ NPs	Synthesis	-	As(III)/total As	GF AAS	0.00181	-	0.0097	68
TTCN-AuNP-Graphene-PE	Chemically modified electrodes	Na₂SO₃	As(III)/total As	PSA	0.0006	-	-	69
AuNP/Fe₃O₄/GCE	Drop dried/electrode position	-	As(III)	SWASV	0.00097	-	-	60
Au-PdNP/GCE	Synthesis	-	As(III)	ASV	0.25	-	-	70
AuNP/BDDE	Electrodeposition	Na₂SO₃	total As	SWASV	-	-	20	This work

* M-PMA : Fe3O4@Poly-Methacrylic acid, MP-AES : Microwave plasma atomic emission spectroscopy, Al2O3 NPs : Aluminum oxide nanoparticles, GF AAS : Graphite furnace atomic absorption spectrometry, TTCN-AuNP-Graphene-PE : 1,4,7-trithiacyclononane- Gold nanoparticles-Graphene-Paste electrode, PSA : Potentiometric stripping analysis, AuNP/Fe3O4/GCE : Magnetic Fe₃O₄ nanoparticles and gold nanoparticles modified glassy carbon electrode, SWASV : Square wave anodic stripping voltammetry, Au-PdNP/GCE : Au-Pd nanoparticles modified glassy

carbon electrode, ASV : Anodic stripping voltammetry, AuNP/BDD : gold nanoparticle-modified boron-doped diamond electrode

3.1.3.6 Interference study

Under the optimal conditions, the interference study was per- formed by adding various interfering substances into a standard solution containing 1.0 µg mL^{-1} of As(III). The tolerance ratio of interference for a ± 5.0% signal change for 1.0 µg mL^{-1} As(III) are listed as follows: 100-fold Ni(II), Mg(II), Zn(II), and Ca(II), and 10-fold Mn(II), Pb(II), and Cd(II). Clearly, most of the ions show no interference for the detection. However, the presence of a one-fold excess of Cu(II) decreased the stripping signal of As(III), and a new peak of Cu(II) was generated at a potential of +0.25 V (Figure 3.9, red line), presumably due to competition between the As(III) and Cu(II) occurring at the active sites of the electrode surface.

To improve the stripping peak signal of As(III) and to solve the problem of Cu(II) interference, ferricyanide was selected as a complexing agent with Cu(II). In the presence of ferricy- anide, the competition between As(III) and Cu(II) was reduced due to the strong complexation between Cu and ferricyanide, leading to a shift in the oxidation potential of Cu(II) to a more negative potential [71]. After 0.25 mmol L^{-1} ferricyanide was added to 1.0 µg mL^{-1} As(III) in the presence of Cu(II), the signals of Cu(II) completely disappeared, and the signals of As(III) remained constant, as shown

in Figure 3.9 (green line). The performance of using 0.25 mmol L^{-1} ferricyanide as the complexing agent for different concentrations of Cu(II) was studied. The current response for 1.0 µg mL^{-1}. As(III) using mPAD is set as 100%, compared to the signal obtained from the addition of 0.25 mmol L^{-1} ferricyanide to 1.0 µg mL^{-1}. As(III) in the presence of various concentrations of Cu(II) (1.0 to 100 µg mL^{-1}). These results show that the percent deviation of all are less than 5%, even though the concentration of the interfering substance was as high as 100 times that of As(III). This result indicates that the mPAD presents outstanding selectivity in the detection of As(III).
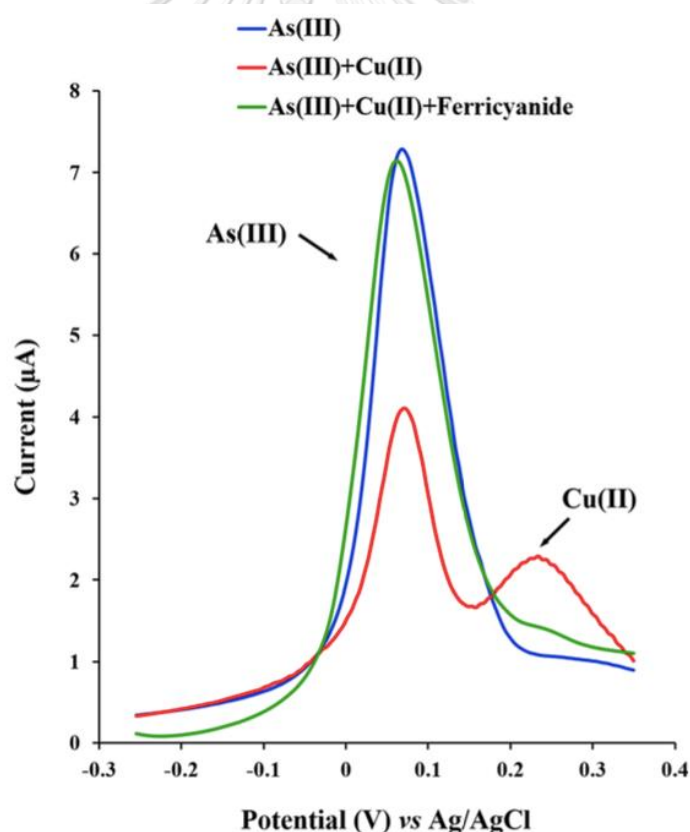
Figure 3.9 SWASVs of 1.0 µg mL^{-1} As(III) (blue line) and 1.0 µg mL^{-1} As(III) in the presence of 1.0 µg mL^{-1} Cu(II) (red line) and 0.25 mmol L^{-1} ferricyanide added to 1.0

µg mL^{-1} As(III) in the presence of 1.0 µg mL^{-1} Cu(II) (green line) at the AuNPs/BDD electrode on an ePAD. Conditions: deposition potential -0.3 V vs. Ag/AgCl and deposition time 120 s.

3.1.3.7 Application in rice samples

mPAD was applied to determine the total inorganic arsenic level in rice samples. After the preparation of rice samples, 1 mL of sample solution was pipetted into a 10.0 mL calibrated flask and determined under the optimum conditions. As(III) was not found in the rice samples, as shown in Table 3.2. The maximum content of total arsenic in rice, as recommended by the Food Standards Australia New Zealand, is 1.0 µg mL^{-1} [39]. To verify the feasibility, a recovery test was carried out by adding different amounts of As(III) and As(V) standards (0, 5.0 and 1.0 µg mL^{-1}) to the sample matrix. The recovery results are shown in Table 3.2, the recoveries and %RSDs of As(III) were found to be in the ranges of 87.82– 107.8% and 2.12–9.31%, respectively. Finally, the results obtained by this present method were compared with those obtained by the ICP-OES method. A paired t-test at the 95% confidence level was performed, and the calculated t-value of As(III) was below the critical t-value (2.57 for 2 degrees of freedom). This result shows that there is no significant difference between the two methods. Therefore, this present method can be used to determine total inorganic arsenic in rice samples with high acceptability and reliability.

Table 3.2 Recovery tests of the proposed method and standard method for the determination of total As in rice samples (n = 3).

Samples	Spiked			Proposed method			ICP-OES		
	As(III)	As(V)	Total As (µg mL^{-1})	Found	%Recovery	%RSD	Found	%Recovery	%RSD
Sample 1	0	0	0	*ND*	-	-	*ND*	-	-
	0.5	0	0.5	0.44±0.04	87.82	9.11	0.39±0.03	77.6	7.69
	1	0	1	0.94±0.04	94.15	4.25	0.81±0.03	81.1	3.70
Sample 2	0	0	0	*ND*	-	-	*ND*	-	-
	0.5	0	0.5	0.45±0.03	89.91	6.68	0.51±0.02	100.2	3.92
	1	0	1	0.94±0.02	94.28	2.12	1.07±0.01	107.5	0.93
Sample 3	0	0	0	*ND*	-	-	*ND*	-	-
	0	0.5	0.5	0.54±0.01	107.8	1.69	0.44±0.01	88.51	1.84
	0	1	1	1.01±0.01	100.8	9.31	0.97±0.01	97.07	0.66
Sample 4	0	0	0	*ND*	-	-	*ND*	-	-
	0	0.5	0.5	0.45±0.02	89.51	4.61	0.40±0.01	84.77	1.05
	0	1	1	0.95±0.05	95.23	6.10	0.97±0.01	97.44	0.51
Sample 5	0	0	0	*ND*	-	-	*ND*	-	-
	0.25	0.25	0.5	0.49±0.02	98.01	3.73	0.42±0.01	79.71	0.59
	0.5	0.5	1	0.97±0.07	97.42	7.58	0.97±0.01	95.72	0.69

*ND = not detectable

3.1.4 Conclusions

A multistep paper-based analytical device (mPAD) for the determination of total inorganic arsenic was demonstrated. The combination of the modification of BDD electrode with AuNPs and the determination of the total inorganic arsenic was integrated in one paper device. Thiosulfate was used as reducing agent to reduce

As(V) to As(III), and then the total inorganic arsenic was determined by SWASV. The study of interference of the tested elements, only Cu(II) found to be an interference for determination of total inorganic arsenic. However, Cu(II) can be easily eliminated using ferricyanide. Finally, this mPAD was successfully applied for the detection of total inorganic arsenic in rice samples. This device shows excellent benefits, such as low cost, ease of use, less time requirement, high selectivity, sensitivity, stability and reproducibility. However, the reusability of this electrode was limit to only 5 times. In addition, mPAD was still required professional skill for electrodeposition of AuNPs on BDD electrode. Even though these weaknesses require a further improvement, the strength of the present sensor such as fast and straightforward fabrication allows the total analysis step to be accomplished within 3 min.
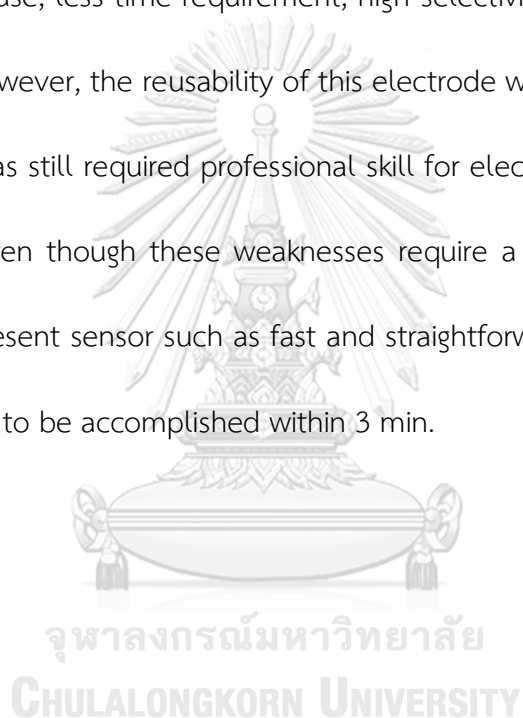
Part II

3.2 Enhanced sensitivity and separation for simultaneous determination of tin and lead using paper-based sensors combined with a portable potentiostat

(Sensors and Actuators B: Chemical)

Kingkan Pungjunun[a], Siriwan Nantaphol[a], Narong Praphairaksit[a], Weena Siangproh[b], Sudkate Chaiyo[a, c, d**], Orawon Chailapakul[a, e*]

[a] Electrochemistry and Optical Spectroscopy Center of Excellence, Faculty of Science, Chulalongkorn University, Bangkok, 10330, Thailand

[b] Department of Chemistry, Faculty of Science, Srinakharinwirot University, Bangkok, 10110, Thailand

[c] The Institute of Biotechnology and Genetic Engineering, Chulalongkorn University, Bangkok, 10330, Thailand

[d] Food Risk Hub, Research Unit of Chulalongkorn University, Bangkok, Thailand

[e] Nanotec-CU Center of Excellence on Food and Agriculture, Department of Chemistry, Faculty of Science, Chulalongkorn University, Bangkok 10330, Thailand

Corresponding author: Prof. Dr. O. Chailapakul

E-mail: corawon@chula.ac.th Tel.: +66 2 218 7615

*** Co-corresponding author:***   Dr. S. Chaiyo

E-mail: <u>sudkate.c@chula.ac.th</u> Tel.: +66 2 218 8078

Abstract

Due to similar properties in the electroanalysis of tin (Sn(II)) and lead (Pb(II)), the voltammograms of tin and lead overlap and it is difficult to simultaneously determine these two metals. Herein, we develop a simple fabricated sensor based on a bismuth nanoparticle-modified screen-printed graphene electrode (BiNP/SPGE) on a paper-based analytical device (PAD) for the simultaneous determination of Sn(II) and Pb(II) and combine it with a portable potentiostat. To overcome crossing interference, the use of hexadecyltrimethylammonium bromide (CTAB) can provide improved separation and enhanced sensitivity for Sn(II) and Pb(II) detection in oxalic acid as a supporting electrolyte while using square-wave anodic stripping voltammetry. Under optimal conditions, the linear range of both metals was determined to be 10 to 250 ng mL^{-1}, and the calculated limit of detection (3SD/slope) was 0.26 ng mL^{-1} and 0.44 ng mL^{-1} for Sn(II) and Pb(II), respectively. This sensor was also applied to simultaneously determine Sn(II) and Pb(II) in canned food samples. The results obtained from the portable potentiostat were similar to the results obtained by a standard method. Therefore, the proposed device can be further improved for the realization of a rapid on-site detector for Sn(II) and Pb(II) detection in real samples.

Keywords: paper-based device, portable sensor, metal nanoparticles, tin, lead, simultaneous detection, CTAB

3.2.1 Introduction

Currently, the consumption of canned food has rapidly increased because it is ready to be eaten without further preparation. However, contamination from packaging material is a major concern regarding human health [72, 73]. Tin (Sn(II)) and lead (Pb(II)) are the most common heavy metals that contaminate canned products[74]. These heavy metals contaminants can cause gastrointestinal irritation; moreover, they can potentially affect the cardiovascular system, nervous system, bone marrow and kidney[75]. In addition, they are also classified as human carcinogens and may help cause epithelial ovarian cancer, stomach cancer and lung cancer[76]. For this reason, the maximum concentration limit of Sn and Pb in canned food has been set by the Food and Agriculture Organization/World Health Organization (FAO/WHO) at 250 mg kg^{-1}[77] and 1 mg kg^{-1}[78], respectively. Therefore, a sensitive and rapid quantitative analysis of Sn and Pb in canned products is an urgent need. Typically, conventional methods for heavy metal determination are ICP-OES[79], ICP-MS[80] and AAS[13]. Unfortunately, there are some limitations with these techniques, including a high-cost and the need for a bulky instrument; additionally, these techniques are time-consuming and require a well-trained analyst, which may hinder its use for on-site analysis.

Presently, there is a demand for simple and portable analytical tools that offer a rapid detection among scientific communities. To achieve these goals, a

paper-based analytical device (PAD) is an alternative device that provides a simple fabrication and low cost and are also disposable and portable [81]. Various detection methods have been broadly utilized with paper-based platforms. Among them, electrochemical and colorimetric detection are the most widely used techniques that are integrated with a PAD[82-85]. However, colorimetric detection still has some drawbacks, including biased data and poor sensitivity. On the other hand, an electrochemical analysis with a PAD is of interest due to its fast analysis time, high sensitivity, portability and practical convenience [86].

Previously, an electrochemical technique for heavy metal detection was developed using a hanging mercury drop electrode (HMDE)[87] or a thin film mercury electrode[88]. However, mercury is environmentally toxic, and mercury poisoning causes prominent nervous system effects[89]. Therefore, alternative electrode materials for heavy metal detection are being explored. Recently, metal nanoparticles such as bismuth nanoparticles (BiNPs)[90], gold nanoparticles (AuNPs)[91], and silver nanoparticles (AgNPs)[92] are of remarkable interest as electrode modifiers. These nanomaterials exhibit good electrocatalytic activity, excellent conductivity and high surface area ratios [81]. Therefore, they have been widely exploited in several electrochemical sensors. Notably, not only metal nanoparticles but also carbon-based nanomaterials have been enormously used in electrochemical sensors on paper-based device [93, 94]. Graphene, an allotrope of carbon consisting of a single layer of carbon atoms in a hexagonal lattice, shows superior electronic properties

and is broadly utilized in electrochemical sensors[95]. Interestingly, it has been reported that a nanocomposite between metal nanoparticles and carbon-based nanomaterials may synergistically enhance the performance of an electrochemical sensor[96]. Thus, the use of a nanocomposite between these two nanomaterials will be highlighted in this work.

In the present work, we focused on the simultaneous determination of Sn(II) and Pb(II) in canned food using an electrochemical paper-based analytical device. Generally, the simultaneous detection of these two metals often results in an overlapped peak caused by oxidation potentials that are close to each other. Interestingly, surfactants such as hexadecyltrimethylammonium bromide, aka, cetyltrimethylammonium bromide (CTAB) and tetramethylammonium bromide (TMAB) present the specific amphiphilic structure. At the low concentration of surfactant, the adsorption can occur at below the critical micelle concentration (CMC) of surfactant onto electrode surface. Meanwhile, at the higher CMC of surfactant, the micelle can be formed and target analyte also diffuse inside the micelle. Consequently, surfactants can alter the redox potential, diffusion coefficient and electron transfer coefficient of two overlapping species due to an adsorption or aggregation process [97]. Therefore, a surfactant can be used as an additive to enhance the signal and improve the peak separation between Sn(II) and Pb(II).

Herein, the objective of this work is to develop a new PAD using a BiNPs-modified graphene electrode in the presence of a CTAB surfactant for the

simultaneous determination of Sn(II) and Pb(II) and then combine it with a portable

potentiostat. An electrode fabrication of a BiNPs-modified electrode can be simply

prepared by mixing BiNPs in a conductive graphene ink. Excellent signal

enhancement toward target analytes was clearly achieved with the BiNPs-modified

screen-printed graphene electrode (BiNP/SPGE). Importantly, the as-prepared sensor

is a disposable and portable device, indicating its potential for on-site analysis with a

small required sample volume (100 µL).

3.2.2 Experimental

3.2.2.1 Materials and reagents

Bismuth nanoparticles (BiNPs, 40-60 nm) was purchased from Nanostructured

& Amorphous materials (USA). Conductive graphene (code no. C2171023D1), carbon

(code no. C2130307D1) and silver/silver chloride (Ag/AgCl) (code no. C2130809D5) ink

was ordered from Gwent group (Torfaen, United Kingdom). Tin(II)chloride and sodium

chloride were purchased from Carlo Erba Reagenti-SDS (Val de Reuil, France).

Lead(II)nitrate, magnesium sulfate, hexadecyltrimethylammonium bromide,

nafion117, sodium dodecyl sulfate, tween®20, were acquired from Sigma-Aldrich (St.

Louis, USA). Standard solutions of 1000 µg mL^{-1} Bi(III), Cu(II), Zn(II), Cd(II), oxalic acid

dehydrate, calcium nitrate tetrahydrate, potassium chloride, iron(II)sulfate,

Iron(III)chloride hexahydrate, 37% hydrochloric acid fuming, 65% nitric acid, 100%

acetic acid and 95-97% sulfuric acid were obtained from Merck (Darmstadt, Germany). All reagents were analytical-grade chemicals and all aqueous solutions were prepared in deionized water (18.2 MΩ.cm^{-1}) from a Milli-Q system (Millipore, UK).

3.2.2.2 Apparatus

The electrochemical analysis was performed using a CHI1240B electrochemical analyzer (CH Instruments, Inc., USA) and a portable electrochemical reader (Metrohm DropSens, Spain). A three screen-printed electrodes system was employed, including a bismuth nanoparticles-modified screen-printed graphene electrode (BiNP/SPGE) as the working and counter electrode, and Ag/AgCl as the reference electrode. A Xerox Color Qube 8570 series (Xerox, Japan) wax printer was used to create wax pattern on paper-based devices. The field emission scanning electron spectroscopy (FESEM) investigations were performed by a JSM-7001F model at 15 kV (JEOL Ltd., England). The energy dispersive x-ray spectra (EDX) was recorded on INCA penta FETx3 model (Oxford Instruments plc, United Kingdom). The accuracy of this method was studied by comparing between the results obtained from this present sensor and those obtained from inductively coupled plasma-optical emission spectroscopy (iCAP 6000 series, Thermo Scientific, USA).

3.2.2.3 Fabrication of BiNP/SPGE on a PAD

To define an electrochemical detection zone, a wax-printing method was utilized. A circular wax pattern (1 cm) was created by Adobe Illustrator CS6 and a solid-wax printer (Xerox Color Qube 8570) was used to print wax on a filter paper (Whatman No. 1). Next, the printed paper was heated on a hot plate (170 °C, 40 s) to melt the printed wax. In each detection zone, a three-electrode system was fabricated. The working electrode (a circle 4 mm in diameter) and counter electrode were screened with a mixture of 10 g graphene ink and 25 mg BiNPs. After the mixture of graphene ink had been heated at 55 °C for 1 h, Ag/AgCl ink was screened as a pseudo-reference electrode and a conductive pad was also patterned onto the paper. Next, the PAD was baked in an oven at 55 °C for 1 h, as shown in Figure 3.10A. Finally, the current was measured directly by inserting the complete device into a portable potentiostat (Figure 3.10B).
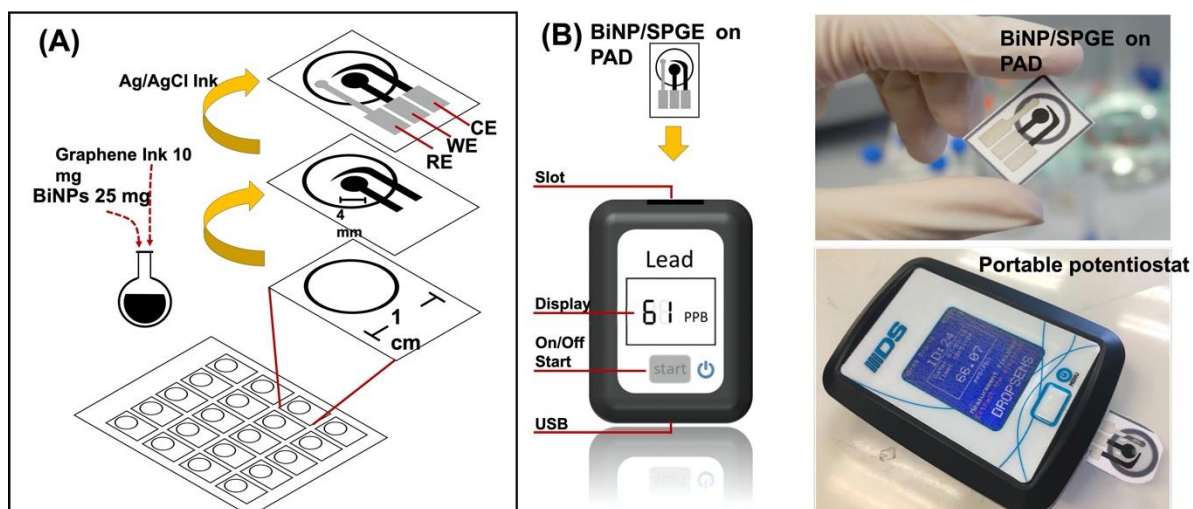
Figure 3.10 The fabrication of BiNP/SPGE (A) and the complete device into a portable potentiostat (B)

3.2.2.4 Electrochemical measurement

Square wave anodic stripping voltammetry (SWASV) was performed for the simultaneous detection of Sn(II) and Pb(II). The overall electrochemical procedure consisted of 2 steps: (i) the metal accumulation step and (ii) the anodic stripping step. First, a 100-µL aliquot using 0.1 M oxalic acid as the supporting electrolyte was dropped onto the electrochemical detection zone and covered the three electrodes. After that, an accumulation potential at -1.1 V vs. Ag/AgCl was applied for 80 s. After a 2 s equilibration period, the square wave anodic stripping voltammograms (SWASVs) were recorded between −1.1 V and −0.5 V vs. Ag/AgCl with a frequency of 25 Hz, a potential increment of 15 mV, and an amplitude of 50 mV at 25 °c.

3.2.2.5 Sample preparation

Five canned food samples consisting of canned mushrooms (sample No. 1-2) and canned bamboo shoots (sample No. 3-5) were purchased from a local market (Bangkok, Thailand). There are two phases in canned food samples, namely, the liquid phase and the solid phase, and these were measured using BiNP/SPGE on a PAD. For liquid samples, 500 µL of each sample solution was diluted 2-fold to 1 mL with 0.1 M oxalic acid and 0.1 mM CTAB before analysis. For solid samples, the samples were ground into a fine powder using a blender. A portion (1 g) was added to 1 mL of 2% v/v HNO_3 and mixed for 5 min. Then, the pH was adjusted to pH 7 using NaOH solution. After that, 500 µL of each sample solution was diluted 2-fold to a 1 mL mixture of 0.1 M oxalic acid and 0.1 mM CTAB. Following the above preparations, 100 µL of solution was dropped onto the BiNP/SPGE using a CHI1240B electrochemical analyzer.

Moreover, we developed a proposed method for on-site analysis using BiNP/SPGE on a DRP Dropstat as a portable electrochemical reader. In the sample preparation step, each sample was cut into a small piece. Both phases of the sample (5 mL using a measuring spoon) were placed into a Ziplock bag. Then, 5 mL of 2% v/v HNO_3 was added and mixed for 5 min. Then, the pH was adjusted to pH 7 using NaOH solution. Next, 500 µL of sample solution was diluted 2-fold to a 1 mL mixture of 0.1 M oxalic acid and 0.1 mM CTAB. Finally, 100 µL of the sample was dropped on the BiNP/SPGE using the portable potentiostat.

3.2.3 Results and discussion

3.2.3.1 Characterization of the modified electrode

An electrochemical response obtained from the screen-printed carbon electrode (SPCE) (b) and screen-printed graphene electrode (SPGE) (a) was studied and compared using a cyclic voltammetry technique, as shown in Figure 3.11A. Cyclic voltammograms were recorded between a potential range of -0.05 V to 0.05 V vs. Ag/AgCl in 0.1 M KNO_3. The double layer capacitance value was calculated from the 0.1 M KNO_3 material electrode. The double layer capacitances were found to be 1.09 $\pm$ 0.01 μF cm^{-2} and 4.63 $\pm$ 0.01 μF cm^{-2} for SPGE and SPCE, respectively. The low double layer capacitance value of SPGE indicates that the SPGE on a PAD shows good electrochemical properties with a low background current. To confirm the performance of SPGE, the CVs of 1.0 mM $[Fe(CN)_6]^{3-/4-}$ in 0.1 M KNO_3 were recorded from -0.8 V to 0.7 V vs. Ag/AgCl for each electrode on a PAD (Figure 3.11B). Clearly, the anodic and cathodic peak potentials of $[Fe(CN)_6]^{3-/4-}$ were found at 0.3 V and -0.2 V vs Ag/AgCl on both electrodes. In addition, clearly, the peak currents of $[Fe(CN)_6]^{3-/4-}$ with the SPGE (line a) were higher than with the SPCE (line b) due to the low capacitive current and excellent electronic properties of graphene. These results suggest that the use of the SPGE on a PAD provides good performance for the field determination of heavy metals.

The surface morphologies of SPCE, SPGE and BiNP/SPGE were displayed in FE-SEM images. The FE-SEM image of SPCE (Figure 3.11C) exhibited a rough surface because of the morphology of carbon, while the SPGE surface (Figure 3.11D) presented a smooth surface of graphene sheets. Meanwhile, for BiNP/SPGE, it was obvious that the BiNPs were extensively deposited over the whole sheet of graphene (Figure 3.11E). To confirm the presence of BiNPs on the surface, an energy dispersive X-ray (EDX) analysis was performed. As shown in Figure 3.11F, the EDX signals at 1.9, 2.5 and 3.2 keV were attributed to the localized energies of the Bi electrons. Moreover, %atomic and %wt of element for SPGE and BiNP/SPGE also indicated the %Bi increase in BiNP/SPGE as shown in Table 3.3, thereby confirming that BiNPs existed on the electrode surface.
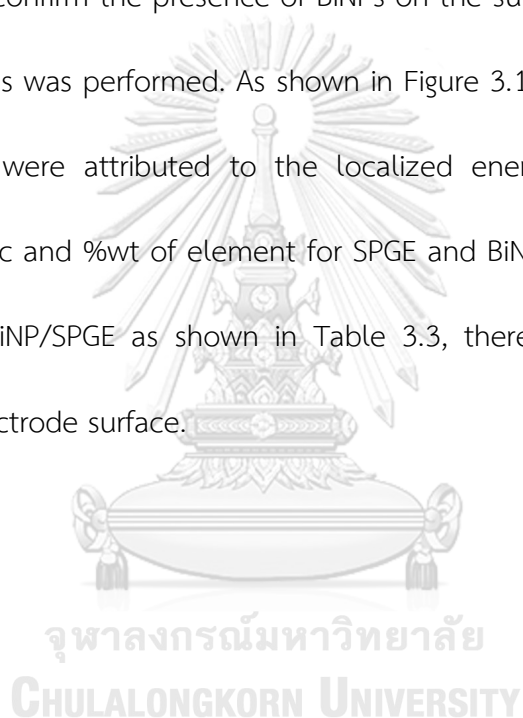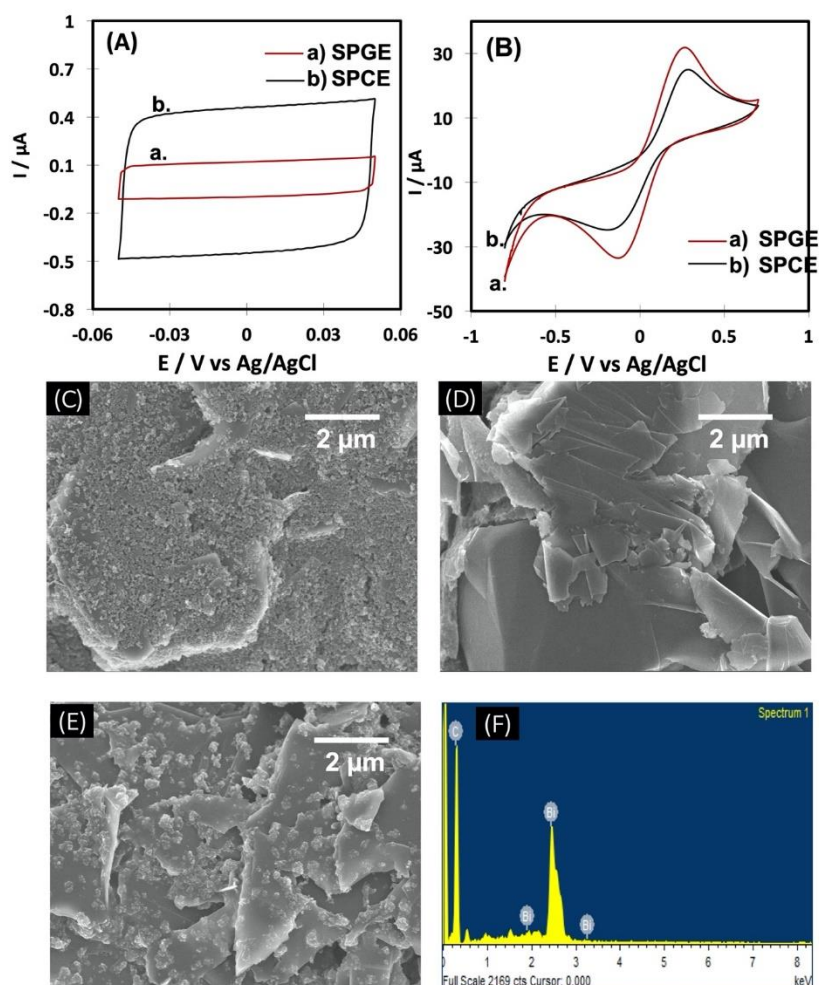
Figure 3.11 CVs in 0.1 M KNO$_3$, recorded at 0.2 V s^{-1} over the potential range of −0.05 to 0.05 V vs Ag/AgCl (A) and 1.0 mM [Fe(CN)$_6$]$^{3-/4-}$ in 0.1 M KNO$_3$ over the potential range of -0.8 V to 0.7 V vs Ag/AgCl with scan rate 0.1 V s^{-1} when compared SPGE (black line:a) with SPCE (red lind:b). FESEM images for SPCE (C), SPGE (D), BiNP/SPGE (E) and EDX spectra of BiNP/SPGE (F) using a magnification of 10,000X and acceleration voltage of 5.0 kV.

Table 3.3 Elemental data of SPGE and BiNP/SPGE from an energy dispersive X-ray (EDX) analysis

Electrode	Element	Line Type	Wt%	Atomic %
SPGE	C	K series	100	100
	Total:		100	100
BiNP/SPGE	C	K series	62.1	96.6
	Bi	M series	37.9	3.4
	Total:		100	100

3.2.3.2 Electrochemical characterization of various electrodes for Sn(II) and Pb(II) determination

The electrochemical behavior of Sn(II) and Pb(II) was examined using a SWASV technique, as shown in Figure 3.12. First, a bare SPGE on a PAD was employed for the simultaneous determination of Sn(II) and Pb(II). The black line (a) shows the SWASVs of the supporting electrolyte (0.1 M oxalic acid), which did not show a significant electrochemical signal. The gray line (b) exhibits a small broad peak current of 100 ng mL^{-1} Sn(II) and Pb(II) on the bare SPCE at -0.8 V vs Ag/AgCl. To compare with the bare SPCE, at the same potential, the oxidation peak current of 100 ng mL^{-1} Sn(II) and Pb(II) on the bare SPGE was higher than on the bare SPCE at the blue line (c). However, the peaks of Sn(II) and Pb(II) overlapped. Hence, the modified electrode was required for a sensitive simultaneous analysis of Sn(II) and Pb(II). As mentioned above, bismuth is widely used as a working electrode to measure Sn(II) and Pb(II) through the formation of intermetallic compounds during the deposition process. Therefore, a bismuth nanoparticle-modified screen-printed graphene electrode (BiNP/SPGE) was chosen for the detection of Sn(II) and Pb(II) in this work. The SWASVs

of Sn(II) and Pb(II) on the BiNP/SPGE (red line (d)) illustrate a higher sensitivity and sharper peak current than when using the bare SPGE. An increase in anodic stripping current was observed with the BiNP/SPGE due to the formation of intermetallic species between the bismuth and metal analytes, which were easily oxidized. Moreover, BiNPs can provide a high electroactive surface, mass transfer effect and rate of electron transfer [98]. Nevertheless, the peaks of Sn(II) and Pb(II) still overlapped, which cannot be separated using only the BiNP/SPGE system. To overcome this problem, CTAB was chosen to be used with the BiNP/SPGE for peak separation. Interestingly, two well-defined peaks of Sn(II) and Pb(II) were observed in the presence of CTAB. Using CTAB, the redox potential of Sn(II) was shifted in the negative direction from -0.8 V to -0.87 V vs Ag/AgCl. Pb(II) was shifted in the positive direction from -0.8 V to -0.75 V vs Ag/AgCl. In addition, the stripping peak of Sn(II) and Pb(II) was significantly enhanced by BiNP/SPGE containing 0.1 mM CTAB (green line:e). CTAB at low concentrations can form a bilayer and act as a positive charge at the electrode surface during the electrodeposition step [99]. Moreover, Sn(II) and Pb(II) can form complexes with oxalate ions such as $[Sn(C_2O_4)_2]^{2-}$ [100] and $[Pb(C_2O_4)_2]^{2-}$ [101], respectively. Consequently, the negative electroactive complexes could be immobilized on the CTAB bilayer at the electrode surface due to electrostatic interaction, which resulted in a sensitivity enhancement [102]. In addition, the Sn(II) and Pb(II) complexes could be reduced to Sn(0) and Pb(0) complexes, respectively, during the electrodeposition step. In the stripping step, the form of CTAB with the Sn(0)-

and Pb(0)-oxalate complexes could alter the oxidation potential of Sn(0)/Sn(II) and Pb(0)/Pb(II). Therefore, the Sn(II) and Pb(II) peak current signals exhibited a high resolution when using CTAB in the system. Furthermore, when comparing the stripping peak current between the proposed BiNP/SPGE (Figure 3.13: red line:a) with a conventional Bi film electrode on a screen-printed graphene electrode (BiF/SPGE) (Figure 3.13: black line:b) in the presence of CTAB, the developed BiNP/SPGE showed increased electrochemical signals of approximately 2.68 times for Sn(II) and 1.76 times for Pb(II). The improved anodic stripping peaks was attributed to the higher surface area of 3D BiNPs compared to the 2D Bi film (in situ) on an SPGE surface. Therefore, the BiNP/SPGE containing CTAB was employed for the simultaneous determination of Sn(II) and Pb(II) in this study.
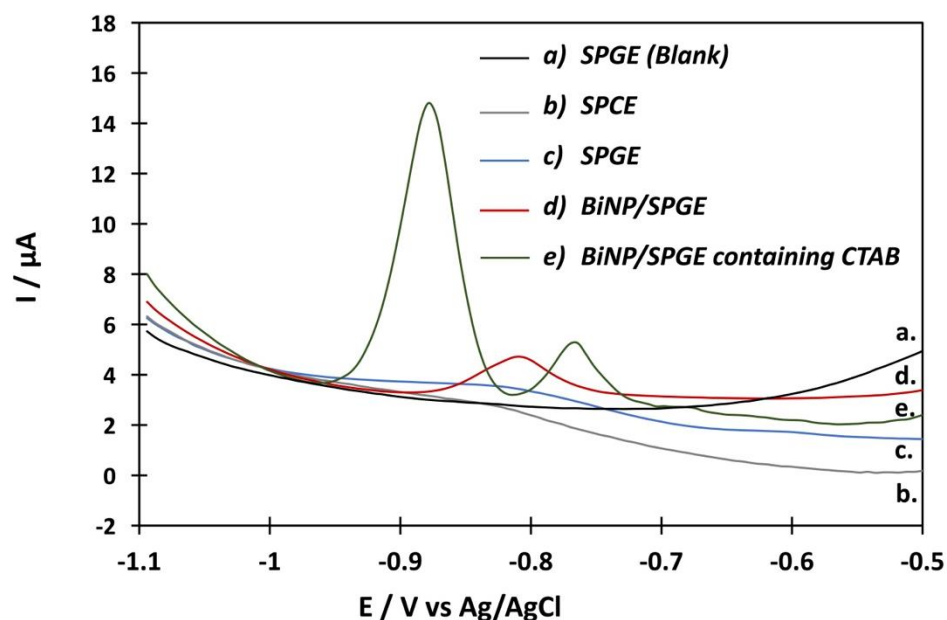
Figure 3.12 SWASVs of blank solution (0.1 M oxalic acid) on SPGE (black line:a) and 100 ng mL^{-1} Sn(II) and Pb(II) containing 0.1 M oxalic acid on bare SPCE

(gray line:b), bare SPGE (blue line:c), BiNP/SPGE (red line:d), BiNP/SPGE with 0.2 mM CTAB (green line:e).
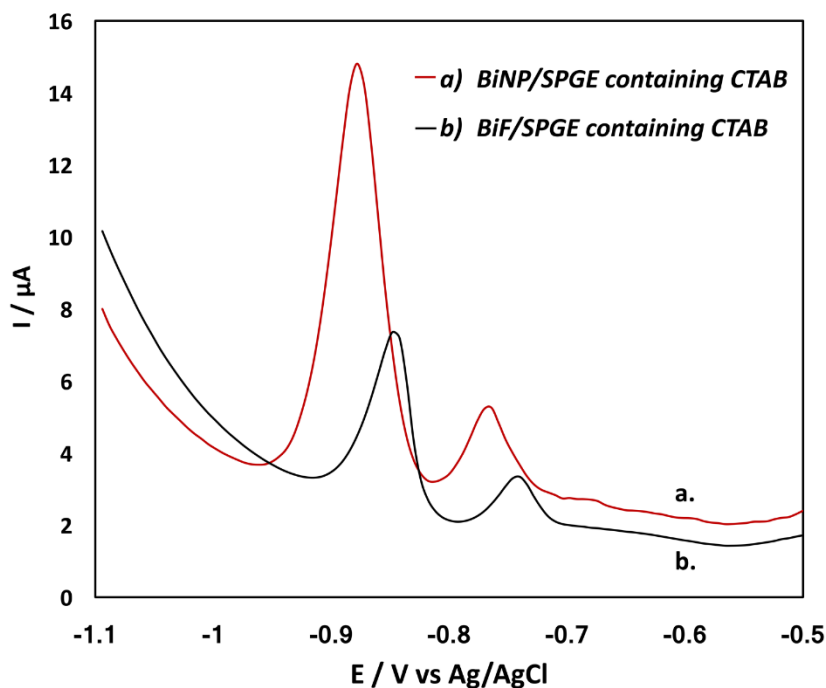
Figure 3.13 SWASVs of 100 ng mL^{-1} Sn(II) and Pb(II) containing 0.1 M oxalic acid and 0.1 mM CTAB on BiNP/SPGE (red line:a), BiF/SPGE (black line:b) (in situ operation: 500 µg mL^{-1} Bi(III)). Conditions: -1.1 V vs Ag/AgCl of deposition potential and 60 s of deposition time.

3.2.3.3 Optimization of operating conditions

The operating conditions and parameters, such as the percentage of BiNPs (% w/w) in graphene ink, deposition potential and deposition time, were subsequently investigated. The best results for Sn(II) and Pb(II) detection were obtained with the

following parameters: 0.25% w/w of BiNPs (Figure 3.14), -1.1 V (Figure 3.15A) and 80 s (Figure 3.15B). Moreover, effect of types and concentrations of surfactants and supporting electrolytes was also studied because the addition of a surfactant plays a key role in enhancing the signal and improving the peak resolution. The highest resolution and peak current of both metals was obtained using 0.1 M oxalic acid (Figure 3.2.7A-B) and 0.2 mM CTAB (Figure 3.16C-D) as supporting electrolyte.

3.2.3.3.1 Effect of percentage of BiNPs (% w/w)

Different amounts of BiNPs were mixed with graphene conductive ink and utilized as working electrode for a further study toward Sn(II) and Pb(II) detection. As shown in Figure 3.2.14, it was observed that the highest peak current for both Sn(II) and Pb(II) was found to be at 0.25% w/w. The stripping currents of Sn(II) and Pb(II) increased with increasing amount of BiNPs from 0.10 %w/w to 0.25 %w/w. Because of the forming of BiNPs with Sn(II) and Pb(II) as intermetallic complex, the enhancement of the electrochemical signal was observed. However, at higher %w/w of BiNPs than 0.25, there was a significant decrease in the peak current of both metals. These results might be caused by the overwhelming of BiNPs that may hinder mass transfer on interface of working electrode. Therefore, 0.25% w/w of BiNPs was chosen to apply in graphene ink as a working electrode.
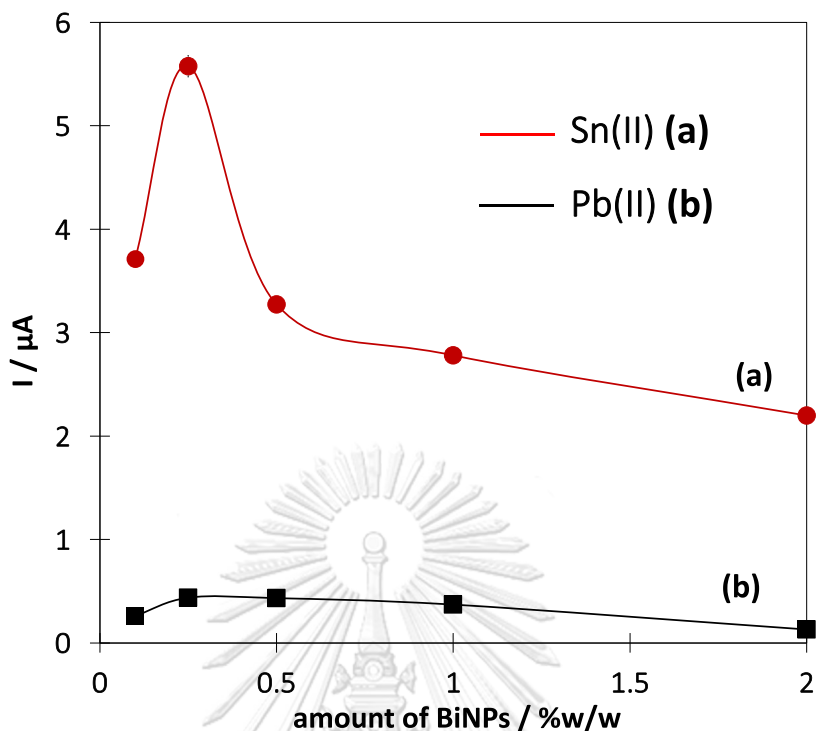
Figure 3.14 Effect of the amount of BiNPs in graphene conducting ink

3.2.3.3.2 Effect of deposition potential and deposition time

The electrodeposition potential was studied in the range of -1.3 V to -0.9 V vs Ag/AgCl (Figure 3.15A). There was a rapid increase in both anodic stripping current signals using electrodeposition potential between -0.9 V to -1.1 V vs Ag/AgCl. However, the peak currents dropped significantly from -1.1 V to -1.3 V vs Ag/AgCl due to hydrogen bubble formation. Thus, the electrodeposition potential of -1.1 V vs Ag/AgCl was chosen because it exhibits the highest stripping peak current and further used as an optimal condition. The deposition time was also optimized in the range of 20 s to 120 s (Figure 3.15B). The stripping peak current increased with increasing

deposition time. However, beyond 80 s, the current is rather constant because of the limited of active surface area and longer analysis time is undesired. Therefore, the deposition time of 80 s was selected in this work.
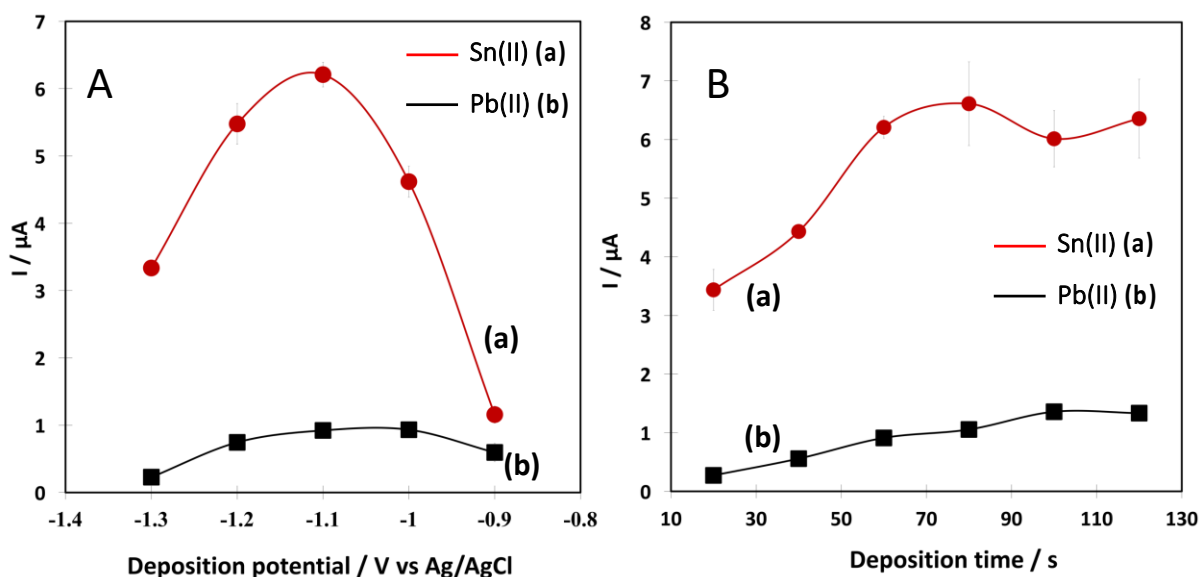
Figure 3.15 The effect of the electrodeposition potential (A) and the electrodeposition time (B) on BiNP/SPGE for 100 ng mL^{-1} Sn(II) and Pb(II) simultaneous detection.

3.2.3.3.3 Effect of the types and concentration of supporting electrolytes

The types of supporting electrolytes strongly influence the formation of metal complex, therefore, the effect of types and concentration of supporting electrolytes on stripping peak currents were evaluated. Figure 3.16A. displays SWASVs for Sn(II) and Pb(II) detection using different types of supporting electrolyte including

HNO_3, acetate buffer, HCl, H_2SO_4, and oxalic acid on BiNP/SPGE. No electrochemical signals were observed for HNO_3 electrolyte (black line:a). whereas an overlapping peak of Sn(II) and Pb(II) was observed using acetate buffer (gray line:b)., HCl (green line:c) and H_2SO_4 (blue line:d) electrolyte. Nevertheless, the well-defined peaks of Sn(II) and Pb(II) was obtained using oxalic acid as supporting electrolyte (red line:e).

The concentration of oxalic acid was evaluated in the range of 0.025 M to 0.15 M (Figure 3.16B). It was found that the stripping peak current of Sn(II) and Pb(II) greatly increased from 0.025 M to 0.1 M because of stable complexation mechanism of metals-oxalate and electrostatic attraction with bilayer of CTAB on electrode surface. The maximum current was observed at 0.1 M of oxalic acid. Conversely, at concentration higher than 0.1 M the current signal declined significantly due to the hydrogen evolution. Thus, the supporting electrolyte of 0.1 M oxalic acid was chosen as supporting electrolyte for the detection of Sn(II) and Pb(II).

3.2.3.3.4 Effect of types and concentrations of surfactants and supporting electrolytes

In the present work, the addition of a surfactant plays a key role in enhancing the signal and improving the peak resolution. Therefore, the selection of optimal conditions for surfactants (types and concentrations of surfactants) could provide better performance for Sn(II) and Pb(II) detection. Hence, various types of surfactant,

including Tween® 20, SDS and CTAB, were analyzed in this study (Figure 3.16C). As presented in Figure 3.16C, no peak was observed using a neutral charge surfactant, namely, Tween®20 (black line:a). Meanwhile, a small peak of Sn(II) and Pb(II) was observed using a negative charge surfactant, namely, SDS (blue line:b), which provided a single overlapping peak of Pb(II) and Sn(II). Interestingly, the use of CTAB, which is a positive charge surfactant (red line:c) showed the sharpest and highest peak currents with well-resolved peaks of Sn(II) and Pb(II). As mentioned earlier, the Sn(II)-oxalate and Pb(II)-oxalate potential at the CTAB bilayer on the electrode surface (positive charge) can be separated. Furthermore, various concentrations of CTAB were tested to obtain the highest sensitivity for the simultaneous determination of Sn(II) and Pb(II) (Figure 3.16D). The stripping currents of Sn(II) and Pb(II) gradually increased up to 0.2 mM CTAB. Above 0.2 mM, the stripping currents dropped since the thick layer of CTAB may obstruct the mass transfer of both metals onto the electrode surface. The highest stripping current peak was presented at 0.2 mM of CTAB, which was chosen as the optimal concentration in this work. Thus, the supporting electrolyte of 0.2 mM CTAB coupling with 0.1 M oxalic acid was chosen as supporting electrolyte for the simultaneous detection of Sn(II) and Pb(II) with high resolution and sensitivity.
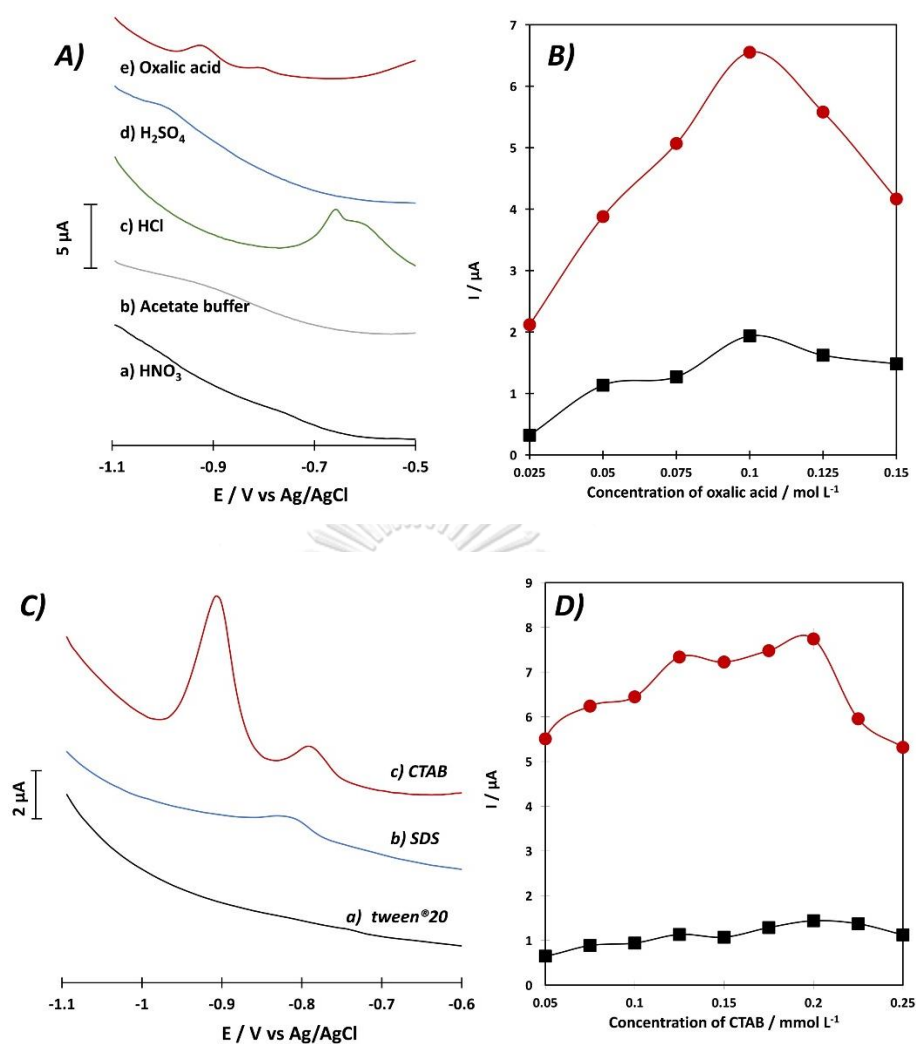
Figure 3.16 SWASVs for 100 ng mL^{-1} Sn(II) and Pb(II) containing 0.2 mM CTAB in 0.1 M of supporting electrolyte solution on BiNP/SPGE; HNO$_3$(black line:a); acetate buffer pH 4.5 (gray line:b); HCl (green line:c); H$_2$SO$_4$ (blue line:d); oxalic acid (red line:e) as electrolyte solution (A). The effect of the concentration of oxalic acid as supporting electrolyte (B). SWASVs of 100 ng mL^{-1} Sn(II) and Pb(II) in 0.1 M oxalic acid on BiNP/SPGE containing 0.2 mM tween®20 (black line:a), SDS (blue line:b), and CTAB (red line:c) (C).The effect of the concentration of CTAB (D);Conditions: -1.1 V vs Ag/AgCl of deposition potential and 60 s of deposition time.

3.2.3.4 Analytical performance

A mixture of Sn(II) and Pb(II) was simultaneously determined using the BiNP/SPGE under optimal conditions. The effects of the Pb(II) and Sn(II) concentrations (50, 100 and 250 ng mL^{-1}) on the electrochemical signals of Sn(II) and Pb(II) were tested in this work, as shown in Figure 3.17. Figure 3.17A, C, and E have shown SWASVs of various concentrations of Sn(II) at fixed Pb(II) concentration (50, 100 and 250 ng mL^{-1}). It can be clearly seen that the linearity of Sn(II) was found in the range of 10 to 250 ng mL^{-1} (Figure 3.17B, D and F) while the stripping current of Pb(II) was constant. Moreover, at the fixed Sn(II) concentration (50, 100 and 250 ng mL^{-1}), the calibration plot of Pb(II) was linear over the range of 10 – 250 ng mL^{-1} (R^2 = 0.987) (Figure 3.17G, I, and K). The sensitivity and R^2 value of each calibration data presents in Table 1. The sensitivity of Sn(II) detections from calibration plots were not significantly difference at 50, 100 and 250 ng mL^{-1} of Pb(II) (0.0787-0.0781 μA mL ng^{-1}), indicating that the concentration of Pb(II) did not affect to Sn(II) detection. Moreover, there were no significant difference between the sensitivity of Pb(II) at 50, 100 and 250 ng mL^{-1} of Sn(II) (0.0302-00.0319 μA mL ng^{-1}) (Figure 3.17H, J and L). Therefore, the simultaneous detection of Sn(II) and Pb(II) would not cause interference with each other.

A)

B)

y = 0.0783x - 1.3528
R² = 0.98581

C)

D)

y = 0.0787x - 1.6827
R² = 0.99049

E)

F)

y = 0.0781x - 1.0504
R² = 0.99531

G)

H)

y = 0.0319x - 0.4256
R² = 0.99514
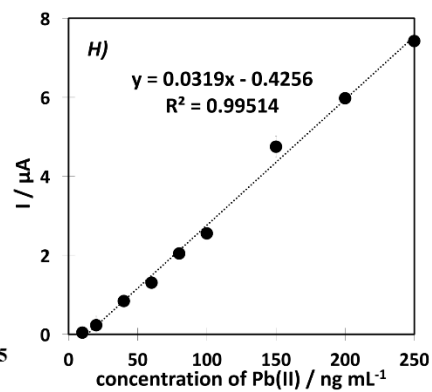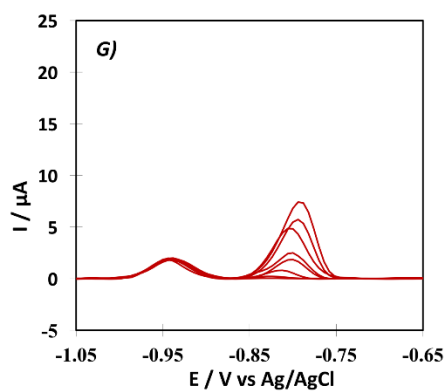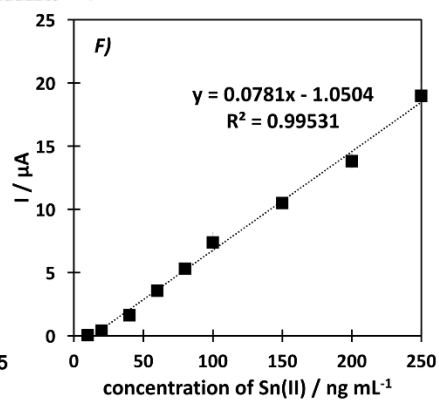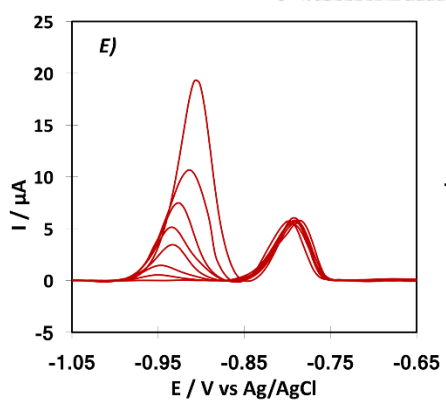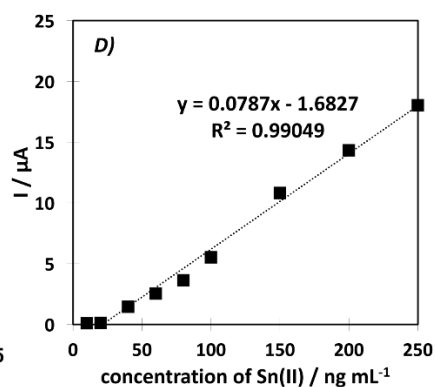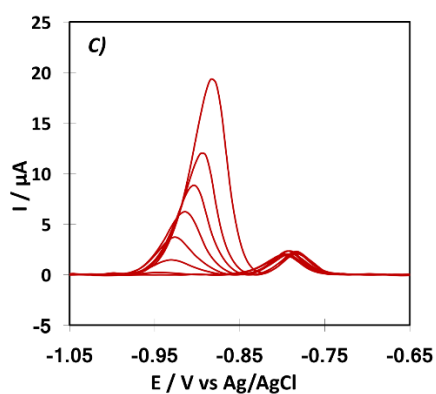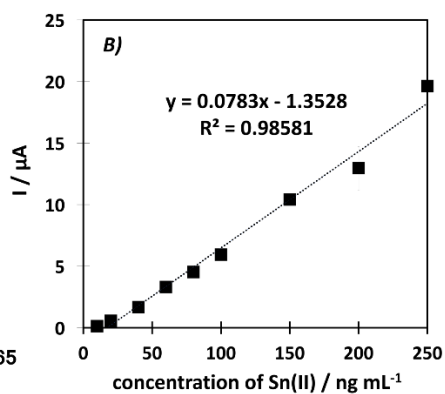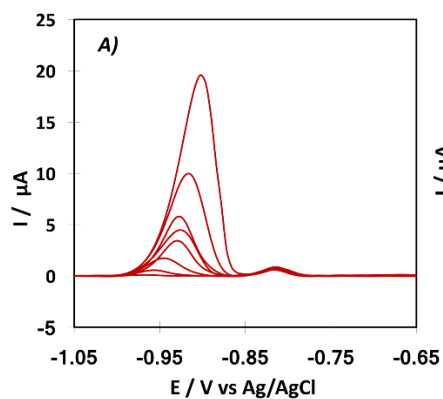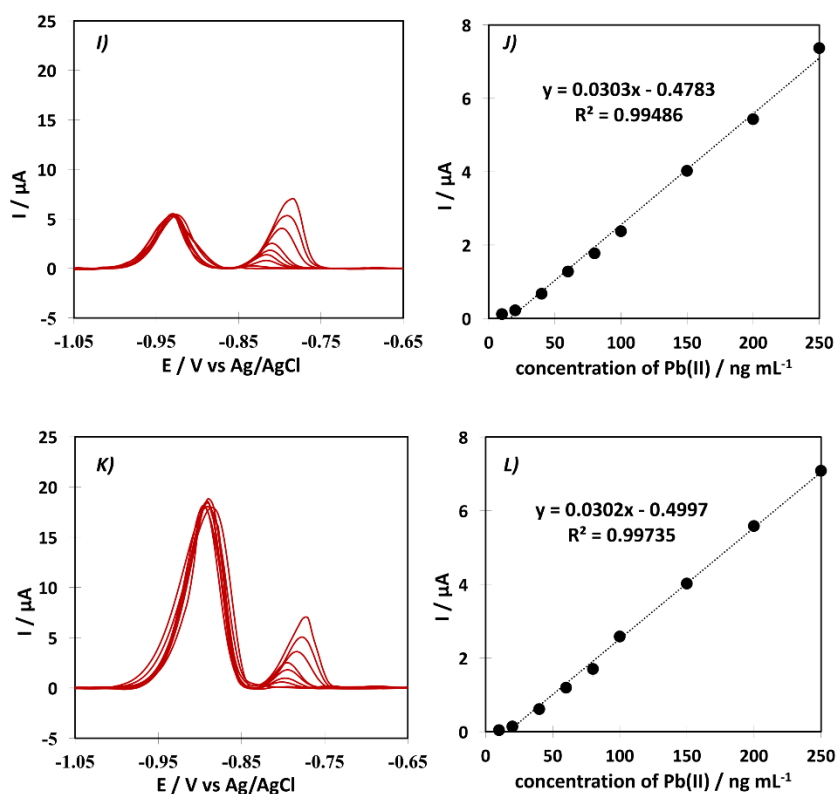
Figure 3.17 Typical SWASVs of various concentrations of Sn(II) at fixed Pb(II) concentration (50 (A-B), 100 (C-D) and 250 (E-F) ng mL^{-1}), various concentrations of Pb(II) at the fixed Sn(II) concentration (50 (G-H), 100 (I-J) and 250 (K-L) ng mL^{-1}). Inset: linear calibration plots for Sn(II) and Pb(II). The error bars were the standard deviations for 3 times of parallel detection and all the tests were under the optimal conditions.

As the results demonstrate, simultaneous detection of Sn(II) and Pb(II) can be obtained because they do not interfere with each other. Thus, the determination of both metals with various concentrations of Sn(II) and Pb(II) was performed simultaneously (Figure 3.18). A linear range was found in a range of 10 to 250 ng mL^{-1}

for both metals (R^2 = 0.9946 for Sn(II) (●) and 0.9907 for Pb(II) (■)) (inset). The limits of detection as calculated (3σ/slope) for Sn(II) and Pb(II) were 0.26 ng mL^{-1} and 0.44 ng mL^{-1}, respectively. The reproducibility in terms of a % relative standard deviation with different BiNP/SPGEs (n=7) for simultaneous measurements of 40, 100 and 250 ng mL^{-1} of Sn(II) and Pb(II) were found to be less than 4.7%. This result clearly shows that the BiNP/SPGE with CTAB is promising for use in the simultaneous determination of metals with good sensitivity and reproducibility. The analytical performance was compared with those of previous literature (Table 3.4). In this work, BiNP/SPGE provided much lower LOD and wider linearity compared to those of other reported electrodes. Moreover, the BiNP/SPGE on a PAD presents the advantages of portability, disposability, ease of use, ease of fabrication and requires only a small sample   volume.
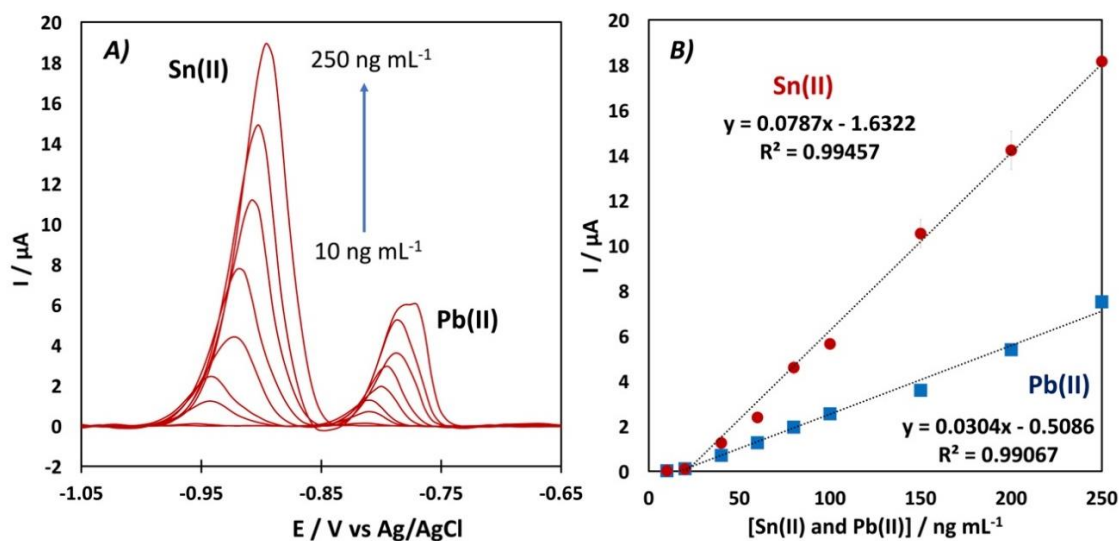
Figure 3.18 SWASVs of Sn(II) and Pb(II) at a BiNP/SPGE on a PAD in in 0.1 M

oxalic acid containing 0.2 mM CTAB at the concentrations of 10–250 ng mL^{-1} (A).

Linear relationship of currents versus Sn(II) and Pb(II) concentration (B).

Table 3.4 Comparison between various electrochemical methods for

detecting Sn(II) and Pb(II)

Working electrode	Modification steps	Sample volume (mL)	LOD (ng mL^{-1})		Ref.
			Sn(II)	Pb(II)	
Glassy carbon electrode	Deposition of Bi film on a glassy carbon electrode	25	0.74	1.13	[103]
HMDE	No steps	30	237.4	414.4	[97]
Boron-doped diamond electrode	-	100	27.4	-	[104]
Carbon paste electrode	Fe(II)-clinoptilolite nanoparticles mixed with carbon paste	10	11.9	-	[105]
Nanoporous bismuth electrode	-	10	Sn(II)	Pb(II)	[106]

| Working electrode | Modification steps | Sample volume (mL) | LOD (ng mL^{-1}) | | Ref. |
			Sn(II)	Pb(II)	
screen-printed Bi-C nanocomposite electrodes	-	20	-	2.3	[107]
BiNP/Nafion modified graphene electrode	-	-	-	0.28	[90]
BiNP/SPGE on paper	-	0.1	0.26	0.44	This work

3.2.3.5 Interference study

An interference study was performed by adding other metals to a standard solution containing 100 ng mL^{-1} of Sn(II) and Pb(II). The tolerance limit was estimated from ±5% of the error. The experimental results showed that 1000-fold mass ratios of Cu(II), Zn(II), Mg(II), Na(I) and K(I); 100-fold mass ratios of Ni(II), Ca(II), Fe(II) and Fe(III); 10-fold mass ratios of Al(III) and 2-fold mass ratios of Cd(II) did not interfere with the determination of Sn(II) and Pb(II). However, a significant amount of cadmium can interfere with the simultaneous detection of Sn(II) and Pb(II), but most canned foods report that the quantity of cadmium is less than both metals in ng kg^{-1} units. Therefore, the developed sensor can be applied for analysis of real samples without any interference from other common metals.

3.2.3.6 Real sample analysis

The BiNP/SPGE was successfully applied for the simultaneous determination of Sn(II) and Pb(II) in canned food samples. First, sample analysis was performed with both the liquid and solid phases of canned food and determined by a CHI1240B electrochemical analyzer. The experimental results are presented in Table 3.5. The % recoveries were determined by spiking known concentrations of Sn(II) and Pb(II) (40, 100 and 250 ng mL^{-1}) into real samples and were found in a range of 83.5 – 108.7% for both metals. To compare the results with the conventional method, a parallel experiment using inductively coupled plasma–optical emission spectroscopy (ICP-OES) was performed. The paired t-test value at 95% confidence was performed and found that there was no significant difference between the two methods, which can confirm the accuracy and reliability of the simultaneous determination of Sn(II) and Pb(II).

In addition, a DRP Dropstat electrochemical reader was used as a portable reader for the on-site analyses. Five samples were also tested to determine the quantity of Sn(II) and Pb(II) with the BiNP/SPGE using the portable potentiostat. The % recoveries that were measured by spiking known concentrations, namely, 50, 100 and 200 ng mL^{-1}, were found to be from 100.6 to 111.2 % for both metals which compared well with ICP-OES, as shown in Table 3.6. A pair t-test of the results between this proposed sensor and ICP-OES indicated that there was no significant statistical diferrence at a 95% confidence level. Therefore, the proposed method can

be used to determine Sn(II) and Pb(II) in real samples with not only high accuracy but

also portability for on-site analysis.

Table 3.5 Recovery tests of the proposed sensor and conventional method

for the simultaneous determination of Sn(II) and Pb(II) in a liquid phase and a solid

phase of canned food samples (n = 3)

Samples	Spiked (ng mL^{-1})		this purposed sensor				ICP-OES			
	Sn(II)	Pb(II)	Found Sn(II) $\bar{x} \pm SD$	%recovery	Found Pb(II) $\bar{x} \pm SD$	%recovery	Found Sn(II) $\bar{x} \pm SD$	%recovery	Found Pb(II) $\bar{x} \pm SD$	%recovery
Solid Phase										
Sample 1	0.00	0.00	ND	-	ND	-	ND	-	ND	-
	40.00	40.00	35.70±1.08	89.2	38.72±0.73	96.8	39.14±3.89	97.8	34.51±3.59	86.3
	100.0	100.0	108.2±1.22	108.2	98.33±3.87	98.3	107.9±1.67	107.9	99.38±4.04	99.4
	250.0	250.0	242.7±3.04	97.1	238.8±8.41	95.5	229.7±6.45	91.9	236.3±2.04	94.5
Sample 2	0.00	0.00	ND	-	ND	-	ND	-	ND	-
	40.00	40.00	36.81±2.83	92.0	39.14±3.21	97.8	40.73±1.85	101.8	38.58±1.17	96.4
	100.0	100.0	99.28±2.47	99.3	106.81±6.13	106.8	99.13±3.35	99.1	87.00±0.71	87.0
	250.0	250.0	246.4±9.87	98.5	234.4±1.33	93.8	220.5±6.39	88.2	235.1±4.42	94.0
Sample 3	0.00	0.00	ND	-	ND	-	ND	-	ND	-
	40.00	40.00	37.01±2.73	92.5	35.97±0.99	89.9	39.35±2.44	98.4	40.77±4.96	101.9
	100.0	100.0	102.5±4.56	102.5	108.0±3.92	108.0	107.8±4.03	107.8	101.7±4.16	101.6
	250.0	250.0	241.6±7.08	96.6	240.4±11.88	96.2	231.3±6.39	92.5	240.3±3.87	96.1
Sample 4	0.00	0.00	ND	-	ND	-	ND	-	ND	-
	40.00	40.00	37.76±2.65	94.4	37.21±1.03	93.0	40.66±4.63	101.6	36.32±3.52	90.8
	100.0	100.0	105.4±0.62	105.4	106.4±4.89	106.4	105.6±2.14	105.6	102.9±3.06	102.9
	250.0	250.0	240.0±7.55	96.0	240.2±3.07	96.1	238.6±5.92	95.4	242.5±6.07	97.0
Sample 5	0.00	0.00	ND	-	ND	-	ND	-	ND	-
	40.00	40.00	36.96±2.85	92.4	33.39±3.13	83.5	35.68±1.96	89.2	37.22±3.37	93.0
	100.0	100.0	107.8±5.05	107.8	91.93±3.73	91.9	101.6±4.40	101.6	103.3±0.88	103.3
	250.0	250.0	242.8±3.35	97.1	252.3±2.79	100.9	232.0±9.09	92.8	246.6±1.96	98.6
Liquid Phase										
Sample 1	0.00	0.00	ND	-	ND	-	ND	-	ND	-
	40.00	40.00	33.78±2.51	84.4	42.39±0.73	106.0	37.84±5.07	94.6	37.48±1.32	93.7
	100.0	100.0	93.00±0.53	93.0	98.68±7.57	98.7	96.24±0.40	96.2	94.32±1.13	94.3
	250.0	250.0	244.3±8.10	97.7	245.4±3.43	98.2	240.8±0.90	94.1	235.8±1.78	94.3
Sample 2	0.00	0.00	ND	-	ND	-	ND	-	ND	-
	40.00	40.00	38.76±1.42	96.9	36.34±1.40	90.8	37.24±3.7	93.1	43.5±1.17	108.8
	100.0	100.0	99.29±4.96	99.3	94.12±1.00	94.1	96.64±8.12	96.6	103.5±1.80	103.5
	250.0	250.0	229.3±3.04	91.7	247.7±0.49	99.1	241.6±6.51	96.6	258.8±1.54	103.5
Sample 3	0.00	0.00	ND	-	ND	-	ND	-	ND	-
	40.00	40.00	37.46±3.06	93.7	39.69±1.34	99.2	39.69±1.17	99.2	40.9±3.26	102.2
	100.0	100.0	108.7±2.45	108.7	102.6±1.03	102.6	97.56±0.72	97.6	92.52±3.33	92.5
	250.0	250.0	246.9±5.59	98.8	244.8±3.21	97.9	243.9±0.46	97.6	231.3±3.57	92.5
Sample 4	0.00	0.00	ND	-	ND	-	ND	-	ND	-
	40.00	40.00	34.45±2.54	86.1	36.90±0.71	92.2	38.98±0.50	97.4	41.1±2.02	102.8
	100.0	100.0	94.57±3.48	94.6	90.06±2.81	90.1	96.72±2.00	96.7	94.72±1.87	94.7
	250.0	250.0	227.5±7.92	91.0	238.1±3.32	95.2	241.8±2.68	96.7	236.8±2.79	94.7
Sample 5	0.00	0.00	ND	-	ND	-	ND	-	ND	-
	40.00	40.00	38.99±1.42	97.5	37.17±1.86	92.9	38.55±0.12	96.4	43.66±1.18	109.2
	100.0	100.0	99.38±4.95	99.4	96.38±4.98	96.4	95.20±2.01	95.2	101.3±0.68	101.3
	250.0	250.0	229.1±3.03	91.6	249.4±0.61	99.8	238.0±2.28	95.2	253.2±4.47	101.3

*ND = not detectable

1   **Table 3.6** Recovery tests of the proposed sensor combined with a portable

2   potentiostat and conventional mwthod for the simultaneous determination of Sn(II)

3   and Pb(II) in canned food samples (n = 3)

Samples	Spiked (ng mL^{-1})	a portable potentiostat				ICP-OES			
		Sn(II)		Pb(II)		Sn(II)		Pb(II)	
		Found (ng mL^{-1})	%recovery	Found (ng mL^{-1})	%recovery	Found (ng mL^{-1})	%recovery	Found (ng mL^{-1})	%recovery
Sample 1	0.00	ND	-	ND	-	ND	-	ND	-
	50.00	52.14±2.15	104.3	55.62±2.01	111.2	48.23±0.15	96.5	47.19±0.28	94.4
	100.0	102.1±2.14	102.1	109.4±1.14	109.4	100.9±2.34	100.9	98.59±2.98	98.6
	200.0	202.1±3.14	101.0	203.3±2.57	101.6	210.2±2.28	105.1	205.1±2.56	102.6
Sample 2	0.00	ND		ND		ND	-	ND	-
	50.00	52.14±1.24	104.3	51.09±2.01	102.2	49.38±1.23	98.8	48.76±1.12	97.5
	100.0	107.2±2.91	107.2	102.4±1.97	102.4	102.8±0.98	102.8	105.2±0.13	105.2
	200.0	201.2±2.14	100.6	205.9±3.21	103.0	205.6±2.13	102.8	208.9±2.14	104.4
Sample 3	0.00	ND	-	ND	-	ND	-	ND	-
	50.00	54.27±2.88	108.5	52.14±2.14	104.3	51.71±0.34	103.4	49.01±0.23	98.0
	100.0	108.9±3.01	108.9	104.9±2.98	104.9	102.0±1.92	102.0	103.9±1.17	103.9
	200.0	203.5±4.14	101.8	203.2±3.38	101.6	208.1±2.49	104.0	208.4±2.11	104.2

4   *ND = not detectable*

5   **3.2.4 Conclusion**

6   In this work, we report a new portable electrochemical sensor for the

7   simultaneous determination of Sn(II) and Pb(II) using a BiNP/SPGE on a PAD. The

8   effect of CTAB was evaluated for the simultaneous determination of Sn(II) and Pb(II).

9   The results demonstrated that CTAB can enhance not only the resolution between

10   Sn(II) and Pb(II) but also the sensitivity for detecting both metals. The reusability of

11   this electrode was limited to a 1 time use due to the currently used paper sensor.

12   However, the reproducibility testing of sensor-to-sensor (n = 7) provided less than

13   5% deviation for Sn(II) and Pb(II) detection. Moreover, this sensor offers several

1   benefits, namely, it is disposable, simple, inexpensive, portable, and easy to

2   fabricate. This sensor can be an alternative tool for the simultaneous determination

3   of Sn(II) and Pb(II) in canned food because it has excellent analytical characteristics,

4   such as high selectivity, sensitivity, stability and reproducibility. In addition, the total

5   analysis process can be accomplished within 2 min and requires only a 100-μL

6   aliquot of sample.

7

CHAPTER 4

THE DEVELOPMENT OF ePAD FOR ENVIRONMENTAL MONITORING APPLICATION

4.1 Electrochemical detection of NOx gas based on disposable paper-based analytical device using a copper nanoparticles-modified screen-printed graphene electrode

(Biosensors and Bioelectronics)

Kingkan Pungjunun[a], Sudkate Chaiyo[a,b], Narong Praphairaksit[a], Weena Siangproh[c], Astrid Ortner[d], Kurt Kalcher[e], Orawon Chailapakul[a,f **], Eda Mehmeti[e*]

[a] Electrochemistry and Optical Spectroscopy Center of Excellence, Department of Chemistry, Faculty of Science, Chulalongkorn University, 254 Phayathai Road, Pathumwan, Bangkok 10330, Thailand

[b] The Institute of Biotechnology and Genetic Engineering, Chulalongkorn University, Patumwan, Bangkok, 10330, Thailand

[c] Department of Chemistry, Faculty of Science, Srinakharinwirot University, Sukhumvit 23, Wattana, Bangkok 10110, Thailand

[d] Institute of Pharmaceutical Sciences, Karl-Franzens University Graz, Schubertstrasse 1, Graz A-8010, Austria

[e] Institute of Chemistry, Karl-Franzens University, Universitätsplatz 1, Graz A-8010, Austria

[f] Nanotec-CU Center of Excellence on Food and Agriculture, Chulalongkorn University, Bangkok 10330, Thailand

* Corresponding author: Dr. Eda Mehmeti

E-mail addresses: eda.mehmeti@uni-graz.at

** Co-corresponding author: Prof. Dr. Orawon Chailapakul

E-mail addresses: corawon@chula.ac.th Tel.: +66 2 218 7615; Fax: +66 2 218 7615

Abstract

A disposable gas-sensing paper-based device (gPAD) was fabricated in origami design which integrates the gas adsorbent and the electrochemical detection zone in a single device. The gPAD for the determination of NOx gas uses a screen-printed graphene electrode modified with copper nanoparticles (CuNP/SPGE) to achieve high sensitivity and selectivity. The gPAD detects both, NO and NO2 (as NOx) with same current responses. The measurement could be performed directly through differential pulse voltammetry (DPV) with a detection limit as low as 0.23 vppm and 0.03 vppm with exposure times of 25 min and 1 h, respectively. The reproducibility in terms of relative standard deviation was less than 5.1% (n = 7 devices) at 25, 75 and 125 vppm NO2 and the life- time of this device was more than 30 days. The gPAD was applied to detect NOx in air and exhaust gases from cars. In comparison with spectrophotometry, there are no significant differences between both methods using a paired t-test of the results on a 95% confidence level. The designed gPAD can provide a new template model for other gas sensors with features of disposability and portability for fieldwork analysis at low cost.

Keywords: Gas sensing, Differential pulse voltammetry Nitric oxide, Nitrogen dioxide, NOx gas

4.1.1 Introduction

Nowadays, nitrogen oxides (NOx) are the important pollution components causing not only the greenhouse effect and acid rain, but they have also enormous impacts on the health of humans, such as adverse effects on the respiration system and acute symptoms at a high level [108, 109]. NOx represents a sum of nitrogen monoxide (NO) and nitrogen dioxide (NO_2). However, NO in ambient air is of low toxicity, but is easily oxidized to NO_2 which is a potent toxic oxidant. Therefore, most frequently NOx is determined as NO_2 [110]. The maximum NO_2 concentration limit set by the United States Environmental Protection Agency (EPA) and the Occupational Safety and Health Administration (US) is 0.2 vppm (3.76 mg m^{-3}, at 25.0 °C and 1 atm) in ambient air and 5 vppm (3.76 g m^{-3}, at 25.0 °C and 1 atm) in gas-exposed industry [111, 112]. Therefore, analytical methods to monitor and control the NOx gas are strongly important.

Convenient techniques for the determination of NOx comprise gas sensors, such as spectrophotometric [113], chemiluminescence [114], laser-induced fluorescence (LIF) [115] and resistive sensors [116, 117]. These techniques have some limitations including bulky instrumentation and high material costs. Recently, electrochemical sensors have rapidly gained significant attention for the determination of NOx because of advantages such as high selectivity, inexpensiveness and portability [118, 119]. Voltammetric techniques, in particular differential pulse voltammetric (DPV), are

attractive because of high sensitivity and tunable selectivity for NOx [120, 121]. Many reports indicate that electrochemical devices can be miniaturized on paper-based design, so-called electrochemical paper-based analytical devices (ePADs). Such concepts are simple, low in cost, portable and including disposability [122, 123]. Moreover, PAD is one of the most promising substrate material which can be applied in point-of-care diagnostic assays [94], food safety assessment [124] and environmental monitoring [125]. Origami [126] and rotational paper-based devices [127] generate high flexibility and simplicity for even complex analytical protocols.

Carbon electrodes, especially, screen-printed graphene electrodes (SPGEs) have been extensively employed in ePADs due to their easy fabrication, low cost, and inherence for large-scale production [128, 129]. However, a limitation of SPGEs is some low sensitivity due to poor electron transfer. To overcome this drawback, we have developed nanoparticle-modified SPGEs because they can exhibit improved electroactive surface and good catalytic properties [81, 130]. Copper nanoparticle (CuNP)-modified carbon-based electrodes for determination of NOx were reported in some studies because of the catalytic property of Cu towards the electrochemical conversion of NOx or their follow-up products [131, 132].

In this work, we describe a novel sensitive method for quantifying NOx with a disposable gas-sensing paper-based device (gPAD). The latter was designed in a way that the analyte (NO, NO_2) is adsorbed on activated carbon and detected electrochemically with a copper nanoparticle-modified screen-printed graphene

electrode (CuNP/SPGE). The two compartment zones of the gPAD consisted of (i) the NOx adsorber with activated carbon as adsorbent for gas collection because of its high surface area and micro-porous morphology [133, 134]; and of (ii) the detection zone containing the CuNP/SPGE as working electrode. The whole sensor was fabricated with origami technique and presents a new strategy for low-cost, simple, disposable and portable sensor design in combination with excellent analytical performance for the detection of NOx in gaseous samples, such as air and exhaust gases from cars.

4.1.2 Experimental

4.1.2.1 Materials and reagents

Conductive inks of graphene, carbon and silver/silver chloride (Ag/AgCl) were purchased from Gwent group (Torfaen, United Kingdom). Copper(II) acetate anhydrous, copper fine powder, glacial acetic acid, sodium acetate trihydrate, potassium hydroxide, sodium hydroxide, sodium nitrite, iron(II) sulfate heptahydrate, sodium chloride, sodium oxalate, sodium sulfite, sulfuric acid (95-97%), nitric acid, sodium thiosulfate heptahydrate, potassium iodate, sodium iodide and ethyleneglycol were purchased from Merck (Darmstadt, Germany). Sodium phosphate dibasic heptahydrate and sodium phosphate monobasic monohydrate used for the preparation of phosphate buffer solution (PBS, 0.1 M) were purchased from Carl Roth (Karlsruhe, Germany). Activated carbon, sulfanilamide, N-(1-naphthyl)

ethylenediamine dihydrochloride (NED), triethanolamine were purchased from Sigma-Aldrich (Buchs, Switzerland). Nitrogen and nitrous oxide were acquired from Messer (Bierbaum, Austria). All reagents used in this work were of analytical grade and were used without further purification. All the solutions were prepared using ultrapure water with a resistivity of 18 MΩ obtained by a cartridge purification system (Millipore, UK).

NO which was used as primary analyte in this work was prepared following the procedure described elsewhere [135]. Briefly, a mixture of iron(II) sulfate heptahydrate (4.25 g), sodium chloride (4.25 g) and sodium nitrite (2.00 g) was sintered under moderate warming. The evolved gas was washed by deaerated NaOH solution (1.0 M) and collected over ultrapure water degassed with nitrogen. For experiments with NO, the pure gas was diluted with nitrogen, for studies with NO_2 it was diluted with air where oxidation occurred according to eqn.

$$2\ NO + O_{2(air)} \rightarrow 2\ NO_2$$

4.1.2.2 Apparatus

Electrochemical analysis was performed with a potentiostat (PGSTAT 128 N, AutoLab, Metrohm, Switzerland) controlled by corresponding software (Nova 2.0). A three-electrode system was employed, including a copper nanoparticle-modified

eworking lectrode (CuNP/SPGE), a graphene ink counter electrode, and a Ag/AgCl reference electrode, all screen-printed onto the paper support.

Field emission scanning electron spectroscopy (FESEM) was done with an electron microscope at 15 kV (JSM-7001F, JEOL, U.K. Ltd., England). The energy dispersive x-ray spectra (EDS) was recorded on an INCA penta FETx3 model (Oxford Instruments plc, United Kingdom).

The accuracy of the sensor method was studied by comparing the results with those obtained from the Griess-Saltzman method using a UV-Visible spectrophotometer (Cary 50, Varian, United States) for absorbance measurements with a 1.0 cm path length quartz cuvette.

4.1.2.3 Preparation of activated carbon for NOx adsrption

Activated carbon powder (0.5 g) was mixed with a 1 M KOH solution (100 mL) and stirred for 4 hrs. Then the solution was filtered using a paper filter (Whatman No.1) and the residue was dried at 50 °C for 2 hrs [136].

4.1.2.4 Design and fabrication of the gPAD for NOx

The pattern for the paper device was created using Adobe Illustrator (CC2019) followed by printing onto filter paper (Whatman No.1, A4 size) by a wax printer (Color Qube 8570 series, Xerox, Japan). The wax-patterned paper (wax zones are indicated in blue, Figure 4.1) was divided two zones; (i) the adsorption paper zone (each circle

8.0 mm in diameter) and (ii) the detection paper zone (4.0 mm in diameter and for working electrode: 8.0 mm in total) (Figure 4.1). The wax-impregnated paper was placed into an oven at 175 °C (40 s) for accomplishing impregnation by wax penetrating trough the paper and forming a hydrophobic barrier. On the detection zone, graphene ink was printed as working and counter electrode on the substrate. Ag/AgCl ink was then screen-printed for the reference electrode (Figure 4.2). After that, each device was cut as shown in Figure 4.3a (i). The origami folding of the paper is also shown in the figure. A double-faced adhesive tape with a punched hole of 8 mm in diameter was attached on the adsorption zone and then 10 mg of activated carbon impregnated with KOH was filled into the hole (ii). Next, the other side of adsorption paper zone was folded onto the side of activated carbon (iii). After assembly of the adsorption compartment, 10 µL aliquot of a 10 mmol L^{-1} Cu(II)-acetate solution in phosphate buffer (0.1 M, pH 6) was dropped directly onto the working electrode and dried at room temperature (iv). To accomplish the gPAD, the adsorption paper zone was folded onto the detection zone attaching it with an 8 mm punched double-faced adhesive tape (v). The final positions of the layers in the gPAD are displayed in Figure 4.3b.
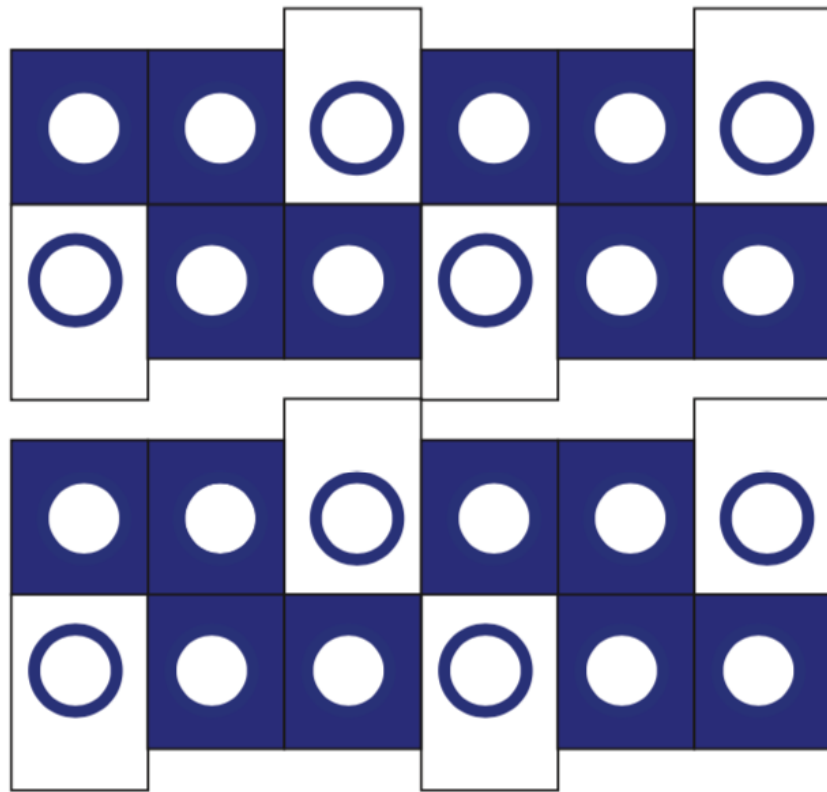
Figure 4.1 Pattern of wax printing
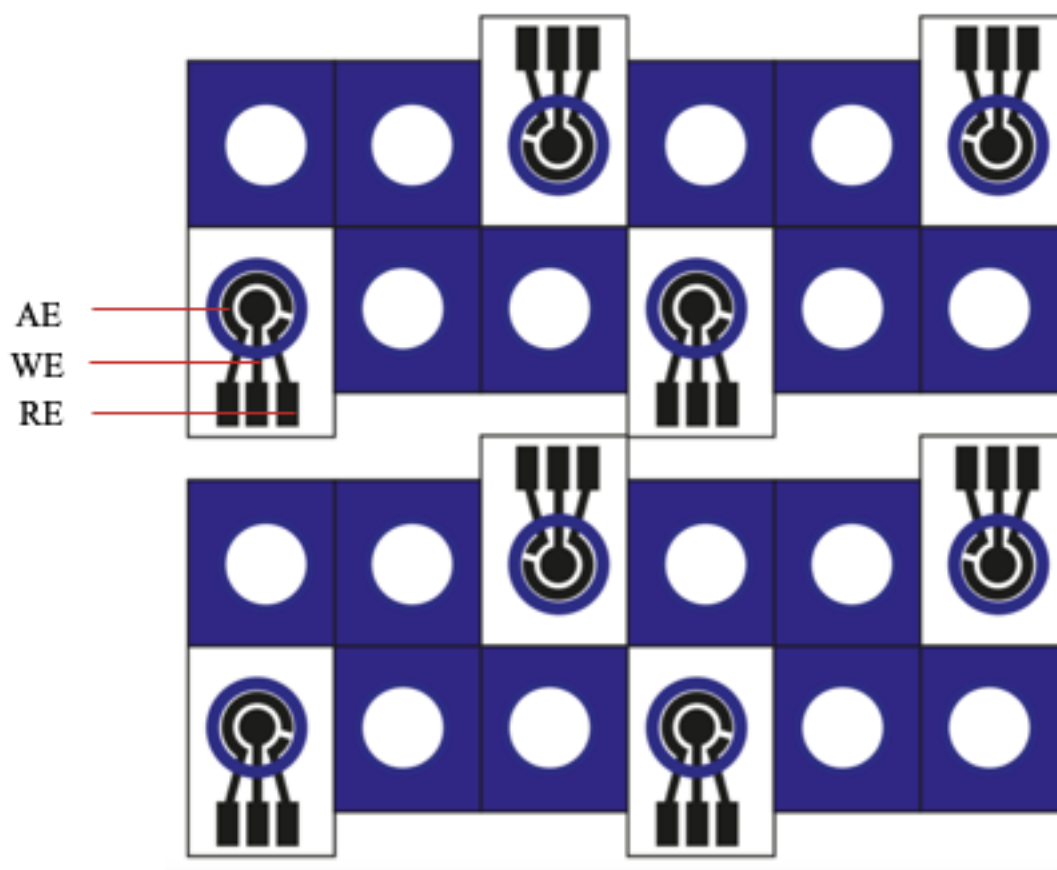
Figure 4.2 Pattern of manufacturing the screen-printed electrode (WE working

electrode, RE reference electrode, AE auxiliary electrode)
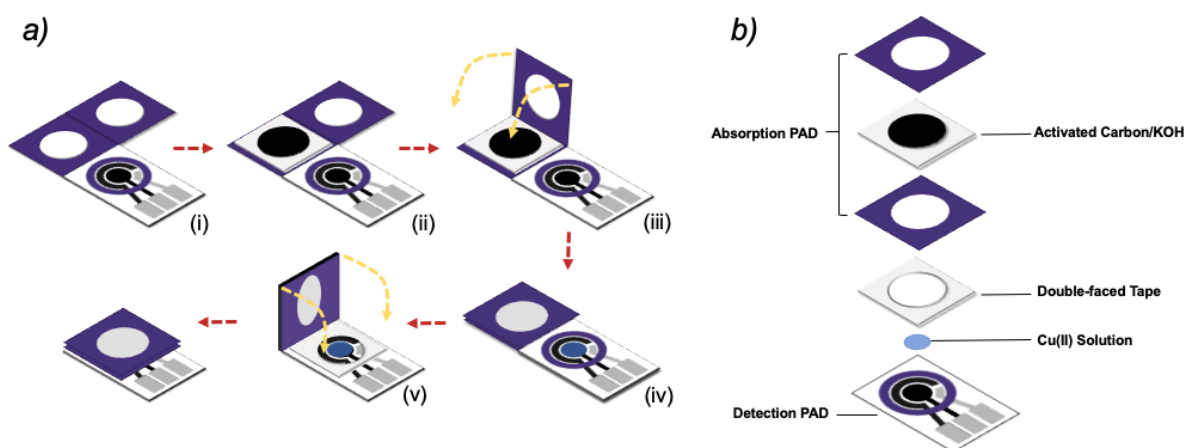
Figure 4.3 Schematic representation of the fabrication and investigation procedure of the gPAD a) and the layers of the final device (b).

4.1.2.5 NOx Adsorption Studies

Investigations were made in a static gas detection system, which was an air-tight box (volume 18 L), equipped with a computer cooling fan for easy gas mixing, a septum (1.5 cm in diameter) for injecting gases, and an inlet and an outlet, normally sealed with a silicon stopper to prevent gas exchange with the ambient air, to facilitate sampling of the total volume inside the box (Figure 4.4). The sensors were placed on the bottom of the receptacle before closing the receptacle. The box was either filled with nitrogen for studies with NO, or with air for investigations with NO_2. Defined volumes of NO or other gases for interference studies were introduces with syringes through the septum.

Studies with ozone were done by generating ozone in a separate box (total volume 18 L) which was equipped with a septum, an in- and outlet, a corona discharge

ozonizer (ATWFS, model Au-003-yg, purchased from www.amazon.de), and a computer cooling fan to generate ozone-containing atmospheres. The ozone concentration was quantified with standard potassium iodide titration. Corresponding volumes of ozone-containing air were sampled and added to the static gas detection system for interference studies.
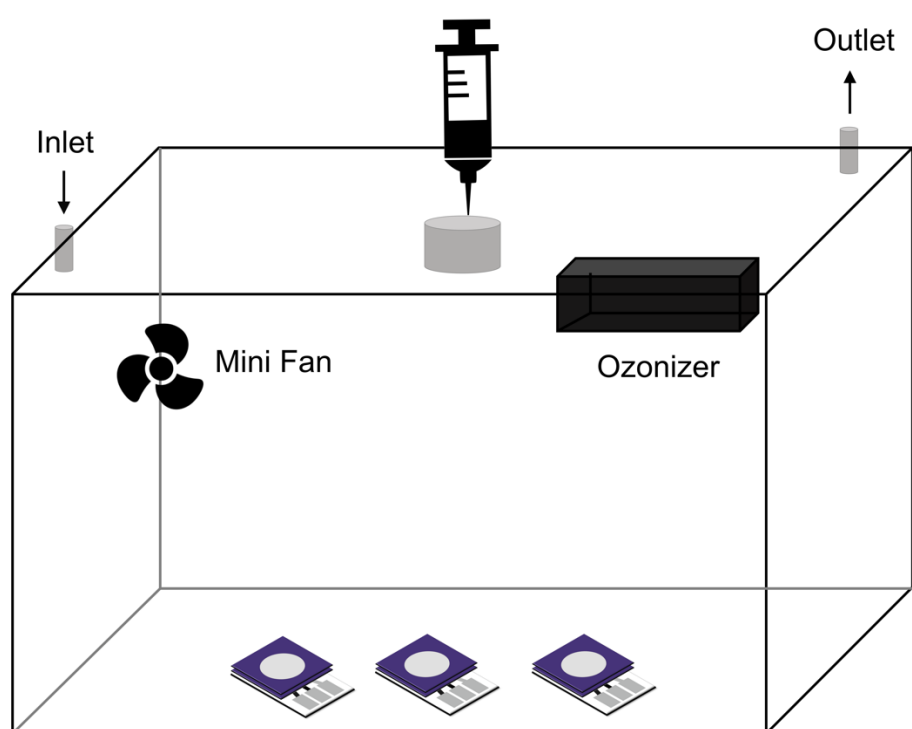
Figure 4.4 Static gas detecting system

4.1.2.6 Electrode modification and electrochemical measurements

The gPAD was placed in the static gas detecting system, as shown in Figure 4.4. Then, an NO gas standard was injected. In this step, NO_x gas was absorbed on the activated carbon in adsorption paper zone for 25 min. After removal of the

sensors from the chamber, 100 µL of phosphate buffer (0.1 M, pH 6) was dropped onto adsorption paper zone which consequently passed through the activated carbon, eluted the adsorbed NO_2 (due to handling in air, adsorbed NO was converted to NO_2 and covered the three electrodes. The ensuing electrochemical procedure consisted of two steps: electrode modification and oxidation of follow-up products of NO_2. For the former, a potential of -1.2 V vs Ag/AgCl was applied for 60 s during which CuNPs were grown on the SPGE. In this step, so-called copper nanoparticles-modified SPGE. After modification and an equilibration time of 2 s, differential pulse voltammograms were recorded between 0.2 V and 1.3 V vs. Ag/AgCl with a scan rate of 20 mVs^{-1}, a pulse amplitude of 25 mV, a pulse rate 0.5 s and a pulse width of 60 ms. Current signals were evaluated from the maximum peak height.

4.1.2.7 Sample preparation

Indoor and outdoor air was collected at the Karl-Franzens University in Graz. The open chamber was exposed to the air for 5 min and then the gPADs were placed in before closing. Likely, exhaust gases from cars were passed through the chamber for 2 min. The exposure time for the sensors was 25 min.

For comparative measurements with spectrophotometry, gas samples from the chamber were passed through 10 mL of absorbing reagent (11 % v/v triethanolamine, 3.6 % v/v ethylene glycol and 25 % acetone in water) from which 1

mL was added to 4 mL of the Griess-Saltzman reagent (0.1 % m:m NED, 1 % m:m sulfanilamide in 5 % m:m phosphoric acid). The concentration of NO_2 gas in the sample was evaluated using UV-Visible spectrophotometry at 540 nm and calibration curves [113].

4.1.3 Results and discussion

4.1.3.1 Morphological characterization of the adsorption layer and the working electrode

The surface morphologies of activated carbon packed in the adsorption PAD were investigated using scanning electron spectroscopy (SEM) as shown in Figure 4.5a, d-g. The properties of activated carbon treated with KOH were investigated using surface area and pore size analysis. Nitrogen adsorption and desorption isotherms of activated carbon treated with KOH are shown in Figure 4.5b. The BET (Brunauer-Emmett-Teller) surface area and total pore volume were calculated to be 798 m^2 g^{-1} and 0.490 cm3 g^{-1} respectively. The micro-pore size distribution was calculated from the data using the MP-plot. The mean pore diameter was found to be 0.7 nm indicating that activated carbon treated with KOH presents micro-porous structure. The results correspond very well with the findings of Lee et al. [136]. Activated carbon in the gPAD treated with KOH solution has high capacity for NO_2 adsorption due to the high surface area and the micro-porous structure.
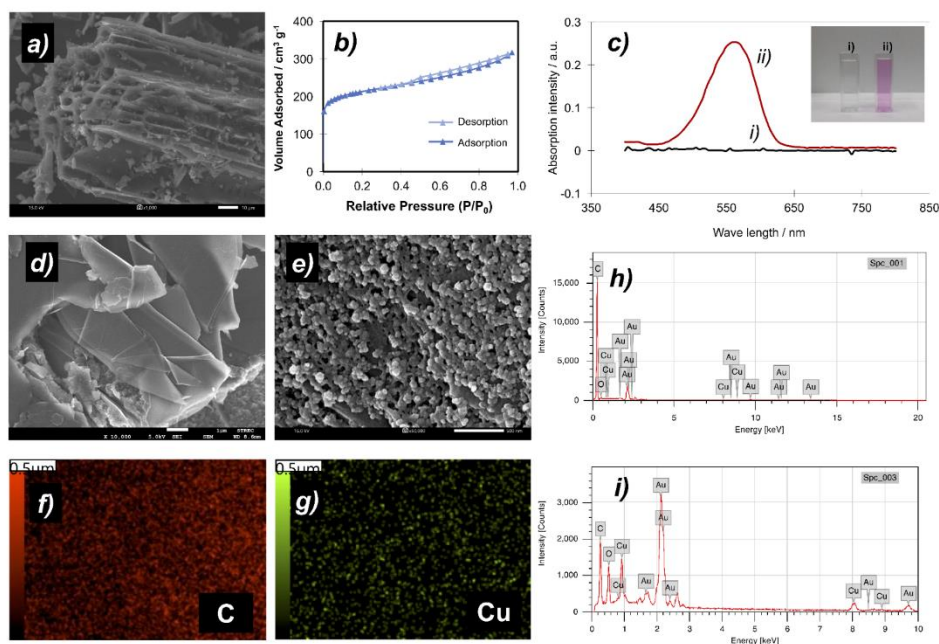
Figure 4.5 Characterization of the adsorption layer (a-c), a bare SPGE (d, h) and a CuNP/SPGE (e, f, g, i): SEM images of activated carbon treated with KOH solution (a), a bare SPGE (d), a CuNP/SPGE (e); element mapping of carbon (f) and copper (g) of a CuNP/SPGE; Griess-Saltzman solution (b) after elution from activated carbon without (i) and with (ii) adsorbed NO2 with corresponding UV-VIS absorption spectra (c); EDS spectra of a bare SPGE (h) and a CuNP/SPGE (i). Micrographs: the length of the white bar corresponds to the following lengths: 10 μm (a), 1 μm (d), 500 nm (e, f, g); the gradient bars of the element maps (f,g) designate practically pure carbon as light red and pure copper as light green.

To confirm adsorption of NO_2 on the surface of the activated carbon, a Griess-Saltzman solution was passed through the adsorption layer of the PAD in the absence and in the presence of adsorbed NO_2 (Figure 4.5c inset). The presence of

NO_2 is proven by the pink color of the solution due to the diazotization reaction. Figure 4.5c displays the corresponding absorption spectra with a typical absorption maximum of the diazo compound at 540 nm. The results underline that the activated carbon impregnated in KOH can adsorb NO_2 gas.

The adsorption mechanism of NOx on KOH-activated carbon was studied by Lee et al. who found that potassium hydroxide is included in the carbon structure along with increased microporosity [136]. Identified reaction products were potassium nitrite and nitrate. Beside NOx the modified carbon material showed good affinity for SO_2.

The surface morphologies of the bare SPGE and the CuNP/SPGE were also investigated by SEM. Successful modification with CuNPs on the SPGE was confirmed as shown in Figure 4.5 (d-i) that presents SEM images of the SPGE (d) and CuNP/SPGE (e) at 10,000X and 50,000X magnification, respectively. Clearly, there are significant differences in surface structure between the SPGE and the CuNP/SPGE. The bare SPGE has a smooth area of graphene sheets whereas the SEM image of a CuNP/SPGE shows that the spherical copper nanoparticles are dispersed on the SPGE surface with an average size of 59 nm in diameter. Moreover, energy dispersive X-ray spectra (EDS) manifested the presence of copper nanoparticles (Figure 4.5h, i) along with element mapping for carbon and copper (Figure 4.5f, g).

4.1.3.2 Electrochemical response of NOx at the gPAD

Cyclic voltammetry was performed to study the electrochemical behavior of NO_2 at a bare SPGE and a CuNP/SPGE as working electrodes on gPADs. Figure 4.6a shows cyclic voltammograms in the absence (i,iii) and presence of 100 vppm NO_2 in 0.1 M PBS pH 6 (ii, iv) recorded from -1.0 V to 1.5 V vs. Ag/AgCl on a bare SPGE(i, ii) and a CuNP/SPGE (iii, iv). No anodic peak was observable with 100 vppm NO_2 at a bare SPGE. However, anodic and cathodic peaks of NO_2 were found at 0.8 V and -0.7 V vs Ag/AgCl with a CuNP/SPGE.
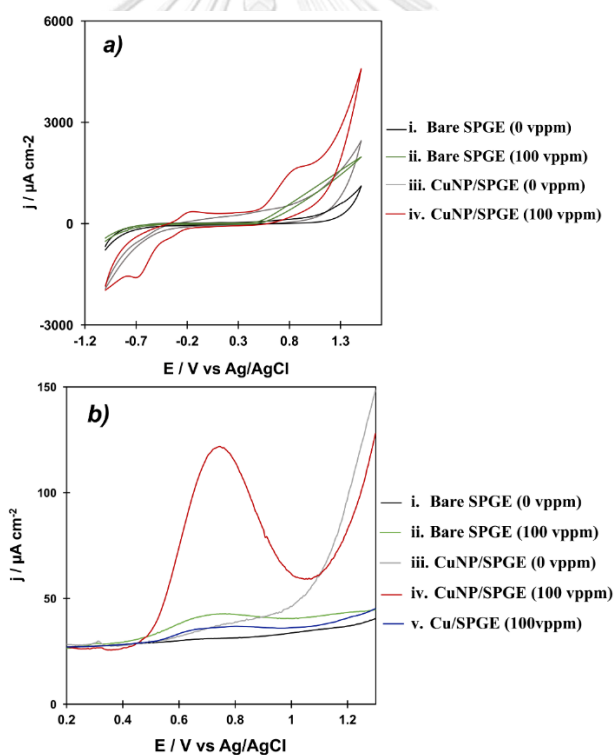
Figure 4.6 Representation CVs (a) and DPVs (b) of different electrodes in the absence (i, ii) and presence (ii, iv, v) of NO_2; bare SPGE (i, ii), CuNP/SPGE (iii, iv) and Cu/SPGE (v). NO_2 concentration (i, iii, v): 100 vppm; experimental conditions: PBS (0.1

M, pH 6); conditioning time at -1.2 V: 60 s (i, ii, iii, iv), 0 s (v) and exposure time 25 min; electrode area 0.126 cm^2.

In comparison to a bare SPGE, the peak currents of NO_2 at a CuNP/SPGE were higher due to the catalytic process of copper nanoparticles as shown in Figure 4.6b. To confirm the better performance of a CuNP/SPGE, differential pulse voltammograms of NO_2 were compared. A small signal at +0.75 V vs Ag/AgCl appears with the bare graphene electrode, which is enormously enhanced (around 9.6 times). in the presence of copper. Obviously the reduction of copper at negative potentials, forming catalytically active Cu(0) nanoparticles, co-reduces NO_2 or one of its follow-up products (nitrate) to a form which is easily oxidized at positive potentials, most probably nitrite [137]. Hence, these results demonstrate that the determination of NO_2 using a CuNP/SPGE coupled with activated carbon as adsorber yields a high-performance sensor, suggesting that the resulting gPAD can be an excellent device for NOx determination in the field.

An aim of this study was to uncover if NO and NO_2 behave similarly at the gPAD with respect to their adsorption behavior on activated carbon. NO in N_2 gas also was tested using the sensor under optimal condition (Figure 4.7). The DPV responses did not show any significant difference of both species ($\pm$ 5 % relative error) neither alone or in combination. Thus, it may be concluded that gas sensing of NOx can be successfully achieved with the gPAD.
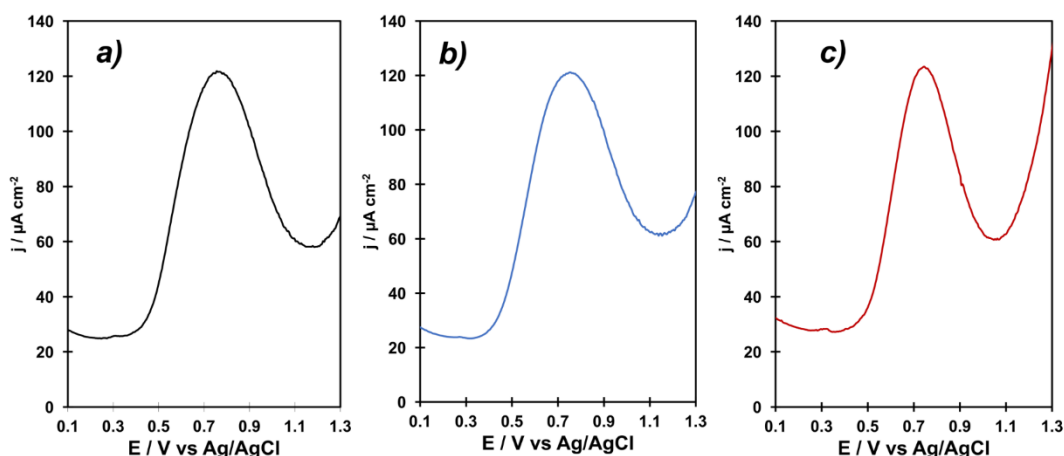
Figure 4.7 Representative DPVs of NO and NO_2; NO_2 100 vppm in air (a), NO 100 vppm in N_2 (b); 50 vppm NO in N_2 + 50 vppm NO_2 in N_2 (c); experimental conditions: PBS (0.1 M, pH 6); conditioning time at -1.2 V: 60 s. Signals shown as current densities (electrode area = 0.1257 cm^2)

Thus, we may conclude that during adsorption potassium nitrite and nitrate are formed, from which the latter is reduced to electrochemically active nitrite by the catalytic action of copper nanoparticles during conditioning at -1.2 V vs Ag/AgCl. During electrochemical detection nitrite is oxidized to nitrate.

4.1.3.3 Optimization

All the experimental parameters, i.e., conditioning time and potential, concentration of the copper solution, pH of the supporting electrolyte as well as exposure time for high concentrations were optimized (Figure 4.8) yielding the following values: conditioning time 60 s, conditioning potential -1.2 V, concentration

of the copper solution 10 mM, pH of the supporting electrolyte 6, and exposure time

for high concentrations (up to 150 vppm) 25 min.
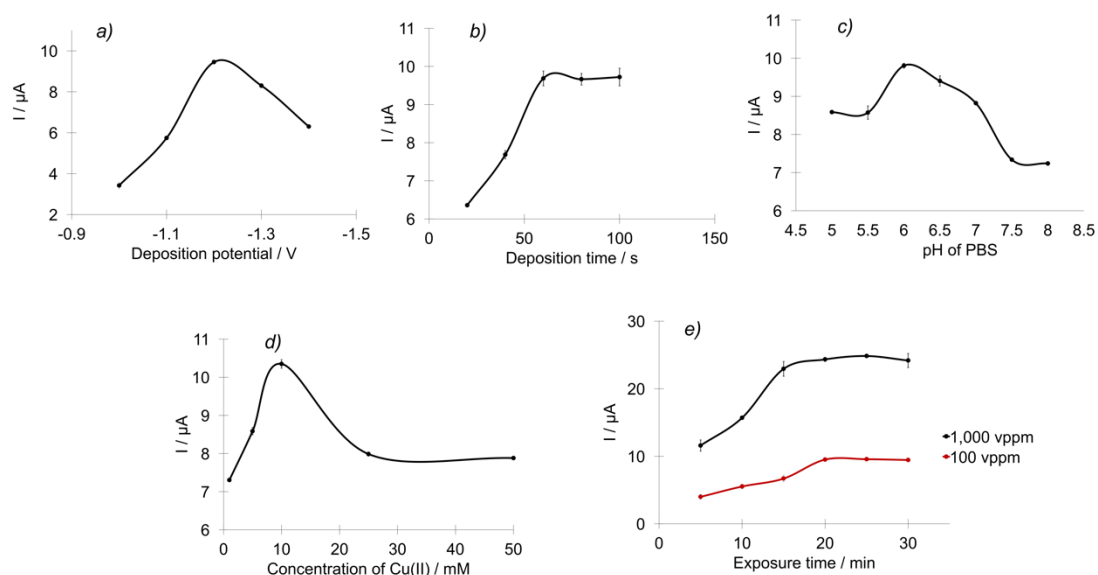
Figure 4.8 Effect of the deposition potential (a), the deposition time (b), the

concentration of Cu(II) (c), the pH of PB (d) and adsorption time (e) for determination

of NOx 100 vppm (n=3). Signals shown as measured currents.

Figure 4.9 shows the adsorption isotherms for two low concentrations of NO_2,

i.e., 0.5 and 1.0 vppm. Increasing the time yields increasing signals up to about 60

min; with longer periods the effect levels off significantly. Thus, with concentrations

higher than 1 vppm 25 minutes seem still proper for quantitative determinations with

respect to reasonable analysis time. For lower concentrations, an exposure time of

one hour should be applied.
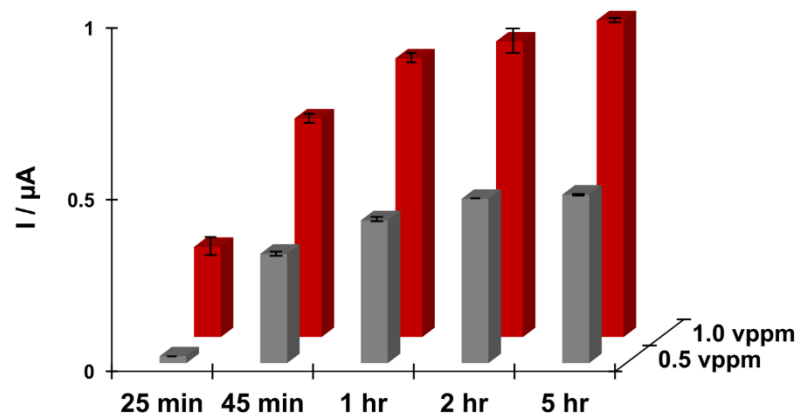
Figure 4.9 Effect of exposure time on the signal of 0.5 and 1.0 vppm NO_2; signals (n = 3) shown as measured values (electrode area = 0.126 cm cm^2); other experimental parameters as in Figure 4.7.
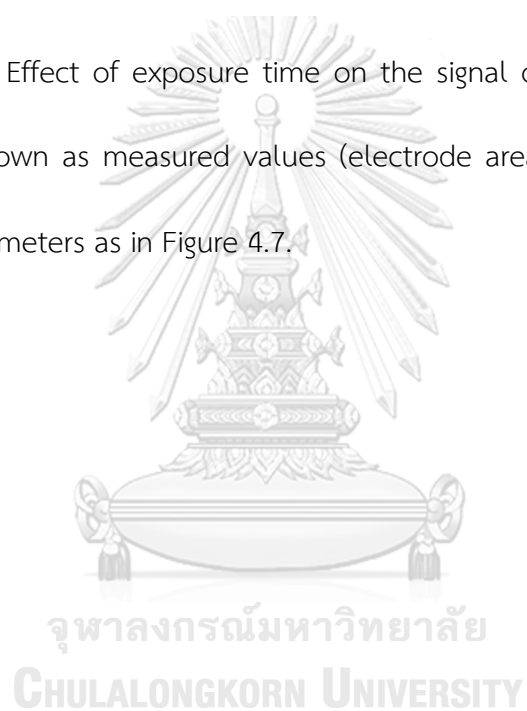
4.1.3.4 Analytical performance of the gPAD
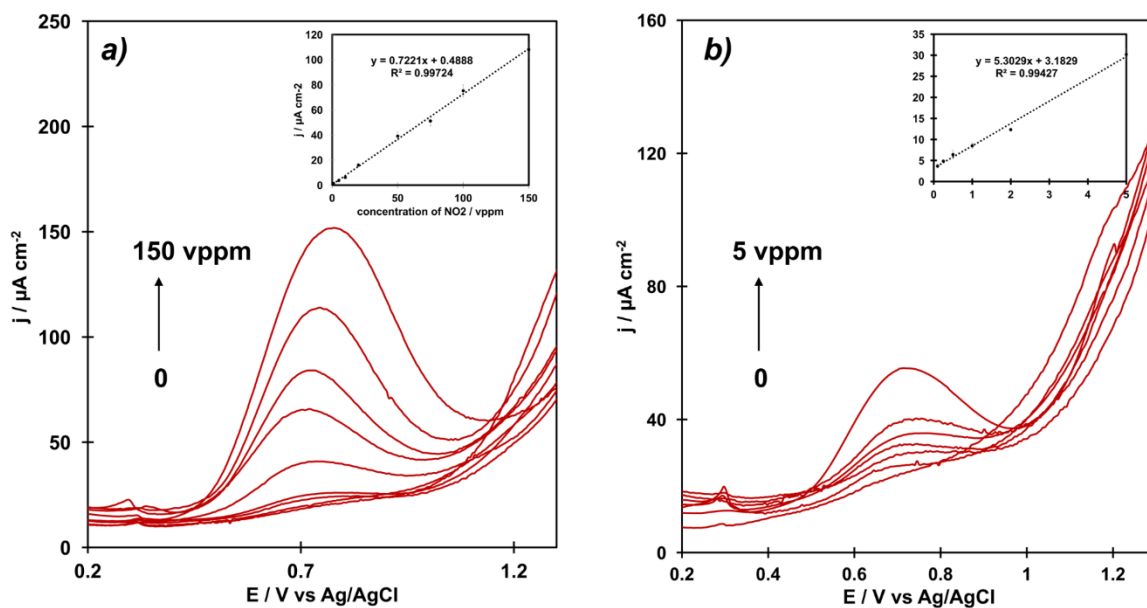
Figure 4.10 Dependence of the DPV current at gPADs on the concentration of

NOx with an exposure time of 25 (a) and 60 min (b). The insets show the calibration

lines. Other experimental conditions as in Fig.4.

Figure 4.10 shows the dependence of the DPV current on the concentration

of NO_2 (as NO in air) with an exposure time of 25 minutes. A linear relation between

signal and concentration was obtained up to 150 vppm (a) with a linearity regression

equation of I (μA) = 0.0907 C_{NOx} (vppm) + 0.0614 (R^2 = 0.99724), as shown in the

inset. Above 150 vppm the signal started to level off. The limit of detection (LOD:

$3\sigma/S$) and limit of quantitation (LOQ: $10\sigma/S$) was calculated to be 0.23 vppm and

0.76 vppm respectively. The LOD of the gPAD with 25 min exposure can be

conveniently used to determine NOx level in exhaust gases from cars for which a

limit of 200 vppm has been set by EPA. The reproducibility in terms of relative standard deviation for the gPAD (n = 7 sensors; 25, 75 and 125 vppm NO_2) were found to be less than 5.1 %.

With an exposure time of 60 min a dynamic range up to 5.0 vppm was determined with a regression equation (R^2 > 0.99), as shown in inset of Fig.5b. The corresponding LOD was estimated as low as 0.03 vppm ($3\sigma/S$), the corresponding LOQ as 0.09 vppm. Hence, gPADs are able to detect maximum allowable NOx-levels in ambient air which EPA have set to 0.1 vppm. In addition, there was no obvious change in the current signal (less than ±10 % of current signal) of 100 vppm NO_2 after storage for 30 days, as shown in Figure 4.11. Thus, gPADs can be used for over 30 days with the same response as at the beginning.
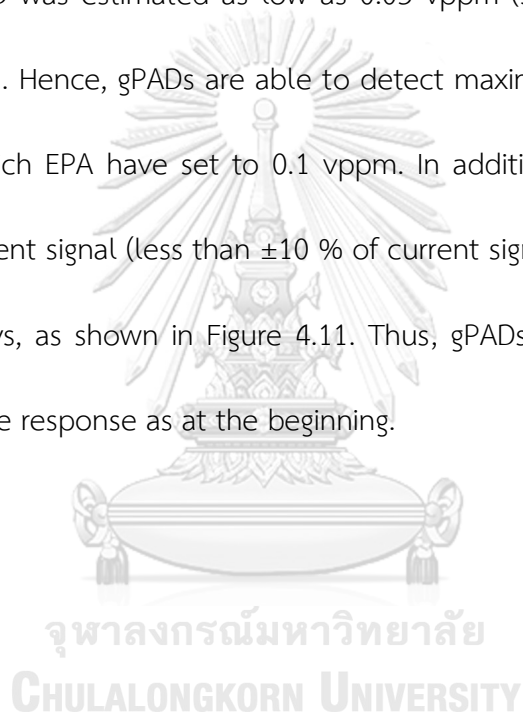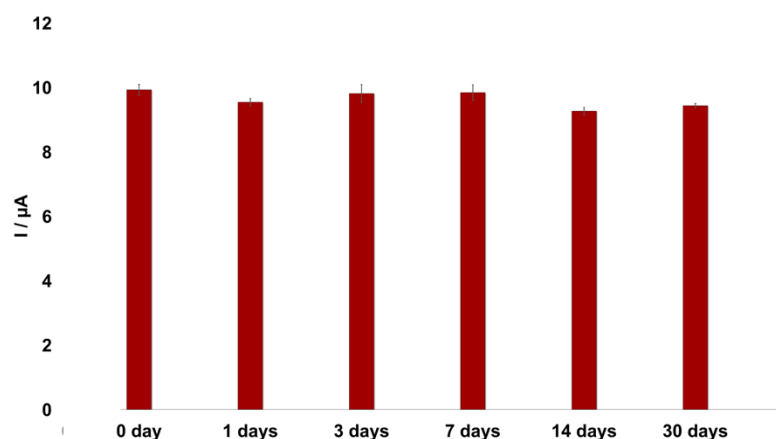
Figure 4.11 Long-term stability of gPADs; 100 vppm of NO_2 (n=3); signals shown as measured currents.

The results demonstrate that the NOx species are adsorbed strongly at the carbon and that the handling time (transfer of the sensors, connection to the instrument, application of the desorbing liquid) has no or only negligible influence on their desorption which is easily explainable by the formation of stable sorption products, such as potassium nitrite and nitrate.

4.1.3.5 Interferences
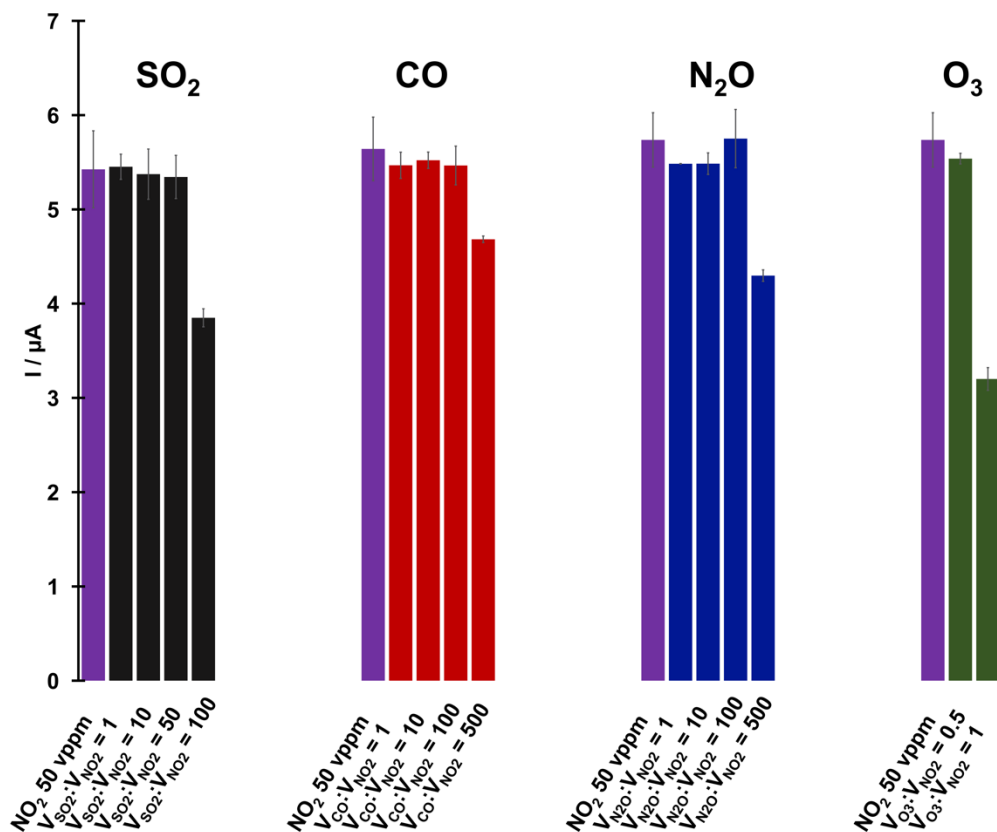
Figure 4.12 Influence of trace gases on the sensor signal of $_{NOx}$ (50 vppm); ratios are given as $v_{(interferent)}$:$v_{(NOx)}$; the signals are shown as means of the measured values (n=3).

For interference studies gases were chosen which can occur in air samples and which were suspected that they might have an influence on the NOx determination. Ozone was included as a potential noxious trace component which can be formed by natural (photochemistry, electrical discharges) or anthropogenic processes. Nitrous oxide was considered as well as it can be released during denitrification by bacterial activity.

To air standards containing 50 vppm NO_x possibly interfering gases were added in defined volume ratios (given as $v_{interferent}:v_{NOx}$) to see their influence on the analytical signal (Figure 4.12). The results show that 100-fold volume ratios of CO and of N_2O as well as a 50-fold ratio of SO_2 changed the signal only within the experimental error. Significant influence was observed with ozone, where the tolerable ratio was 0.5. A ratio of 1 (50 vppm ozone, 50 vppm NOx) caused a decrease of the signal of around 40 % already.

Therefore, the developed sensor can be applied in real sample analysis without serious interferences of other common gases except in the presence of high concentrations of ozone.

4.1.3.6 Application to samples

The gPAD was used to determine NOx gas in three types of gas samples, namely ambient indoor and outdoor air, and exhaust gases from a diesel car. For the air samples 25 and 60 min adsorption time was applied, but no electrochemical signals could be observed in both cases. Comparative spectrophotometric measurements confirmed that the concentrations were below 0.03 vppm. Spiking with NO standards at levels of 1, 75 and 125 vppm yielded recoveries within an acceptable range from 95.9% and 105.1 % (Table 4.1, supplementary material). Exhaust gases from a car were collected in a sealed box, in which gPADs were

exposed for 25 min. The results showed levels of NOx from 67.0 to 124.6 vppm with an RSD of less than 4.2 % which compared well with spectrophotometric determinations. A paired t-test of the results from the two methods uncovered that there was no significant statistical difference on a 95 % confidence level because the calculated t-value (0.825) was lower than the critical value for two-tailed comparison (2.228). Thus, the gPAD presented here demonstrated high performance and high reliability for the determination of NOx in real samples.

Table 4.1 Comparison of the performance of the proposed method using gPADs with a conventional UV-VIS spectrophotometric method in air samples (n=3)

SAMPLE	Spike concentration	This method			UV-VIS spectroscopy		
		Found	% RSD	% recovery	Found	% RSD	% recovery
indoor	non-spiked	ND	-	-	ND	-	-
	1 vppm	0.959	0.91	95.9	1.05	0.67	105.3
	25 vppm	26.04	2.4	104.2	24.8	0.3	99.3
	100 vppm	91.83	2.2	91.8	95.5	0.3	95.5
outdoor	non-spiked	ND	-	-	ND	-	-
	1 vppm	0.978	0.95	97.82	1.045	0.67	104.5
	25 vppm	25.04	5.06	100.1	26.06	0.3	104.2
	100 vppm	105.10	5.20	105.1	95.37	0.2	95.4
car#1	non-spiked	113.6	4.2	-	116.3	0.3	-
car#2	non-spiked	67.04	2.3	-	63.78	0.2	-
car#3	non-spiked	124.6	3.8	-	121.5	0.3	-

ND = not detectable

4.1.4 Conclusion

A novel gas-sensing paper-based analytical device for the determination of NOx is presented. It shows a good potential for simple applications in the field due to low detection limits, reasonable analysis times and good tolerance towards SO_2, CO and N_2O. Moreover, the gPADs presented here are environmentally friendly, disposable, portable and low in production cost. The price for individual fabrication is significantly less than 1 USD per piece and can be still substantially lowered by mass production. As the sensor is designed as a one-shot sensor for single use only, no regeneration of the sensor surface is necessary. The gPAD for NOx determination presented here exhibits high sensitivity and selectivity applicable to environmental gas samples. In addition, it can be expected that similar devices for other gaseous analytes will be developed in the near future where this gPAD may serve as a template.

CHAPTER 5

THE DEVELOPMENT OF ePAD FOR CLINICAL APPLICATION

5.1 Dual-Mode Detection of Thiocyanate in Complexed Viscous Samples via Laser-Engraved Microcapillary Pump Paper-Based Microfluidic Device

Kingkan Pungjunun[a], Abdulhadee Yakoh[a], Sudkate Chaiyo[a,b], Narong Praphairaksit[a], Weena Siangproh[c], Kurt Kalcher[d], Orawon Chailapakul[a*]

[a] Electrochemistry and Optical Spectroscopy Center of Excellence (EOSCE), Department of Chemistry, Faculty of Science, Chulalongkorn University, 254 Phayathai Road, Pathumwan, Bangkok 10330, Thailand

[b] The Institute of Biotechnology and Genetic Engineering, Chulalongkorn University, Patumwan, Bangkok, 10330, Thailand

[c] Department of Chemistry, Faculty of Science, Srinakharinwirot University, Sukhumvit 23, Wattana, Bangkok 10110, Thailand

[d] Institute of Chemistry, Karl-Franzens University, Universitätsplatz 1, Graz A-8010, Austria

* Corresponding author: Prof. Dr. Orawon Chailapakul

E-mail address: corawon@chula.ac.th Tel.: +66 2 218 7615; Fax: +66 2 218 7615

Abstract

A novel microcapillary grooved paper-based analytical device capable of dual-modes sensing (colorimetric and electrochemical detection) was demonstrated for thiocyanate determination. The device comprises of two components: colorimetric PAD (cPAD) for colorimetric detection and electrochemical PAD (ePAD) for electrochemical detection. Herein, the capillary groove constructed via laser-engraved micropatterning functioned as a micropump to facilitate the viscous fluidic transport (e.g. human saliva), which would otherwise impede its analysis on paper device. For the first time, the proposed device exhibits a promising ability to detect salivary thiocyanate on paper device without the needs of sample pretreatment or bulky instrumentations as normally required in conventional methods for saliva analysis. An extensive linear dynamic range covering its detection for both high and trace level regime (5 orders of magnitude) is collectively achieved using such dual sensing modes. Under the optimal condition, the limit of detection was found to be 6 µM with less than 4.95% RSD. An excellent stability of μpumpPAD for over 30 days was also perceived. Real sample analysis from the proposed device was in line with standard chromatographic method. Benefitting from its simple fabrication and operation, portability, disposability, low sample volume (20 µL) and low-cost (< 1 USD), this device is an exceptional alternative tool for the detection of various biomarkers in saliva specimen.

5.1.1 Introduction

Thiocyanate ion (SCN⁻) is known as a vital metabolite, which shows a biological importance in living organism. Broad ranges of SCN⁻ levels are variously presented in several biological fluids such as plasma, urine or saliva [138]. With the current trend of non-invasive detection, the SCN⁻ determination in saliva samples are of interest in this present work. Typically, a low level of SCN⁻ can be found due to a dietary intake of certain foods and contaminants (e.g. milk products and vegetables), drug administration and occupational exposure to organic nitrile [139]. On the contrary, an elevated level of SCN⁻ can also be found in a smoker, as a result of the tobacco degradation [140]. It has been reported that a high level of SCN⁻ has an adverse effect on the protein dialysis and secretion of iodine by thyroid glands [141]. Therefore, a SCN⁻ is considered to be a key indicator to monitor and control the tobacco consumption and accordingly its detection in saliva can be used to differentiate the smokers from non-smokers [142]. In this regard, analytical methods capable of determining SCN⁻ in such wide concentration ranges; both low and high concentration regimes, are of great concern for practical use.

To date, a number of analytical techniques have been employed for the determination of SCN⁻ [143-145]. However, the sensitivity of these developed methods was only limited within a specific range. To avoid this limitation, sample preparation steps are frequently demanded to attain broad utility and applicability [146-148].

Recently, microfluidic paper-based analytical device (μPAD) has gained tremendous interest among scientific community owing to the distinguishing aspects of paper (e.g., high surface area of the fiber network and power-free fluid flow via capillary force) [149]. Numerous μPADs coupled with several detection methods have been previously reported for determination of various target analytes. This includes a series of fluorescence detections [150, 151], colorimetric detections [152, 153] and electrochemical detections [154, 155]. Although the versatile μPADs have been extensively explored for myriad analytes, it should be noted that only a single report from Pena-Pereira et al. was published for the determination of thiocyanate using paper-based device [156]. In view of μPAD, electrochemical and colorimetric detection are two of most common methods employed on μPAD for its simplicity and portability. The electrochemical detection, in particular, offers an excellent sensitivity and selectivity towards SCN^- determination. This method is clearly suitable for trace level quantification of SCN^- [157, 158]. Although sample preparation/dilution steps can be circuitously performed in case of concentrated sample, additional procedures which may prolong total analysis time is clearly undesirable. Likewise, the colorimetric detection is also of significant interest. This technique is relatively simple (i.e., color intensity is related with the analyte concentration). Various chemistries can be tuned and properly selected for specific detection [147, 159, 160].Although this technique offers a more user-friendly platform, its sensitivity is still rather limited for a screening or semi-quantitative analysis in high SCN^- concentration. Another challenging aspect for

colorimetric μPAD is the physical property of the saliva sample. Principally, the rheological behavior of saliva is based on viscous and elastic properties resulting from the mucin conformation and/or the mucin type within glandular saliva [161]. Precipitation of mucins using specific reagents/equipments have been reported to effectively decrease its viscosity [162, 163], however, the use of bulky and sophisticated instrument (such as centrifuge) is inevitable, which impede the practical use for on-field testing. Hence, a straightforward and low-cost paper-device for such analysis is still in high demand. All in all, the hybrid sensing modes between colorimetric and electrochemical detection are believed to expand the working range for broad criteria in practical SCN$^-$ detection.

Herein, we engineered a novel microcapillary-pump paper-based analytical device or "μpumpPAD" via laser-engraving machine. The micropatterning of a microcapillary-pump can facilitate the fluid dynamic behavior of a viscous saliva sample to wick down the channel in paper device without sample preparation needed (Figure 5.1A). This sensing device also integrates dual sensing modes (colorimetric and electrochemical detection) for a broad range application within a single device. The proposed platform comprises of two main components: colorimetric PAD (cPAD) for colorimetric detection and electrochemical PAD (ePAD) for electrochemical detection. A single drop of saliva sample enables a rapid detection of SCN$^-$ via both sensing modes without prior sample preparation required. As conceptually illustrated in Figure 5.1B, once the sample is introduced to the

sample inlet zone of cPAD, the colorimetric screening is spontaneously performed. The rapid visible color change from colorless to red in the color testing zone of cPAD effectively corroborates the presence of the high level of SCN^-. Besides, the semi-quantitative determination can be further performed by image processing. For low level of SCN^-, no distinct color change is generated on cPAD. Hence, just by simply sliding an ePAD to take over the sample zone of cPAD and applying a running buffer, the trace level of SCN^- can be easily detected via electrochemical mode using copper (II) phthalocyanine modified screen-printed graphene electrode (CuPc/SPGE). To demonstrate the applicability of the μpumpPAD device, real saliva samples from smoking and non-smokeing volunteers were tested with the proposed platform. The μpumpPAD demonstrated here would serve an alternative tool for SCN^- determination and could be further exploited for other applications.
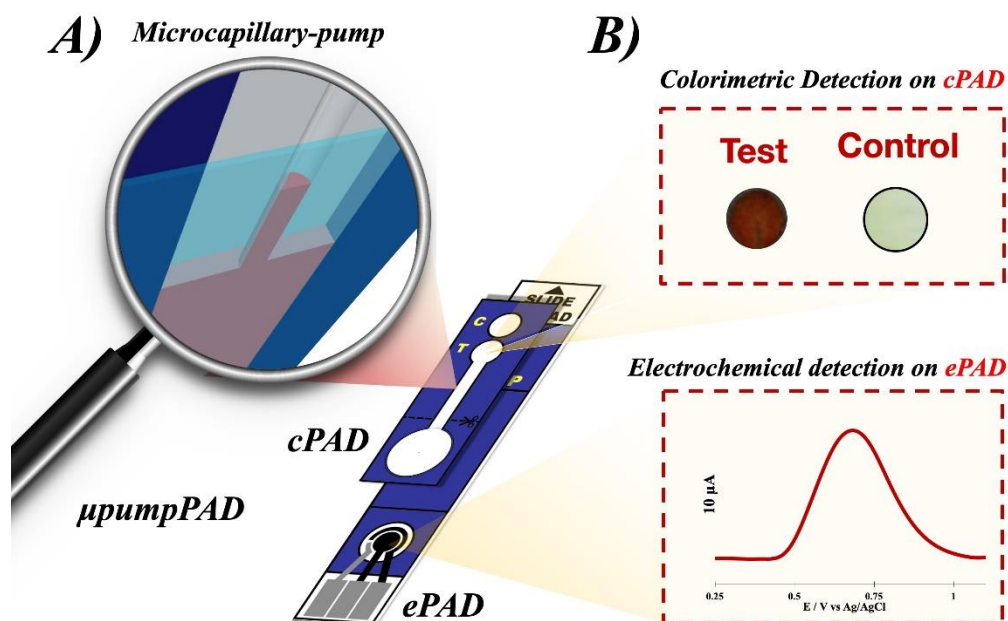
Figure 5.1 Schematic illustration of the microcapillary-pump (A) of the µpumpPAD for dual modes sensing via colorimetric detection on cPAD and electrochemical detection on ePAD (B).

5.1.2. Experimental Section

5.1.2.1 Materials, reagents and equipments

Conductive graphene ink was purchased from Serve science company (Bangkok, Thailand). Conductive ink of silver/silver chloride (Ag/AgCl) was purchased from SunChemical (Bath, UK). Potassium thiocyanate and sodium acetate trihydrate were acquired from Riedel-de Haën (Seelze, Germany). Iron(III) nitrate nonahydrate, polyacrylic acid (PA), L-cysteine, ammonium acetate, hexadecyltrimethylammonium bromide, phosphoric acid, sodium carboxymethyl cellulose (avg Mw~90,000) and nitric acid 65% were obtained from Sigma-aldrich (Missouri, USA). Copper(II)

phthalocyanine (CuPc), potassium chloride, di-potassium hydrogen phosphate, sodium sulphate, sodium sulfite, magnesium chloride, potassium carbonate, boric acid and acetic acid (glacial) 100% were purchased from Merck (Darmstadt, Germany). Potassium dihydrogen orthophosphate, potassium iodide and L-ascorbic acid were purchased from BDH (Dubai, UAE). Citric acid, D (+) glucose anhydrous, sodium chloride, potassium nitrate and potassium fluoride were purchased from Carlo Erba (Val de Reuil, France). Calcium chloride Fused gran was acquired from M & B (London, UK). Sodium nitrite was purchased from Deajung (Gyeonggi-do, Korea). All chemicals used in this work were of analytical grade. All solutions were prepared using milliQ water (18.2 MΩ cm) obtained by a cartridge purification system (Millipore, UK).

A Gemini 200 HR Nano controlled stress rotational rheometer (Malvern-Bohlin Instrument, UK) was used for viscosity measurement of synthetic saliva and real samples (conditions; cone and plate, diameter of 50 mm, 2°, temperature of 25°C). The surface morphology was investigated using a JSM-7610F field emission scanning electron microscope (FE-SEM) (JEOL ltd., Japan).

5.1.2.2 Fabrication of μpumpPAD

The μpumpPAD device comprises of two components; colorimetric PAD (cPAD) for colorimetric detection and electrochemical PAD (ePAD) for

electrochemical detection. The device design as illustrated in Figure 5.1 was created using Adobe Illustrator program (version 23.0.4). A wax-printing method was used to create a wax barrier. For the device fabrication, the designed pattern was printed onto a filter paper (Whatman No.1) and then heated at 150 °C for 40 s. The cPAD consists of the sample inlet zone (diameter: 8 mm), straight channel (length: 15 mm, width: 1.5 mm), colorimetric detection zone (diameter: 4 mm) and control zone (diameter: 4 mm). To provide a fast fluidic flow, a microcapillary pump was fabricated on the cPAD by etching the back of the straight channel of cPAD (length: 20 mm) using a laser engraving machine. A transparent adhesive tape was then attached underneath the cPAD except for the sample zone. For colorimetric testing, a 0.8 µL of coloring reagent containing Fe(III), CTAB and HNO_3 was spotted on the detection zone. After that, 1.5 mg mL^{-1} PA was subsequently added on the detection zone and dried at room temperature. For electrochemical detection, three electrodes were printed on ePAD using a silk screen-printing method. A Ag/AgCl ink was used as a reference electrode (RE) while a mixture of CuPc and graphene ink (10 mg: 2 g) was used as a counter electrode (CE) and working electrode (WE). Lastly, the ePAD was placed in an oven at 55 °C for 1 hr. An adhesive tape was used to attach the back of the electrodes zone.

5.1.2.3 Analytical procedure

For colorimetric detection, photographs were captured using a smartphone (Iphone 11 pro, Apple Inc, USA) in a light controlled box. For semi-quantitative interpretation, the obtained photographs were imported and analyzed using ImageJ program (National Institute of Health, USA).

For electrochemical process, a voltammetric experiment was performed using a CHI1240B electrochemical analyzer (CH Instruments, Inc., USA). After loading a running buffer (mixture of 0.1 mol L^{-1} Britton-Robinson buffer pH 3.5 and CTAB), a potential of -1.2 V vs Ag/AgCl was applied throughout 60 s for the pretreatment electrode step. Subsequently, square wave voltammetry (SWV) was performed using a potential scan between 0.25 and 1.25 V vs Ag/AgCl with a potential increment of 4 mV, an amplitude of 25 mV, a frequency of 15 Hz and an equilibration period of 2 s at room temperature.

5.1.2.4 Sample preparation

Saliva samples were collected form the smoking and non-smoking volunteers (sample 1-10). Volunteers were asked to avoid drinking and eating for 2 hr prior to the saliva collection. All samples were individually kept in a plastic tube container. Blinded saliva samples were also obtained from the institute of biotechnology and genetic engineering, Chulalongkorn University (Thailand) (sample 11-13). In all cases,

samples were stored at -4 °C before the analysis. Then, all of the samples were analyzed with high-performance liquid chromatography (Agilent 1100 series, USA, column: Extend-C18, column size: 4.6 x 150 cm, particle size: 5 μm) and the proposed μpumpPAD device in succession.

5.1.3 Results and Discussion

5.1.3.1 μpumpPAD Operation

Basically, the micro pumping on paper-based analytical device (μpumpPAD) consists of two components: the colorimetric PAD (cPAD) for colorimetric detection and electrochemical PAD (ePAD) for electrochemical detection. These hybrid sensing modes were elaborately designed to extend the dynamic range and integrate strengths of each sensing system for SCN^- determination. This μpumpPAD allows of saliva samples with a wide range of SCN^- concentration to be detected without requiring any sample preparation steps. In particular, the micropatterning of the microcapillary groove (perpendicular to a flow channel of cPAD) was etched via laser engraving machine and served as a microcapillary pump to enhance the capillary flow rate [164], making it especially suited for the viscous saliva sample. For the device assembly (Figure 5.2a), the cPAD was placed onto the ePAD (i), and then the wings of cPAD was folded and wrapped around the back of ePAD (ii). Once assembled, the

final μpumpPAD can be presented in Figure 5.2a (iii). At this stage, the device is ready for colorimetric assay.

For the operation of μpumpPAD, the assay begins by applying a 30 µL of working solution or a real sample onto the sample zone (Figure 5.2b (i)). Then, the solution is rapidly wicked along the straight channel through the microcapillary pump and reached the colorimetric detection zone. Herein, the pre-deposited Fe(III) reacts with the SCN^- and yields a reddish-brown complex of $[FeSCN]^{2+}$, which can be visualized by naked eyes (Figure 5.2b (ii)) [165]. For semi-quantitative analysis, a photograph of the colorimetric reaction was captured using a smartphone in the light controlled box and further analyzed using ImageJ software (Figure 5.2b (iii)). The distinctive colorimetric response on cPAD can thus confirm the high level of SCN^-. It should be noted that a low amount of SCN^- may not sufficiently produce observable signal in colorimetric assay. Therefore, the electrochemical detection using square wave voltammetry (SWV) would be subsequently performed in such case. To begin an electrochemical measurement, the ePAD was slid upward such that the three electrodes lie underneath and coincide with the sample inlet zone of cPAD. At this stage, the sample inlet zone of cPAD is in contact with the underlying electrodes of ePAD. Then, the devices were cut along the dash line to eliminate convective fluid flow (Figure 5.2b (iv)). Next, a 20 µL of supporting electrolyte was introduced to elute the remaining saliva from the sample inlet zone of cPAD to ePAD (Figure 5.2b (v)). Lastly, the SWV experiment was performed (Figure 5.2b (vi)).
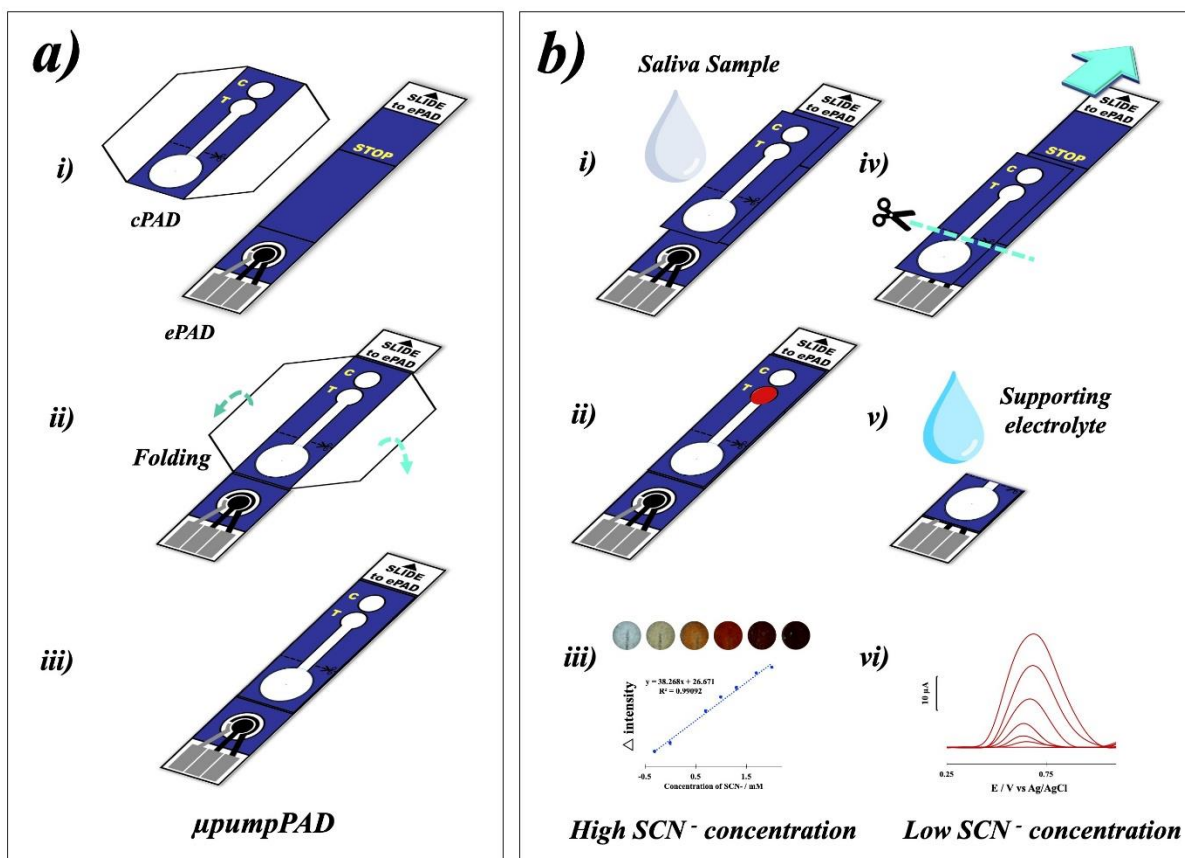
Figure 5.2 Schematic illustration of the device assembly (a) and assay procedure of μpumpPAD (b).

5.1.3.2 Device Design and Characterization

As reported by Noiphung [161] et al., the troublesome physical property of saliva, particularly its viscosity, had a significant impact on the detection using paper-based devices. Therefore, various synthetic salivas with different viscosities were prepared and investigated with differing device geometries. It has been reported that the viscosity of human saliva was in the range of 1.33 to 3.88 mPa.s, depending on the sample collection method and the types of salivas [166]. In this present work, a

synthetic saliva based on sodium carboxymethyl cellulose (SCMC) was prepared following the literature [161]. Different concentrations of SCMC (ranging from 0.1% w/v to 1.25% w/v) result in different viscosities [167]. Initially, the viscosities of these synthetic salivas were investigated using a cone and plate rotational rheometer at varied shear rates. The result exhibited that the viscosity decreased with increasing shear rate, indicating that the viscosity of human saliva has been shown to be non-Newtonian [161], and then leveled off at the shear rate of 600 s^{-1} as shown in Figure 5.3. Moreover, the viscosity values increased with increasing concentration of SCMC. Here, the prepared SCMC-based saliva of 0.10, 0.25, 0.50, 1.00 and 1.25 %w/v SCMC had the mean viscosity value of 1.14±0.17, 2.17±0.10, 2.62±0.10, 4.71±0.01and 5.84±0.01 mPa.s, respectively, at the shear rate of 600 s^{-1}, thereby covering an extended viscosity range in real human saliva [168]. These SCMC-based synthetic salivas (ranging from 1.14±0.17 to 5.84±0.01 mPa.s) were then used for further experiments throughout this work.
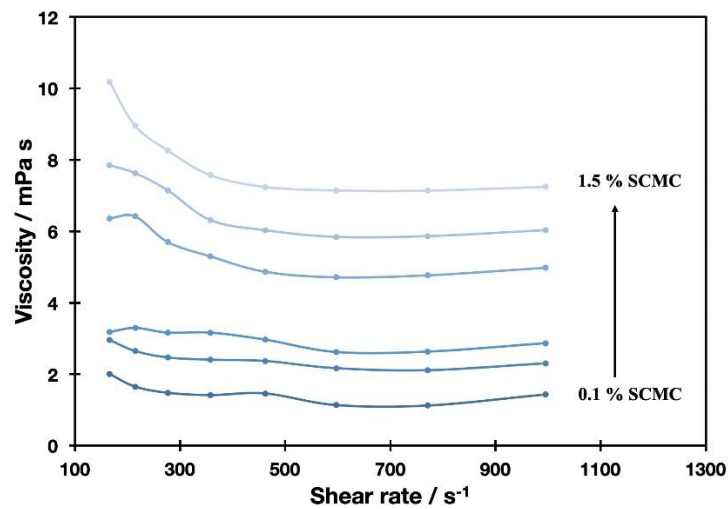
Figure 5.3 The plots between viscosity and shear rate of various concentration of SCMC in substituted saliva (n=3).

Firstly, the effect of viscosity on the flow behavior on a paper device with straight channel (13 mm diameter sample inlet, 1.5 mm channel width and 100 mm channel length) was investigated. In this study, the flow behavior was studied by monitoring the travelled distance of the fluids (red-colored synthetic salivas with different viscosities) along the straight channel. As shown in Figure 5.4, the distance that the artificial saliva traversed was correlated with the viscosity.

0.1   **0.25**   **0.5**   **1.0**   **1.25% w/v SCMC**
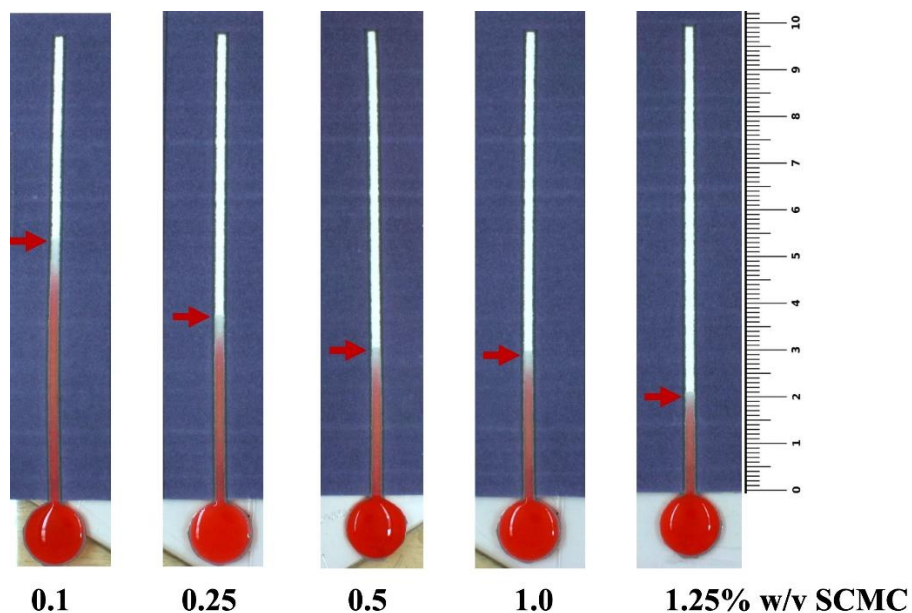
Figure 5.4 The effect of difference viscosities of synthetic salivas to the travelled distance of the fluids along the straight channel

Also, it is clearly evinced in this figure that a synthetic saliva with high viscosity was trapped and retarded within the sample inlet zone. This is because the mass transportation of aqueous solution in PAD is determined using Lucas-Washburn law,

$$L = \sqrt{\frac{\gamma \, rt \, cos\theta}{2\mu}}$$

Where; L is the aqueous transported distance under capillary force, γ is the liquid–air surface tension, r is the porous radius of the cellulose fiber, ϑ is the aqueous–fiber contact angle, μ is the fluid viscosity and t is the transported time. Thus, this result clearly confirms the effect of viscosity on the flow behavior on a paper substrate. To overcome this limitation, the μpumpPAD format was introduced

in this work. In order to confirm the functionality of the proposed platform, a comparative study using different paper-based geometries (including; (i) planar PAD, (ii) planar PAD sealed with transparent tape and (iii) etched microgrooves on PAD sealed with transparent tape) tested with the highest concentration of SCMC-based saliva (1.25% w/v) was performed (Figure 5.5). Obviously, an extremely short distance of fluid flow via porous paper capillary was observed in planar PAD (i), while a longer fluid flow distance was observed with a PAD sealed with a transparent tape. This phenomenon is presumably due to the increasing interlayer force between the paper and transparent tape. To be highlighted, the longest fluid flow distance was obtained with the etched microgrooves on PAD sealed with transparent tape. With this geometry, not only porous paper capillary force and interlayer force, but also the microscale capillary force lied between the microgrooves and transparent tape, collectively uplifted the fluid convective flow. The flow velocities of each geometry were found to be 0.045 ± 0.005, 0.20 ± 0.01, and 0.36 ± 0.01 cm min^{-1} for planar PAD, planar PAD sealed with tape, and μpumpPAD, respectively. This observation is in line with the previous work reported by Jin-Wen Shangguan et al [164]. That is;

$$F_{microscale\ capillary} > F_{interlayer} > F_{porous\ paper}$$

where $F_{microscale\ capillary}$ is the force generated by microscale capillary channel using laser etching, $F_{interlayer}$ is the force generated by transparent tape and paper as double-layer structure, and $F_{porous\ paper}$ is the force generated by microscale capillary of porous paper. Therefore, it can be concluded that the μpumpPAD can effectively

increase the capillary force, which advantageously lead to faster sampling speed. Therefore, the laser-etching microgroove on PAD will be further used throughout this study. Again, a flow behavior tracking from the distance that the fluid can traverse was tested with a series of synthetic saliva with different viscosities using μpumpPAD. As expected, when the concentration of SCMC/viscosity is increased, the slower flow velocity is observed (Figure 5.6). Anyhow, to enable fluid transport in practical samples, the channel length of cPAD was set at 1.5 cm which is close to the maximum distance generated by the synthetic saliva with the highest viscosity.

Furthermore, the geometrical factors affecting the flow behavior which include the laser engraving energy (10, 11, 12, 13, 14 and 15 eV) and channel width (1.5, 1.75 and 2 mm) were optimized. As presented in Figure 5.7, insignificant effect from the channel width towards the flow velocity was observed. Therefore, the channel width of 1.5 mm was selected in this work. On the contrary, the laser engraving energy substantially impacts the longitudinal flow velocity since it directly controls the size and shape of the microscale capillary channel. Although the laser energy of 13 eV provided the highest flow velocity, a laser energy of 12 eV was selected in this work. Here, an energy of 12 eV was selectively biased since the engraved energy higher than 12 eV randomly resulted in a microchannel destruction while those of 14 and 15 eV clearly damaged the microchannel (paper tearing) and eventually decreased the flow velocity. All in all, the channel width of 1.5 mm and laser engraving energy of 12 eV were chosen for the fabrication of μpumpPAD. To

confirm the microcapillary channel structure on paper device, the conventional filter paper and etched filter paper were investigate using a cross-sectional scanning electron microscope (SEM) technique. It is clearly seen in Figure 5.5 b that the capillary microchannel between paper layer and adhesive tape was successfully constructed via laser engraving machine compared to that of conventional paper (Figure 5.5 c). Using an image processing software, the width and height of this micropump channel were estimated to be 95 and 365 µm, respectively (Figure 5.5b).
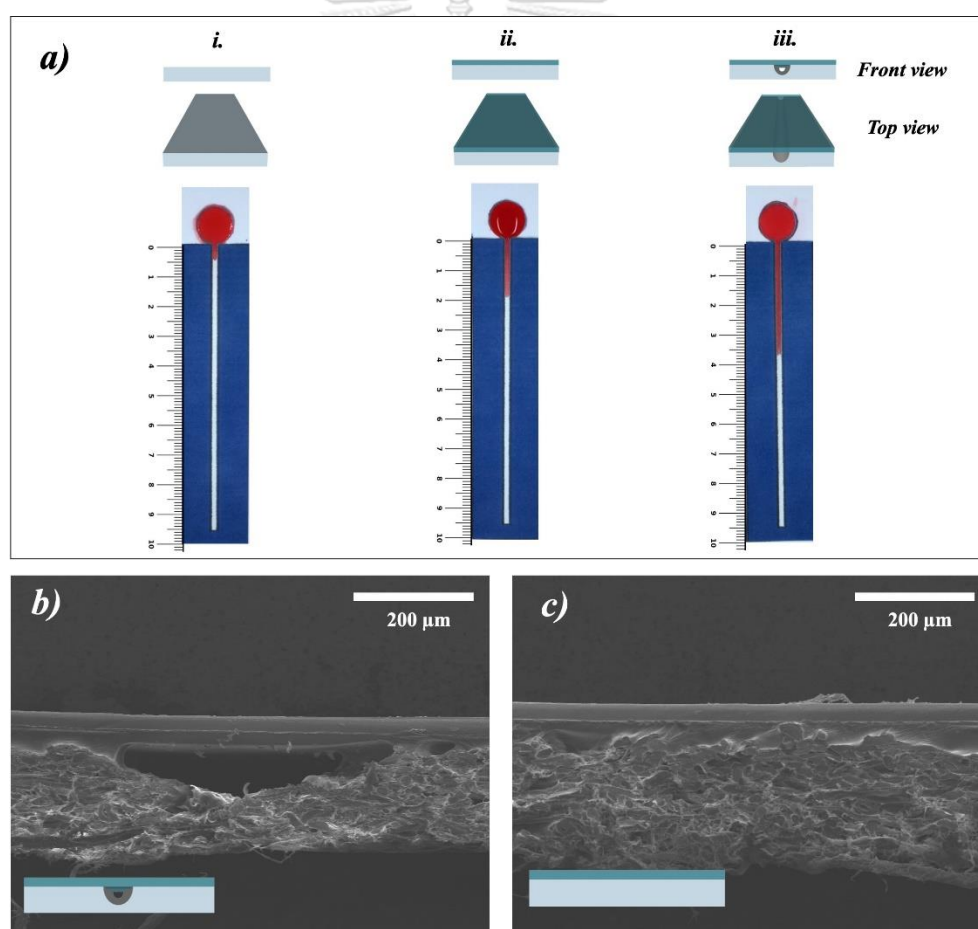
Figure 5.5 A different µPAD structures: i) planar paper, ii) paper sealed with transparent tape and iii) microgrooves onto paper sealed with transparent tape

displayed a hydrodynamic analysis under the conditions: 10mm of diameter; 0.5 mm of width; 100 mm of length; 200 μL of food color dye (a). SEM image of microgrooves onto paper sealed with transparent tape (b) and paper sealed with transparent tape (c) using acceleration voltage of 5.0 kV.
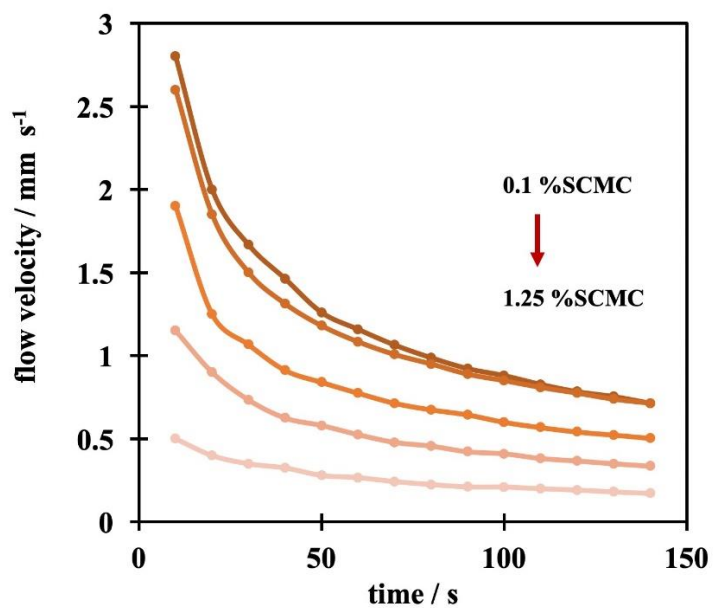
Figure 5.6 The velocity measurement of various concentration of SCMC-based saliva substitutes (n=3).
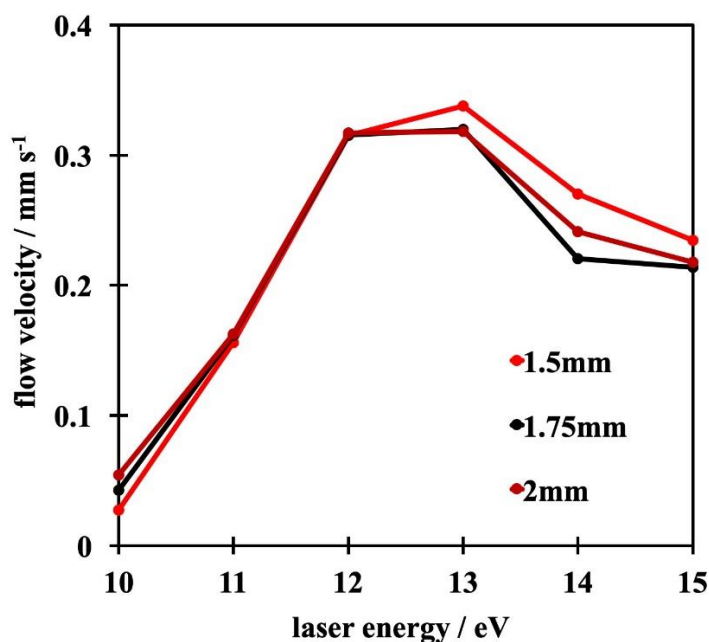
Figure 5.7 The effect of laser energy and channel width to the flow velocity using 1.5 %w SCMC-based saliva substitutes as tester (n=3).

5.1.3.3 Effect of Viscosity on Dual Sensing Modes

As described previously, the viscosity has a potent effect on the detection of paper-based devices. Therefore, a series of SCN^--containing synthetic salivas with varying viscosity were subsequently investigated with the proposed reaction systems; both colorimetric and electrochemical detection. Initially, the colorimetric detection of SCN^- using the Fe(III)-complexation reaction was performed with different device geometries. Noted that polyacrylic acid (PA) was used in this colorimetric detection to stabilize the colorimetric product ($[FeSCN]^{2+}$) and attain a uniform color. The comparative color change with the presence and the absence of PA on the detection zone is shown in Figure 5.8. Without PA, an inhomogeneity of the color distribution

was observed, which may result in the color intensity deviations. This is because the

negative charge of PA can stabilize the positive charge of the colorimetric product

($[FeSCN]^{2+}$) and prevent it from flowing to the edge of the detection zone.
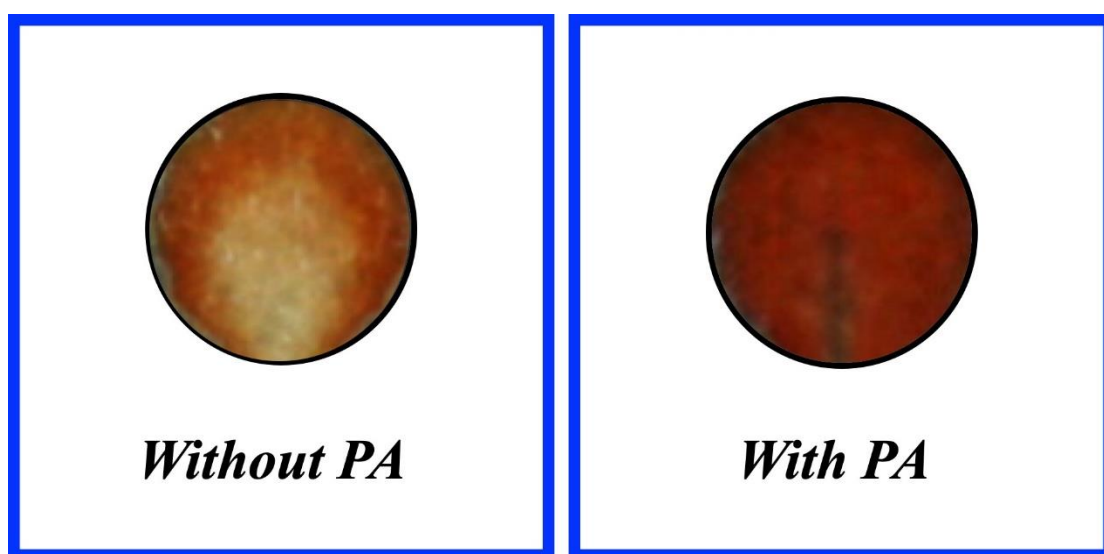
Figure 5.8 The effect of PA on colorimetric detection zone(n=3).

As shown in Figure 5.9a, the synthetic salivas with different viscosities (from

1.14±0.17 to 5.84±0.01 mPa.s) were investigated on the cPAD using 3 different device

systems, (i) planar PAD sealed with transparent tape, (ii) μpumpPAD without CTAB,

and (iii) μpumpPAD with CTAB. In the planar PAD sealed with transparent tape (i), the

saliva with higher viscosity could not flow to the detection zone and eventually

affect the mean color intensity difference (Δintensity = blank - sample). In the case

of μpumpPAD without CTAB (ii), all saliva samples apparently were able to reach the

detection zone as a result of the etched microcapillary pump. However, incomplete

color formation was still observed for the saliva with higher viscosity due to the flow termination. The percentage of relative standard deviation was up to 33.8% as a consequence of this phenomenon. Interestingly, with the assistance of CTAB (iii), a completed fast-flow fluid with homogeneous color change even at high viscosity was obtained. Technically, it has been reported that CTAB could reduce the viscosity of the viscous sample [162]. Moreover, there was no significant different (%RSD less than 5) in mean color intensity using μpumpPAD with CTAB, indicating that the proposed system could provide both high homogeneity and reproducibility. Hence, this proposed colorimetric method outlined here can effectually overcome the limitation from fluid viscosity in saliva sample.

Next, the electrochemical behavior of SCN$^-$ was studied using SWV technique (Figure 5.9b). From the SWV voltammograms, no electrochemical peak from the supporting electrolyte (0.1 mol L^{-1} Britton-Robinson buffer pH 3.5, (curve i)) was detected with a bare screen-printed graphene electrode (SPGE) whereas the presence of 250 μmol L^{-1} of SCN$^-$ (curve ii) showed a small broad peak at +0.8 V vs Ag/AgCl. A notable increase in oxidation currents of SCN$^-$ was found using SPGE in the presence of CTAB in the electrolyte soltion at +0.7 V vs Ag/AgCl (curve iii). Here, the use of 0.3 mmol L^{-1} CTAB reportedly formed a surfactant bilayer and exhibited a positive charge on the electrode surface during the electrodeposition step [99]. Consequently, SCN$^-$ as a negatively charged ion could be trapped on the CTAB bilayer due to the electrostatic interaction, which resulted in a higher peak current.

We further enhanced the detection sensitivity by modifying the electrode surface with copper(II) phthalocyanine (CuPc) owing to its electrocatalytic property toward SCN⁻ [169]. As expected, the highest oxidation peak current of SCN⁻ at +0.65 V vs Ag/AgCl was obtained when CuPc/SPGE was utilized in the presence of CTAB (curve iv). Interestingly, the presence of CTAB could also facilitate the electron transfer and result in a lower oxidation potential compared to that of the solution without CTAB (curve v). Hence, the CuPc/SPGE in the presence of CTAB will be used as an effective electrode for the electrochemical detection of SCN⁻ in this work. The existence of CuPC on the electrode surface was further corroborated by SEM/EDX analysis (Figure 5.10). The surface morphologies of SPGE and CuPc/SPGE were investigated with SEM/EDX analysis. The SEM image of SPGE exhibits a smooth surface of graphene sheets as shown in Figure 5.10a. Meanwhile, CuPc/SPGE presents the rough surface with the massive deposition of CuPc particles onto the graphene sheets as shown in Figure 5.10b. Moreover, the energy dispersive X-ray (EDX) analysis was employed to confirm the element of CuPc on the working electrode. As shown in Figure 5.10c-f, the presence of Cu and N elements corresponded to CuPc from the EDX spectra could confirm the successful modification of the electrode surface.

Following the selection of a suitable electrode for SCN⁻ determination, we then investigated the effect of the viscosity on the electrochemical measurement. As shown in Figure 5.9c, the oxidation peak currents of 0.250 mmol L⁻¹ SCN⁻ in various synthetic salivas with different viscosity showed no statistically difference (%RSD <

3.8) within the studied range (viscosity ranging between 1.14±0.17 and 5.84±0.01 mPa.s.). Thus, it can be concluded here that the variation of the saliva viscosity had no effect on the electrochemical detection using the proposed system.
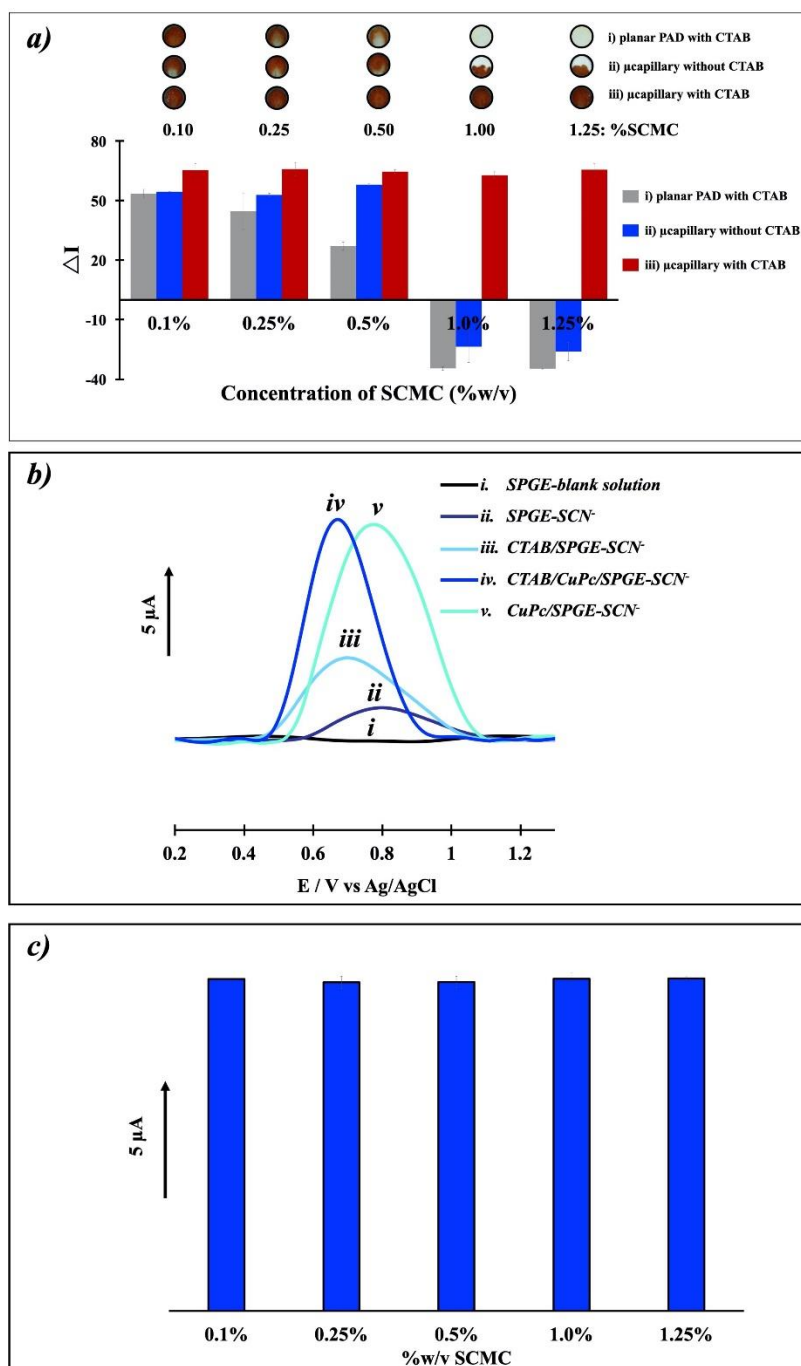
Figure 5.9 The effect of viscosity for the determination of 10 mmol L^{-1} SCN^{-} using complexation with 0.5 mol L^{-1} Fe(III) in 3 differences system; planar PAD with CTAB (i), μpumpPAD without CTAB (ii) and μpumpPAD with CTAB (iii) (a). The SWASVs of blank solution (0.1 mol L^{-1} Britton-robinson pH 7) (i) and 0.250 mmol L^{-1} SCN^{-}

(ii,iii,iv, v) at SPGE (i,ii), SPGE containing CTAB (iii), CuPc/SPGE containing CTAB (iv) and CuPc/SPGE without CTAB (v) in 0.1 mol L^{-1} Britton-robinson pH 7 containing 0.3 mmol L^{-1} CTAB on ePAD (b). The effect of viscosity for determination of 0.250 mmol L^{-1} SCN$^-$ on CuPc/SPGE using 0.1 mol L^{-1} Britton-Robinson buffer pH 3.5 and 0.3 mmol L^{-1} CTAB as supporting electrolyte (n=3) (c).

e) Element	Line Type	Wt%	Atomic %	f) Element	Line Type	Wt%	Atomic %
C	K series	94.15	94.94	C	K series	79.78	84.92
N	K series	5.85	5.06	N	K series	15.48	14.13
Cu	L series	0.00	0.00	Cu	L series	4.73	0.95
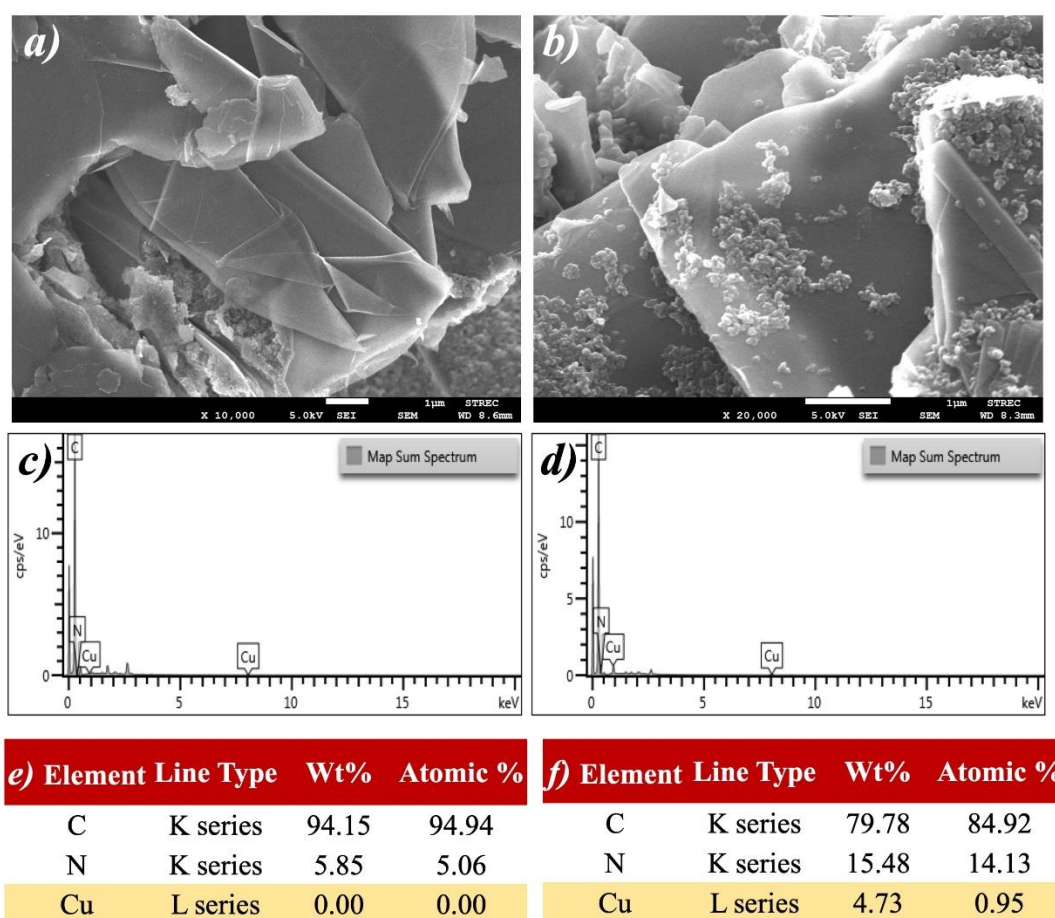
Figure 5.10 SEM image of a SPGE (a) and a CuPc/SPGE (b) using acceleration voltage of 5.0 kV. EDX spectra (c, d) and table of the % atomic and %w of element (e, f) of SPGE (c, e), CuPc/SPGE (d, f) using a magnification of 10,000X and acceleration voltage of 5.0 kV.

5.1.3.4 Optimization of the Assay Condition

To achieve the maximum detection efficiency, various parameters affecting the performance of the sensor; colorimetric detection and electrochemical detection, were optimized. The operating conditions of colorimetric detection, including the concentration of Fe(III), HNO_3, PA, and CTAB, were initially investigated. The highest performance was found with the following conditions; 0.5 mol L^{-1} of Fe(III), 2.0 mol L^{-1} of HNO_3, 1.5 mg mL^{-1} of PA, and 3 mmol L^{-1} of CTAB as shown in Figure 5.11a-d. Moreover, the detection time was also studied in this work. Figure 5.11e presents the relationship between Δintensity and detection time up to 20 min. The color change from colorless to reddish-brown was rapidly developed once the sample reached the detection zone. Using an image processing software, it was found that the Δintensity increased with increasing measurement time earlier and remained steady after 4 min suggesting that the complexation of $[FeSCN]^{2+}$ was completely formed. However, to ensure the reaction completeness and avoid a random error, the detection time at 5 min was selected for the colorimetric determination of SCN^-.
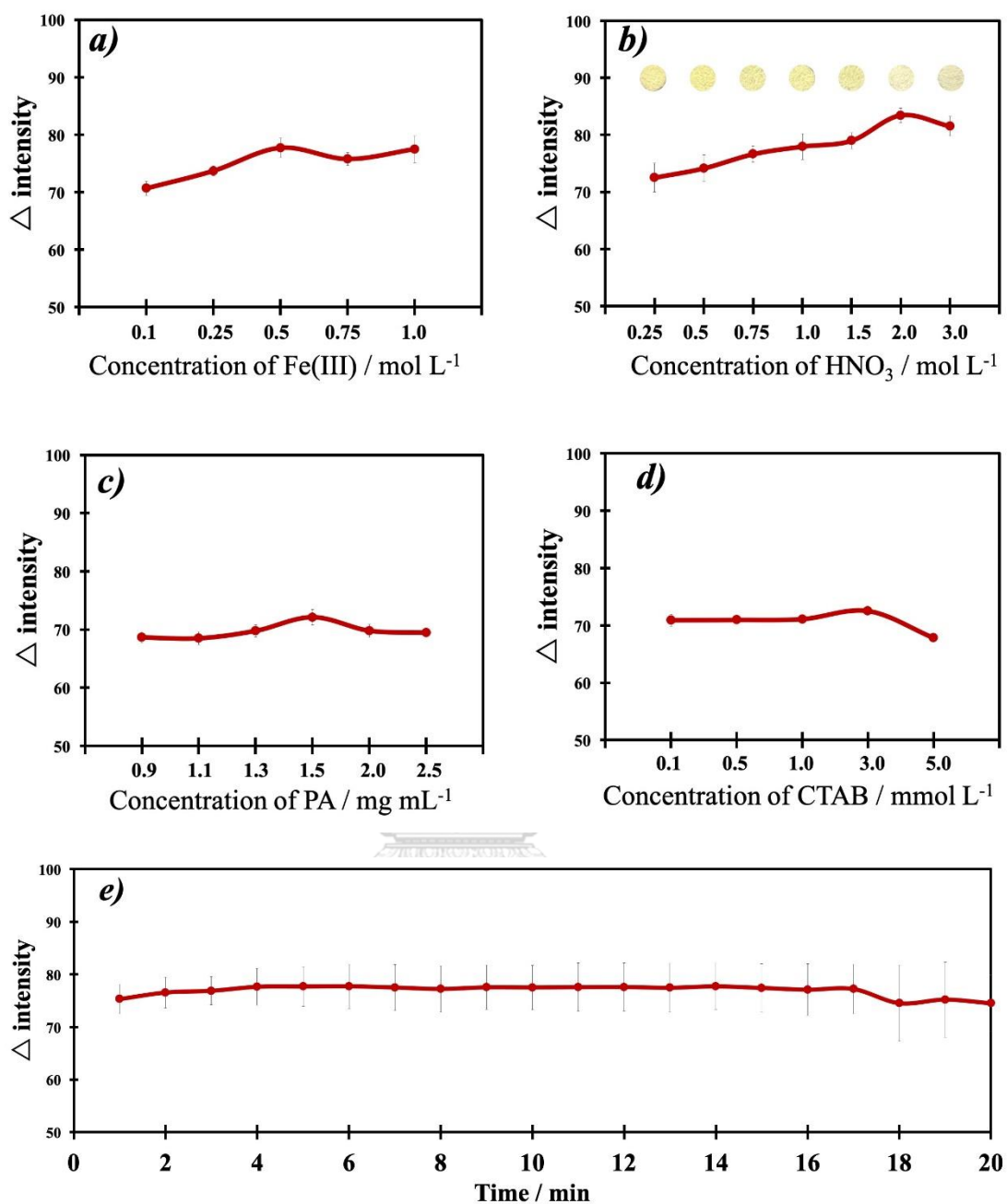
Figure 5.11 The effect of the concentration of Fe(III) (a), concentration of HNO$_3$ (b), concentration of PA (c), concentration of CTAB (d) and reaction time (e) on colorPAD for 10 mmol L^{-1} SCN$^-$ detection (difference 3 devices; n=3).

Next, the optimal electrochemical parameters consisting of concentration of CuPc/SPGE (%w/w), pre-conditioning potential, pre-conditioning time, concentration of CTAB and pH of buffer were optimized. The highest performance was achieved with the following conditions; 0.5 %w/w of CuPc/SPGE, -1.2 V vs Ag/AgCl of pre-conditioning potential, 60 s of pre-conditioning time, 0.3 mmol L^{-1} of CTAB concentration and Britton-Robinson buffer pH of 3.5 as shown in Figure 5.12. More details are presented in the supplementary material.
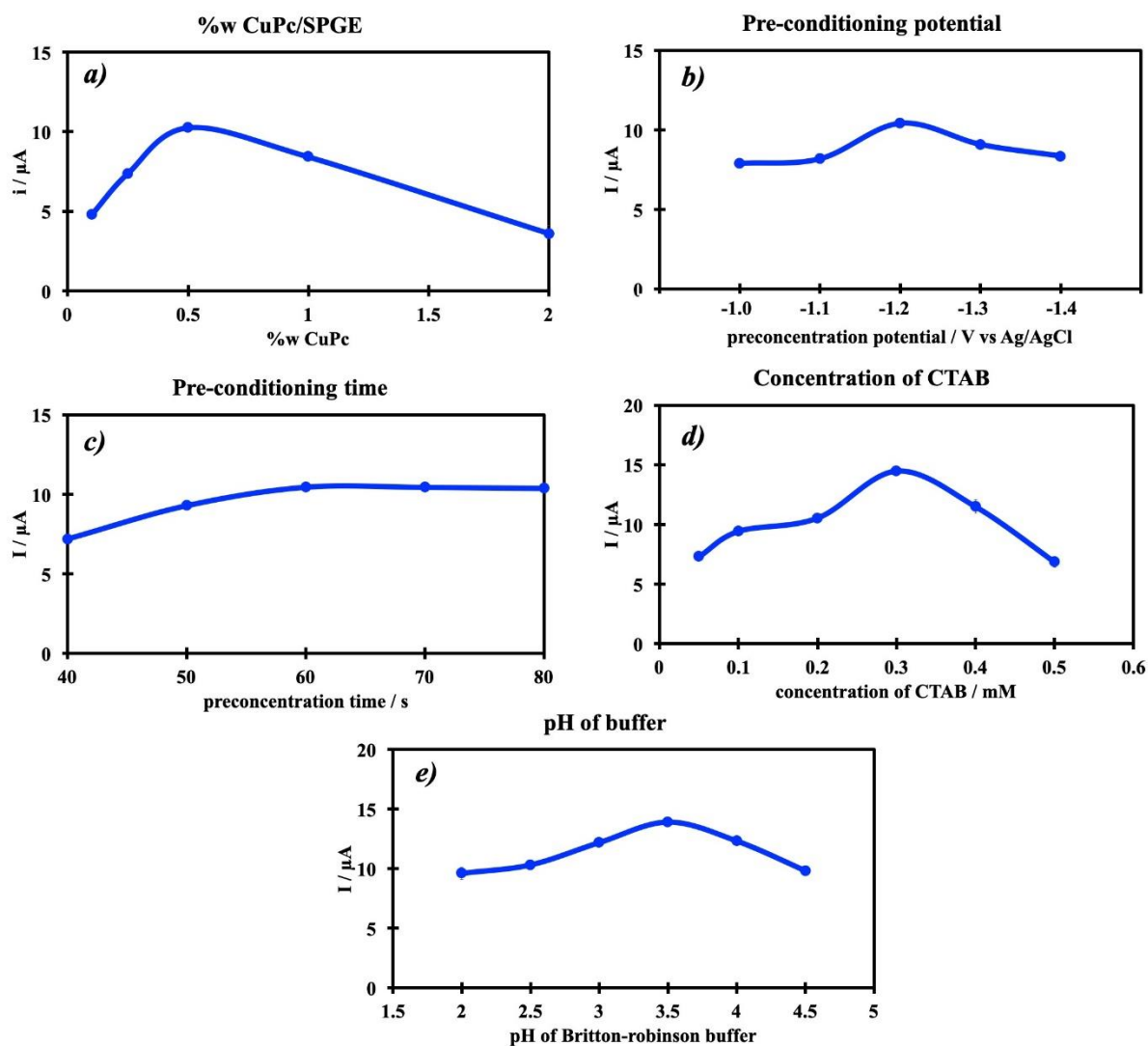
Figure 5.12 The effects of %w CuPc (a), preconditioning potential (b), preconditioning time(c), concentration of CTAB (d) and pH of Britton-robinson buffer (e) on the analytical performance of ePAD for 0.250 mmol L^{-1} SCN^- determination (difference 3 devices; n=3).

5.1.3.5 Analytical Performance of μpumpPAD

Under the optimal conditions, the analytical figure of merits for dual modes sensing of SCN⁻ using μpumpPAD were evaluated. With the developed device, linear calibration plots can be successively established for both sensing modes using only a single drop of SCN⁻ solution. Under the colorimetric mode, the color intensity increased with increasing the concentration of SCN⁻ between 0 and 100 mmol L^{-1} conforming to the color change from colorless to reddish-brown (Figure 5.13a). A good linear logarithmic relationship between the intensity and concentration of SCN⁻ was established from 0.5 to 100 mmol L^{-1} with the regression equation of $\Delta I = 38.268$ log $C_{SCN^-} + 26.671$ ($R^2 = 0.99092$) as shown in the inset. The limit of detection (LOD = $3\sigma/s$) and limit of quantitation (LOQ = $10\sigma/s$) were found to be 0.17 and 0.59 mmol L^{-1} respectively. The repeatability in terms of relative standard deviation for the cPAD by the determination of SCN⁻ at 1, 25 and 70 mmol L^{-1} were less than 2.32% (n=5).

For the electrochemical mode, a linear dynamic range was attained between 0.025 and 0.7 mmol L^{-1} with the regression equation of $\Delta I = 47.307$ $C_{SCN^-} + 1.558$ ($R^2 = 0.99447$) as shown in Figure 5.13b. The LOD and LOQ were calculated to be 0.006 and 0.022 mmol L^{-1}, respectively. The repeatability was estimated using the determination of SCN⁻ at 0.050, 0.300 and 0.500 mmol L^{-1} with 5 different sensors. The relative standard deviation obtained was less than 4.95 %, indicating a good precision and repeatability. Altogether, using dual sensing modes, the dynamic range for SCN⁻ was greatly expanded covering the practical test in real world sample

without a prolonged sample preparation steps needed. A comparison of the analytical performance between the proposed platform and other SCN⁻ sensors was summarized in Table 5.1. Although the detection limit of this approach is inferior to some reports, strong advantages in terms of the widest linear dynamic range, fast analysis time and portability are key factors making this sensor an exceptional alternative for SCN⁻ detection.
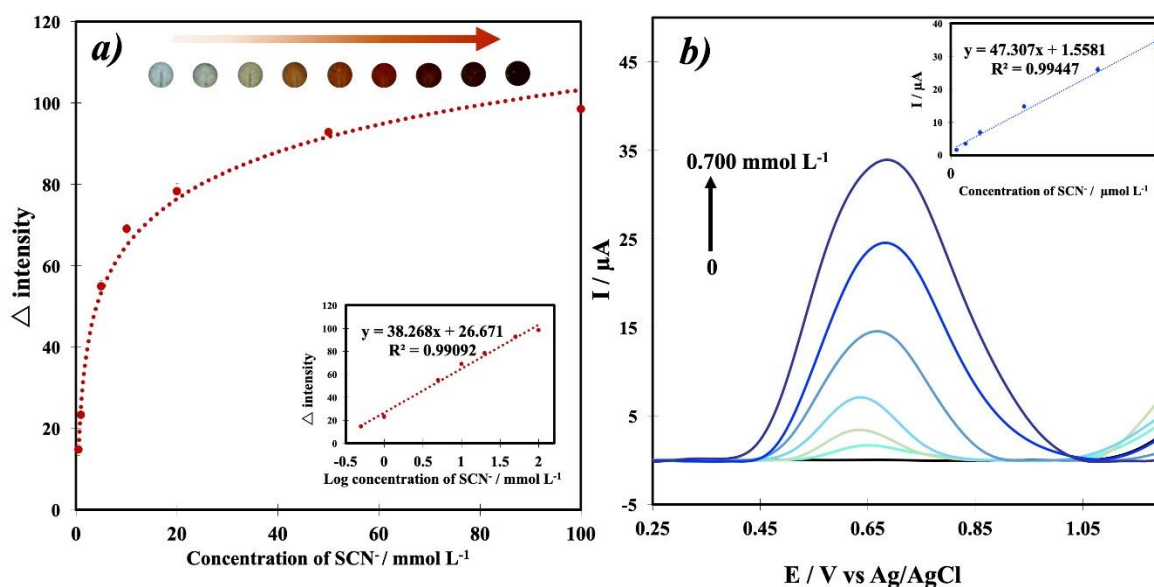
Figure 5.13 A visual image of the cPAD for the determination of SCN⁻ at the concentration of 0 to 100 mmol L^{-1} with 0.5 mol L^{-1} Fe(III) and the dependence of ∆I on the concentration of SCN⁻ using ImageJ software for analysis at cPAD. Inset: the linear relation between ∆I and log concentration of SCN⁻ (a). The SWASVs of SCN⁻ at CuPc/SPGE on ePAD in 0.1 mol L^{-1} Britton-robinson buffer pH 7 at the concentrations of 0 - 0.700 mmol L^{-1}. Inset: the linear relationship of stripping currents versus SCN⁻ concentration (b).

Table 5.1 Summarized results of the determination of SCN⁻ in saliva

samples using the different methods.

Material	Detection methods	Substrate	Analysis time	Linear range	LOD	Ref
Fe(III)	colorimetric	PADs	30 min	0.25-20 mM	0.06 mM	156
AuNPs-CDs	colorimetric fluorescent	-	6 min	0.1 – 2 µM	0.036 µM	170
Au@Pt NCs	colorimetric	-	30 min	0.020 – 40 µM	5 µM	147
Au@Ag NRs	SERS	droplet microfluidic chip	> 1 hr	1 – 256 µM	1 µM	171
Starch-reduced AuNPs	SERS	silicon wafer	> 1 hr	0.05-50 µM	0.05 µM	143
Ds/Fe₃O₄@ g-C₃N₄	electrochemical	-		1-900 nM	0.14 nM	157
PMETAC -MIM resonator	visual	glass		0.005 - 0.3 M	-	140
Fluorescein-AuNPs	fluorescent	-	25 min	1–40 nM	0.5 nM	172
Fe(III) CuPc/SPGE	colorimetric electrochemical	PADs	6 min	0.025 – 100 mM	20 µM	This work

Moreover, the stability of the µpumpPAD was investigated. The stability was

defined as the retention of at least 95% of the initial response. The results as

presented in Figure 5.14a-b clearly showed that the device was able to maintain the

sensing performance for more than 1 month. Therefore, the µpumpPAD

demonstrated here exhibits a strong potential applicability for the determination of

SCN⁻ in saliva sample.
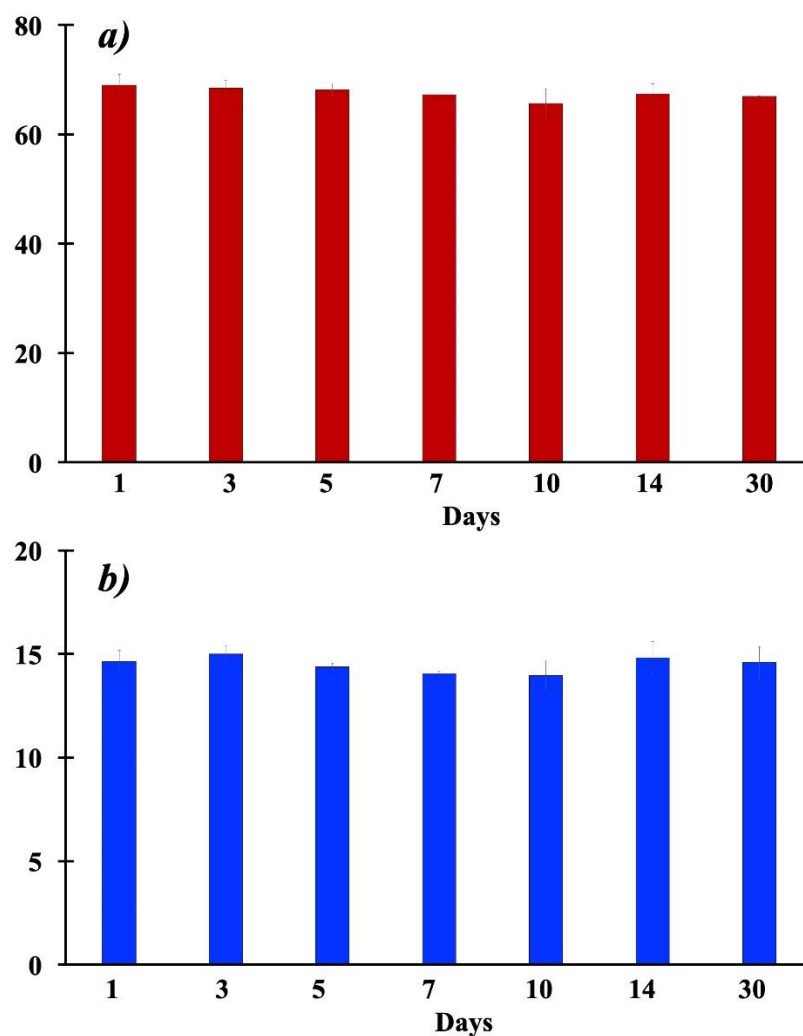
Figure 5.14 The stability of cPAD (a) and ePAD (b) of μpumpPAD (n=3).

5.1.3.6 Interference study

We further studied the influence of other common ions/compounds that are usually present in the real saliva sample on the analytical signal using μpumpPAD. The interference study was performed by adding the ions in the defined mass ratios (given as $m_{interference}$: m_{SCN^-}) to a 10 mmol L^{-1} SCN$^-$ solution for colorimetric detection and 0.250 mmol L^{-1} SCN$^-$ solution for electrochemical detection. For colorimetric

detection on cPAD, the result showed that 100-fold mass ratio of CH_3COO^-, NH_4^+, K^+, CO_3^{2-}, Na^+, SO_4^{2-}, SO_3^{2-}, NO_3^-, Mg^{2+}, Cl^-, citric acid, and glucose as well as 10-fold mass ratio of ascorbic acid, $H_2PO_4^-$ and cysteine did not interfere the analytical signal of SCN^-, producing less than ±5% of the error as shown in Figure 5.15a.

For electrochemical detection on ePAD, the experimental result exhibited that 100-fold mass ratio of CH_3COO^-, NH_4^+, K^+, Na^+, SO_4^{2-}, NO_3^-, Mg^{2+}, Cl^-, $H_2PO_4^-$, citric acid and glucose as well as 10-fold mass ratio of ascorbic acid, SO_3^{2-}, F^-, CO_3^{2-}, NO_2^- and cysteine virtually had no impact on the current signal, generating merely less than ±5% of the error as shown in Figure 5.15b. Therefore, it could be deduced that the proposed dual colorimetric and electrochemical system outlined here show a good selectivity toward SCN^- and provide a promising tool for real sample analysis.

Furthermore, we additionally evaluated the effect of iodide, a particularly troublesome ion well recognized to interfere both colorimetric and electrochemical signals, for it could react as a coloring reagent to Fe(III). However, the result exhibited that, even with the highest concentration of iodide reportedly tested in saliva at 0.010 mmol L^{-1} [156], the error percentage is still within ±5%. Therefore, the μpumpPAD conclusively can be applied for real saliva samples without any serious interferences.
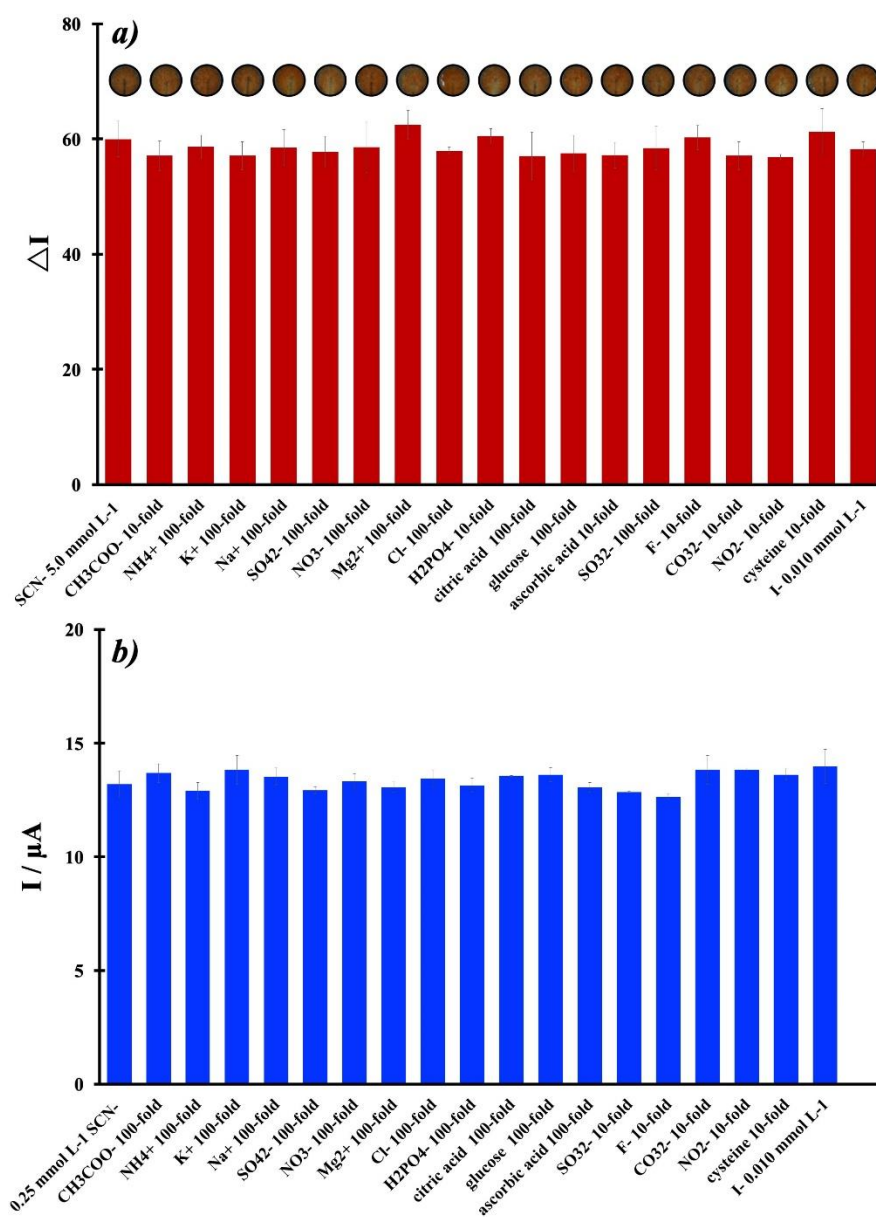
Figure 5.15 Influence of common interfering ion on the signal of SCN^-; ratios are given as $m_{(interferent)}$:$m_{(SCN-)}$ on dual modes sensing (color detection (a) and electrochemical detection (b)); the signals are shown as means of the measured values (n = 3).

5.1.3.7 Application in the Real Human Saliva

Thiocyanate in 10 saliva samples form the smoking and non-smoking volunteers (sample 1-10) were determined using μpumpPAD and validated in parallel with the standard ion exchange-chromatogaphy method to access the applicability of the developed sensor. The experimental results are exhibited in Table 5.2. The paired t-test value at 95% confidence was performed and found that there was no significant difference between these two methods. Moreover, the % recovery was assessed by spiking the known concentrations of SCN$^-$ (0.250 mmol L^{-1} and 1.000 mmol L^{-1}) in each real saliva sample and analyzed with both the proposed platform and the standard method. The result showed that the % recovery was in the range between 99.4 and 104.9 as shown in Table 5.3. Moreover, three blinded saliva samples (BS1-BS3) from The Institute of Biotechnology and Genetic Engineering, Chulalongkorn University (Thailand) were also evaluated using μpumpPAD and found that the %relative errors were less than 3.7% (n=3) (Table 5.4). Based on these results, the μpumpPAD demonstrated here can provide an excellent performance for a SCN$^-$ determination in the wide range of samples with good accuracy and precision.

Table 5.2 Summarized results of the determination of SCN⁻ in saliva samples using the micropumpPAD and conventional method (n = 3).

Sample	µpumpPAD Concentration ± SD (mmol L^{-1})			HPLC-UV-visible Concentration ± SD (mmol L^{-1})		
S1	*ND*			*ND*		
S2	*ND*			*ND*		
S3	*ND*			*ND*		
S4	*ND*			*ND*		
S5	*ND*			*ND*		
S6	0.084	±	0.001	0.087	±	0.001
S7	0.042	±	0.002	0.037	±	0.001
S8	0.024	±	0.002	0.024	±	0.002
S9 (smoker)	1.108	±	0.022	1.121	±	0.014
S10	0.014	±	0.003	0.014	±	0.001

*ND = non-detected

จุฬาลงกรณ์มหาวิทยาลัย

CHULALONGKORN UNIVERSITY

Table 5.3 Recovery tests of the proposed sensor for the determination of

SCN⁻ in saliva samples (n = 3).

Sample	Spike concentration (mmol L⁻¹)	colorimetric			electrochemical			%recovery
		$\bar{x}$	±	SD	$\bar{x}$	±	SD	
S1	-		ND			ND		-
	0.250		ND		0.256	±	0.001	102.5
	1.000	0.995	±	0.042		overloaded		99.5
S2	-		ND			ND		-
	0.250		ND		0.254	±	0.002	101.6
	1,000	0.999	±	0.030		overloaded		99.9
S3	-		ND			ND		-
	0.250		ND		0.246	±	0.013	98.4
	1.000	0.994	±	0.028		overloaded		99.4
S4	-		ND			ND		-
	0.250		ND		0.257	±	0.002	102.8
	1.000	1.001	±	0.048		overloaded		100.1
S5	-		ND			ND		-
	0.250		ND		0.265	±	0.003	104.7
	1.000	0.998	±	0.010		overloaded		99.4
S6	-		ND		0.048	±	0.001	-
	0.250		ND		0.311	±	0.002	104.9
	1.000	1.096	±	0.040		overloaded		104.7
S7	-		ND		0.022	±	0.001	-
	0.250		ND		0.276	±	0.001	101.4
	1.000	0.998	±	0.019		overloaded		99.4
S8	-		ND		0.011	±	0.001	-
	0.250		ND		0.258	±	0.007	98.8
	1.000	1.018	±	0.045		overloaded		100.7
S9	-		ND		0.096	±	0.002	-
	0.250		ND		0.350	±	0.001	101.8
	1.000	1.128	±	0.032		overloaded		103.3
S10	-		ND			ND		-
	0.250		ND		0.266	±	0.002	104.7
	1.000	1.008	±	0.040		overloaded		100.3

Table 5.4 Summarized results of the determination of SCN⁻ in the blinded

saliva samples using the μpumpPAD and conventional method (n = 3).

Samples	μpumpPAD			Concentration (revealed by provider after the test) (mmol L^{-1})	%Relative error
	Concentration ± SD				
	mmol L^{-1}				
BS1	58.19	±	2.74	60.0	3.0
BS2	82.99	±	3.99	80.0	3.7
BS3	15.16	±	0.76	15.0	1.1

5.1.4 Conclusion

The novel micro pumping on paper-based analytical device (μpumpPAD) for dual-mode (colorimetric and electrochemical) sensing of thiocyanate was fabricated to enhance the performance of SCN⁻ analysis in viscous saliva samples. To address for the biased colorimetric detection, the device was developed to improve the capillary transport in paper channel using laser engraving machine without sample preparation needed. Moreover, copper (II) phthalocyanine modified screen-printed graphene electrode (CuPc/SPGE) was employed to improve the detectability of thiocyanate by electrochemical method. An exceptionally wide dynamic range for SCN⁻ between 0.025 – 100 mmol L^{-1} was obtained over the two sensing modes. The μpumpPAD demonstrated here features a low cost and simple fabrication, portability, short-time analysis, and long-term stability. Additionally, benefitting from

the above advantages, we believed that the proposed μpumpPAD could serve as a prototype for a future development of analytical sensors for a series of biomarkers in viscous saliva sample.

CHAPTER 6

CONCLUSIONS AND FUTURE PERSPECTIVE

6.1 Conclusions

The conclusions were divided into four parts as follows;

Part I:

"Anodic stripping voltammetric determination of total arsenic using a gold nanoparticle-modified boron-doped diamond electrode on a paper-based device"

The multistep paper-based analytical device (mPAD) was designed to integrate the electrode modification and the electrochemical analysis process into a single device. An enhanced sensitivity for the determination of total arsenic was achieved using gold nanoparticles modified onto a boron-doped diamond electrode. The electrodeposition of gold nanoparticles onto boron-doped diamond electrode surface was performed in the modification zone before the measurement in the detection zone using the origami method. The linear range of 0.1 to 1.5 µg mL^{-1} and the limit of detection (3SD/slope) of 20 ng mL^{-1} for total arsenic detection was obtained. mPAD was successfully applied for the determination of total arsenic in rice samples with remarkable performance in terms of high accuracy, repeatability, reproducibility, selectivity, and portability.

Part II:

"Enhanced sensitivity and separation for simultaneous determination of tin and lead using paper-based sensors combined with a portable potentiostat"

The bismuth nanoparticle-modified screen-printed graphene electrode coupling with a portable potentiostat was developed for simultaneous detection of tin and lead. To address an overlapped peak caused by oxidation potentials of tin and lead, CTAB as additive could be employed to enhance sensitivity and peak resolution for the determination of both metals. The simple electrode fabrication was made using bismuth nanoparticles directly added into the conductive graphene ink and screen-printed onto the paper-based analytical device. The wide linearity of both metals was found to be from 10 to 250 ng mL^{-1}. The calculated limit of detection (3SD/slope) for tin and lead were as low as 0.26 ng mL^{-1} and 0.44 ng mL^{-1} respectively. The proposed device on PAD combined with a portable potentiostat is also capable of performing on-site analysis for simultaneous detection of tin and lead in food-canned samples.

Part III:

"Electrochemical detection of NOx gas based on disposable paper-based analytical device using a copper nanoparticles-modified screen-printed graphene electrode"

A novel electrochemical gas sensing unit on paper-based analytical device (gPAD) integrating the gas adsorbent and the electrochemical detection zone in a

single device using origami design was demonstrated. The activated carbon, as an absorber of NOx gas, was employed in this research because of its mesoporous structure. Besides, the use of copper nanoparticle-modified screen-printed graphene electrode further enhance the detection sensitivity of NOx gas. The proposed sensing platform is superior to the conventional counterparts in terms of the simple operation at room temperature and higher selectivity. The limits of detection were found to be 0.23 vppm and 0.03 vppm for the adsorption times of 25 min and 1 h, respectively. The designed device provides a new template model for other gas sensing with such beneficial features as portability and disposability for on-field analysis at low cost.

Part IV:

"Enhancing the capillary fluid transport using engraved microfluidic paper-based analytical device for dual mode sensing of thiocyanate in viscous samples"

The novel micro pumping on paper-based analytical device (μpumpPAD) for dual-mode (colorimetric and electrochemical) sensing of thiocyanate was fabricated to enhance the performance of thiocyanate analysis in viscous saliva samples. To address for the biased colorimetric detection, the device was developed to improve the capillary transport in paper channel using laser engraving machine without sample preparation needed. Moreover, copper (II) phthalocyanine modified screen-

printed graphene electrode (CuPc/SPGE) was employed to improve the detectability of thiocyanate by electrochemical method. The exceptionally wide dynamic range for thiocyanate between 0.025 – 100 mmol L^{-1} was obtained over the two sensing modes. The μpumpPAD demonstrated here features a low cost and simple fabrication, portability, short-time analysis, and long-term stability. Additionally, benefitting from the above advantages, we believed that the proposed μpumpPAD could serve as a prototype for a future development of analytical sensors for a series of biomarkers in viscous saliva sample.

6.2 Future perspective

The paper-based analytical device is clearly a very attractive tool due to the potential of its power-free capillary force and low-cost format. It is also a great promising to extend the use of ePAD with an appropriate design for a variety of analytes. Additionally, wireless communication technology such as NFC (near-field communication) technology available on almost every smartphones could be further coupled with the proposed device to facilitate the analysis and become more user-friendly platform.

REFERENCES

1.   Li, H.; Steckl, A. J., Paper Microfluidics for Point-of-Care Blood-Based Analysis and Diagnostics. *Analytical Chemistry* **2019,** *91* (1), 352-371.

2.   Rahbar, M.; Nesterenko, P. N.; Paull, B.; Macka, M., Geometrical Alignment of Multiple Fabrication Steps for Rapid Prototyping of Microfluidic Paper-Based Analytical Devices. *Analytical Chemistry* **2017,** *89* (22), 11918-11923.

3.   Nantaphol, S.; Channon, R. B.; Kondo, T.; Siangproh, W.; Chailapakul, O.; Henry, C. S., Boron Doped Diamond Paste Electrodes for Microfluidic Paper-Based Analytical Devices. *Analytical Chemistry* **2017,** *89* (7), 4100-4107.

4.   Chen, G.-H.; Chen, W.-Y.; Yen, Y.-C.; Wang, C.-W.; Chang, H.-T.; Chen, C.-F., Detection of Mercury(II) Ions Using Colorimetric Gold Nanoparticles on Paper-Based Analytical Devices. *Analytical Chemistry* **2014,** *86* (14), 6843-6849.

5.   Tian, T.; An, Y.; Wu, Y.; Song, Y.; Zhu, Z.; Yang, C., Integrated Distance-Based Origami Paper Analytical Device for One-Step Visualized Analysis. *ACS Applied Materials & Interfaces* **2017,** *9* (36), 30480-30487.

6.   e Silva, R. F.; Longo Cesar Paixão, T. R.; Der Torossian Torres, M.; de Araujo, W. R., Simple and inexpensive electrochemical paper-based analytical device for sensitive detection of Pseudomonas aeruginosa. *Sensors and Actuators B: Chemical* **2020,** *308*, 127669.

7.   Diouf, A.; Moufid, M.; Bouyahya, D.; Österlund, L.; El Bari, N.; Bouchikhi, B., An electrochemical sensor based on chitosan capped with gold nanoparticles combined with a voltammetric electronic tongue for quantitative aspirin detection in human physiological fluids and tablets. *Materials Science and Engineering: C* **2020,** *110*, 110665.

8.   Wu, S.; Li, K.; Dai, X.; Zhang, Z.; Ding, F.; Li, S., An ultrasensitive electrochemical platform based on imprinted chitosan/gold nanoparticles/graphene nanocomposite for sensing cadmium (II) ions. *Microchemical Journal* **2020,** *155*, 104710.

9.   Sahyar, B. Y.; Kaplan, M.; Ozsoz, M.; Celik, E.; Otles, S., Electrochemical xanthine detection by enzymatic method based on Ag doped ZnO nanoparticles by

using polypyrrole. *Bioelectrochemistry* **2019,** *130,* 107327.

10.   Singh, S.; Gill, A. A. S.; Nlooto, M.; Karpoormath, R., Prostate cancer biomarkers detection using nanoparticles based electrochemical biosensors. *Biosensors and Bioelectronics* **2019,** *137,* 213-221.

11.   Yu, H.; Li, C.; Tian, Y.; Jiang, X., Recent developments in determination and speciation of arsenic in environmental and biological samples by atomic spectrometry. *Microchemical Journal* **2020,** *152,* 104312.

12.   Kumar, S.; Prasad, S.; Yadav, K. K.; Shrivastava, M.; Gupta, N.; Nagar, S.; Bach, Q.-V.; Kamyab, H.; Khan, S. A.; Yadav, S.; Malav, L. C., Hazardous heavy metals contamination of vegetables and food chain: Role of sustainable remediation approaches - A review. *Environmental Research* **2019,** *179,* 108792.

13.   Leao, D. J.; Junior, M. M. S.; Brandao, G. C.; Ferreira, S. L. C., Simultaneous determination of cadmium, iron and tin in canned foods using high-resolution continuum source graphite furnace atomic absorption spectrometry. *Talanta* **2016,** *153,* 45-50.

14.   Bayhan, T.; Ünal, Ş.; Çırak, E.; Erdem, O.; Akay, C.; Gürsel, O.; Eker, İ.; Karabulut, E.; Gümrük, F., Heavy metal levels in patients with ineffective erythropoiesis. *Transfusion and Apheresis Science* **2017,** *56* (4), 539-543.

15.   Sodhi, K. K.; Kumar, M.; Agrawal, P. K.; Singh, D. K., Perspectives on arsenic toxicity, carcinogenicity and its systemic remediation strategies. *Environmental Technology & Innovation* **2019,** *16,* 100462.

16.   Borahan, T.; Unutkan, T.; Turan, N. B.; Turak, F.; Bakırdere, S., Determination of lead in milk samples using vortex assisted deep eutectic solvent based liquid phase microextraction-slotted quartz tube-flame atomic absorption spectrometry system. *Food Chemistry* **2019,** *299,* 125065.

17.   Juhászová, L.; Burhenn, S.; Sagapova, L.; Franzke, J.; Dědina, J.; Kratzer, J., Hydride generation atomic absorption spectrometry with a dielectric barrier discharge atomizer: Method optimization and evaluation of analytical performance for tin. *Spectrochimica Acta Part B: Atomic Spectroscopy* **2019,** *158,* 105630.

18.   Proch, J.; Niedzielski, P., In–spray chamber hydride generation by multi–mode

sample introduction system (MSIS) as an interface in the hyphenated system of high performance liquid chromatography and inductivity coupled plasma optical emission spectrometry (HPLC/HG–ICP–OES) in arsenic species determination. *Talanta* **2020,** *208,* 120395.

19.   Pereira, J. S. F.; Moraes, D. P.; Antes, F. G.; Diehl, L. O.; Santos, M. F. P.; Guimarães, R. C. L.; Fonseca, T. C. O.; Dressler, V. L.; Flores, É. M. M., Determination of metals and metalloids in light and heavy crude oil by ICP-MS after digestion by microwave-induced combustion. *Microchemical Journal* **2010,** *96* (1), 4-11.

20.   Prada, D.; López, G.; Solleiro-Villavicencio, H.; Garcia-Cuellar, C.; Baccarelli, A. A., Molecular and cellular mechanisms linking air pollution and bone damage. *Environmental Research* **2020,** *185,* 109465.

21.   Cui, P.-Y.; Zhang, J.-H.; Wu, Y.-P.; Zhang, Y.; Zhou, J.-Z.; Luo, Y.; Huang, Y.-D., Wind-tunnel measurements and LES simulations of air pollutant dispersion caused by fire-induced buoyancy plume inside two parallel street canyons. *Process Safety and Environmental Protection* **2020,** *140,* 151-169.

22.   Adhikari, A., Chapter 1 - Introduction to spatiotemporal variations of ambient air pollutants and related public health impacts. In *Spatiotemporal Analysis of Air Pollution and Its Application in Public Health*, Li, L.; Zhou, X.; Tong, W., Eds. Elsevier: 2020; pp 1-34.

23.   Schepers, D.; Schulze, G.; Frenzel, W., Spectrophotometric flow-through gas sensor for the determination of atmospheric nitrogen dioxide. *Analytica Chimica Acta* **1995,** *308* (1), 109-114.

24.   Zhu, Y.; Shi, J.; Zhang, Z.; Zhang, C.; Zhang, X., Development of a Gas Sensor Utilizing Chemiluminescence on Nanosized Titanium Dioxide. *Analytical Chemistry* **2002,** *74* (1), 120-124.

25.   Bessler, W. G.; Schulz, C.; Lee, T.; Jeffries, J. B.; Hanson, R. K., Carbon dioxide UV laser-induced fluorescence in high-pressure flames. *Chemical Physics Letters* **2003,** *375* (3), 344-349.

26.   Zhou, Y.; Jiang, Y.; Xie, T.; Tai, H.; Xie, G., A novel sensing mechanism for resistive gas sensors based on layered reduced graphene oxide thin films at room temperature. *Sensors and Actuators B: Chemical* **2014,** *203*, 135-142.

27.   Zhang, W.; Du, Y.; Wang, M. L., Noninvasive glucose monitoring using saliva nano-biosensor. *Sensing and Bio-Sensing Research* **2015,** *4*, 23-29.

28.   Carrilho, E.; Martinez, A. W.; Whitesides, G. M., Understanding Wax Printing: A Simple Micropatterning Process for Paper-Based Microfluidics. *Analytical Chemistry* **2009,** *81* (16), 7091-7095.

29.   Bard, A. J.; Faulkner, L. R.; Leddy, J.; Zoski, C. G., *Electrochemical methods: fundamentals and applications*. wiley New York: 1980; Vol. 2.

30.   Ciobanu, M.; Wilburn, J. P.; Krim, M. L.; Cliffel, D. E., 1 - Fundamentals. In *Handbook of Electrochemistry*, Zoski, C. G., Ed. Elsevier: Amsterdam, 2007; pp 3-29.

31.   Oberacher, H.; Pitterl, F.; Erb, R.; Plattner, S., Mass spectrometric methods for monitoring redox processes in electrochemical cells. *Mass Spectrom Rev* **2015,** *34* (1), 64-92.

32.   Skoog, D. A., *Fundamentals of Analytical Chemistry*. Thomson-Brooks/Cole: 2004.

33.   Skoog, D. A.; Holler, F. J.; Crouch, S. R., *Principles of Instrumental Analysis*. Thomson Brooks/Cole: 2007.

34.   Zelić, M., Reverse scan as a source of information in square wave voltammetry. *Croatica chemica acta* **2006,** *79* (1), 49-55.

35.   Tayyab Raza Naqvi, S.; Rasheed, T.; Naeem Ashiq, M.; Najam ul Haq, M.; Majeed, S.; Fatima, B.; Nawaz, R.; Hussain, D.; Shafi, S., Fabrication of iron modified screen printed carbon electrode for sensing of amino acids. *Polyhedron* **2020,** *180*, 114426.

36.   Charoenkitamorn, K.; Chaiyo, S.; Chailapakul, O.; Siangproh, W., Low-cost and disposable sensors for the simultaneous determination of coenzyme Q10 and α-lipoic acid using manganese (IV) oxide-modified screen-printed graphene electrodes. *Analytica Chimica Acta* **2018,** *1004*, 22-31.

37.   Mohamed, H. M., Screen-printed disposable electrodes: Pharmaceutical applications and recent developments. *TrAC Trends in Analytical Chemistry* **2016,** *82*, 1-11.

38.   Arsenic compounds. Toxnet toxicology Data Network: 2010.

39.   Teixeira, M. C.; Tavares, E. d. F. L.; Saczk, A. A.; Okumura, L. L.; Cardoso, M. d. G.; Magriotis, Z. M.; de Oliveira, M. F., Cathodic stripping voltammetric determination of arsenic in sugarcane brandy at a modified carbon nanotube paste electrode. *Food Chemistry* **2014,** *154*, 38-43.

40.   Macedo, S. M.; de Jesus, R. M.; Garcia, K. S.; Hatje, V.; de S. Queiroz, A. F.; Ferreira, S. L. C., Determination of total arsenic and arsenic (III) in phosphate fertilizers and phosphate rocks by HG-AAS after multivariate optimization based on Box-Behnken design. *Talanta* **2009,** *80* (2), 974-979.

41.   Jia, X.; Gong, D.; Wang, J.; Huang, F.; Duan, T.; Zhang, X., Arsenic speciation in environmental waters by a new specific phosphine modified polymer microsphere preconcentration and HPLC–ICP-MS determination. *Talanta* **2016,** *160*, 437-443.

42.   Luo, J.; Xu, F.; Hu, J.; Lin, P.; Tu, J.; Wu, X.; Hou, X., Preconcentration on metal organic framework UiO-66 for slurry sampling hydride generation-atomic fluorescence spectrometric determination of ultratrace arsenic. *Microchemical Journal* **2017,** *133*, 441-447.

43.   Guo, Z.; Yang, M.; Huang, X.-J., Recent developments in electrochemical determination of arsenic. *Current Opinion in Electrochemistry* **2017,** *3* (1), 130-136.

44.   Li, X.; Zhou, H.; Fu, C.; Wang, F.; Ding, Y.; Kuang, Y., A novel design of engineered multi-walled carbon nanotubes material and its improved performance in simultaneous detection of Cd(II) and Pb(II) by square wave anodic stripping voltammetry. *Sensors and Actuators B: Chemical* **2016,** *236*, 144-152.

45.   Rosolina, S. M.; Chambers, J. Q.; Lee, C. W.; Xue, Z.-L., Direct determination of cadmium and lead in pharmaceutical ingredients using anodic stripping voltammetry in aqueous and DMSO/water solutions. *Analytica Chimica Acta* **2015,** *893*, 25-33.

46.   Herzog, G.; Moujahid, W.; Twomey, K.; Lyons, C.; Ogurtsov, V. I., On-chip electrochemical microsystems for measurements of copper and conductivity in artificial seawater. *Talanta* **2013,** *116*, 26-32.

47.   Rodrigues, J. A.; Rodrigues, C. M.; Almeida, P. J.; Valente, I. M.; Gonçalves, L. M.; Compton, R. G.; Barros, A. A., Increased sensitivity of anodic stripping voltammetry at the hanging mercury drop electrode by ultracathodic deposition. *Analytica Chimica Acta* **2011,** *701* (2), 152-156.

48.   Wang, W.; Bai, H.; Li, H.; Lv, Q.; Zhang, Q.; Bao, N., Carbon tape coated with gold film as stickers for bulk fabrication of disposable gold electrodes to detect Cr(VI). *Sensors and Actuators B: Chemical* **2016,** *236*, 218-225.

49.   Punrat, E.; Chuanuwatanakul, S.; Kaneta, T.; Motomizu, S.; Chailapakul, O., Method development for the determination of arsenic by sequential injection/anodic stripping voltammetry using long-lasting gold-modified screen-printed carbon electrode. *Talanta* **2013,** *116*, 1018-1025.

50.   Song, Y.; Swain, G. M., Total inorganic arsenic detection in real water samples using anodic stripping voltammetry and a gold-coated diamond thin-film electrode. *Analytica Chimica Acta* **2007,** *593* (1), 7-12.

51.   Carrera, P.; Espinoza-Montero, P. J.; Fernández, L.; Romero, H.; Alvarado, J., Electrochemical determination of arsenic in natural waters using carbon fiber ultra-microelectrodes modified with gold nanoparticles. *Talanta* **2017,** *166*, 198-206.

52.   Idris, A. O.; Mabuba, N.; Arotiba, O. A., Electrochemical co-detection of Arsenic and Selenium on a Glassy Carbon Electrode Modified with Gold Nanoparticles. *International Journal of Electrochemical Science* **2017,** *12* (1), 10-21.

53.   Idris, A. O.; Mafa, J. P.; Mabuba, N.; Arotiba, O. A., Nanogold modified glassy carbon electrode for the electrochemical detection of arsenic in water. *Russian Journal of Electrochemistry* **2017,** *53* (2), 170-177.

54.   Kit-Anan, W.; Olarnwanich, A.; Sriprachuabwong, C.; Karuwan, C.; Tuantranont, A.; Wisitsoraat, A.; Srituravanich, W.; Pimpin, A., Disposable paper-based electrochemical sensor utilizing inkjet-printed Polyaniline modified screen-printed carbon electrode for Ascorbic acid detection. *Journal of Electroanalytical Chemistry* **2012,** *685*, 72-78.

55.   Ma, C.; Li, W. P.; Kong, Q. K.; Yang, H. M.; Bian, Z. Q.; Song, X. R.; Yu, J. H.; Yan, M., 3D origami electrochemical immunodevice for sensitive point-of-care testing based on dual-signal amplification strategy. *Biosens. Bioelectron.* **2015,** *63*, 7-13.

56.   Nantaphol, S.; Chailapakul, O.; Siangproh, W., A novel paper-based device coupled with a silver nanoparticle-modified boron-doped diamond electrode for cholesterol detection. *Analytica Chimica Acta* **2015,** *891*, 136-143.

57.   Liu, H.; Xiang, Y.; Lu, Y.; Crooks, R. M., Aptamer-Based Origami Paper Analytical

Device for Electrochemical Detection of Adenosine. *Angewandte Chemie International Edition* **2012,** *51* (28), 6925-6928.

58.　　Anezaki, K.;　Nukatsuka, I.; Ohzeki, K., Determination of arsenic(III) and total arsenic(III,V) in water samples by resin suspension graphite furnace atomic absorption spectrometry. *Analytical Sciences* **1999,** *15* (9), 829-834.

59.　　Paik, M.-K.; Kim, M.-J.; Kim, W.-I.; Yoo, J.-H.; Park, B.-J.; Im, G.-J.; Park, J.-E.; Hong, M.-K., Determination of arsenic species in polished rice using a methanol-water digestion method. *Journal of the Korean Society for Applied Biological Chemistry* **2010,** *53* (5), 634-638.

60.　　Cui, H.; Yang, W.; Li, X.; Zhao, H.; Yuan, Z., An electrochemical sensor based on a magnetic Fe3O4 nanoparticles and gold nanoparticles modified electrode for sensitive determination of trace amounts of arsenic(iii). *Analytical Methods* **2012,** *4* (12), 4176-4181.

61.　　Alvarado-Gamez, A. L.; Alonso-Lomillo, M. A.; Dominguez-Renedo, O.; Arcos-Martinez, M. J., Vanadium determination in water using alkaline phosphatase based screen-printed carbon electrodes modified with gold nanoparticles. *Journal of Electroanalytical Chemistry* **2013,** *693*, 51-55.

62.　　Yamada, D.; Ivandini, T. A.; Komatsu, M.; Fujishima, A.; Einaga, Y., Anodic stripping voltammetry of inorganic species of As3+ and As5+ at gold-modified boron doped diamond electrodes. *Journal of Electroanalytical Chemistry* **2008,** *615* (2), 145-153.

63.　　Davis, P. H.; Dulude, G. R.; Griffin, R. M.; Matson, W. R.; Zink, E. W., Determination of total arsenic at the nanogram level by high-speed anodic stripping voltammetry. *Analytical Chemistry* **1978,** *50* (1), 137-143.

64.　　Ramanavicius, A.; German, N.; Ramanaviciene, A., Evaluation of Electron Transfer in Electrochemical System Based on Immobilized Gold Nanoparticles and Glucose Oxidase. *Journal of The Electrochemical Society* **2017,** *164* (4), G45-G49.

65.　　Long, G. L.; Winefordner, J. D., Limit of Detection A Closer Look at the IUPAC Definition. *Analytical Chemistry* **1983,** *55* (07), 712A-724A.

66.　　Administration, U. S. F. a. D., Analytical results from inorganic arsenic in rice and rice products sampling. 2013.

67. Ahmad, H.; Ahmad, A.; Islam, S. S., Magnetic Fe 3 O 4@ poly (methacrylic acid) particles for selective preconcentration of trace arsenic species. *Microchimica Acta* **2017,** *184* (7), 2007-2014.

68. Hassanpoor, S.; Khayatian, G.; Judy Azar, A. R., Ultra-trace determination of arsenic species in environmental waters, food and biological samples using a modif ied aluminum oxide nanoparticle sorbent and AAS detection after multivariate optimization. *Microchimica Acta* **2015,** *182*.

69. Sanghavi, B. J.; Gadhari, N. S.; Kalambate, P. K.; Karna, S. P.; Srivastava, A. K., Potentiometric stripping analysis of arsenic using a graphene paste electrode modified with a thiacrown ether and gold nanoparticles. *Microchimica Acta* **2015,** *182* (7), 1473-1481.

70. Lan, Y.; Luo, H.; Ren, X.; Wang, Y.; Liu, Y., Anodic stripping voltammetric determination of arsenic(III) using a glassy carbon electrode modified with gold-palladium bimetallic nanoparticles. *Microchimica Acta* **2012,** *178* (1), 153-161.

71. Kadara, R. O.; Tothill, I. E., Resolving the copper interference effect on the stripping chronopotentiometric response of lead(II) obtained at bismuth film screen-printed electrode. *Talanta* **2005,** *66* (5), 1089-1093.

72. Massadeh, A. M.; Al-Massaedh, A. A. T., Determination of heavy metals in canned fruits and vegetables sold in Jordan market. *Environmental Science and Pollution Research* **2018,** *25* (2), 1914-1920.

73. Palisoc, S. T.; Bentulan, J. M. O.; Natividad, M. T., Determination of trace heavy metals in canned food using Graphene/AuNPs/[Ru(NH3)6]3+/Nafion modified glassy carbon electrodes. *Journal of Food Measurement and Characterization* **2019,** *13* (1), 169-176.

74. Fiamegos, Y.; Vahcic, M.; Emteborg, H.; Snell, J.; Raber, G.; Cordeiro, F.; Robouch, P.; de la Calle, B., Determination of toxic trace elements in canned vegetables. The importance of sample preparation. *TrAC Trends in Analytical Chemistry* **2016,** *85*, 57-66.

75. Cima, F., Tin: Environmental Pollution and Health Effects☆. In *Reference Module in Earth Systems and Environmental Sciences*, Elsevier: 2018.

76.   Njati, S. Y.; Maguta, M. M., Lead-based paints and children's PVC toys are potential sources of domestic lead poisoning – A review. *Environmental Pollution* **2019,** *249*, 1091-1105.

77.   Blunden, S.; Wallace, T., Tin in canned food: a review and understanding of occurrence and effect. *Food and Chemical Toxicology* **2003,** *41* (12), 1651-1662.

78.   Noureddine El Moussawi, S.; Ouaini, R.; Matta, J.; Chébib, H.; Cladière, M.; Camel, V., Simultaneous migration of bisphenol compounds and trace metals in canned vegetable food. *Food Chemistry* **2019,** *288*, 228-238.

79.   Park, Y. M.; Choi, J. Y.; Nho, E. Y.; Lee, C. M.; Hwang, I. M.; Khan, N.; Jamila, N.; Kim, K. S., Determination of macro and trace elements in canned marine products by inductively coupled plasmaoptical emission spectrometry (ICP-OES) and ICPmass spectrometry (ICP-MS). *Analytical Letters* **2019,** *52* (6), 1018-1030.

80.   Gray, P. J.; Cunningham, W., Inductively Coupled Plasma Collision Cell Quadrupole Mass Spectrometric Determination of Extractible Arsenic, Cadmium, Chromium, Lead, Mercury, and Other Elements in Food Using Microwave-Assisted Digestion: Results from an FDA Interlaboratory Study. *Journal of Aoac International* **2019,** *102* (2), 590-604.

81.   Pungjunun, K.; Chaiyo, S.; Jantrahong, I.; Nantaphol, S.; Siangproh, W.; Chailapakul, O., Anodic stripping voltammetric determination of total arsenic using a gold nanoparticle-modified boron-doped diamond electrode on a paper-based device. *Microchimica Acta* **2018,** *185* (7), 8.

82.   Deng, M. H.; Liao, C. H.; Wang, X. F.; Chen, S. D.; Qi, F. G.; Zhao, X. L.; Yu, P., A paper-based colorimetric microfluidic sensor fabricated by a novel spray painting prototyping process for iron analysis. *Canadian Journal of Chemistry* **2019,** *97* (5), 373-377.

83.   Ding, R.; Krikstolaityte, V.; Lisak, G., Inorganic salt modified paper substrates utilized in paper based microfluidic sampling for potentiometric determination of heavy metals. *Sensors and Actuators B: Chemical* **2019,** *290*, 347-356.

84.   Ding, J.; He, N.; Lisak, G.; Qin, W.; Bobacka, J., Paper-based microfluidic sampling and separation of analytes for potentiometric ion sensing. *Sensors and Actuators B: Chemical* **2017,** *243*, 346-352.

85. Lisak, G.; Cui, J.; Bobacka, J., Paper-based microfluidic sampling for potentiometric determination of ions. *Sensors and Actuators B: Chemical* **2015,** *207,* 933-939.

86. Sun, X.; Li, B.; Qi, A.; Tian, C.; Han, J.; Shi, Y.; Lin, B.; Chen, L., Improved assessment of accuracy and performance using a rotational paper-based device for multiplexed detection of heavy metals. *Talanta* **2018,** *178,* 426-431.

87. Cruz-Hernandez, Y.; Villalobos, M.; Gonzalez-Chavez, J. L.; Martinez-Villegas, N., OPTIMIZING THE DIFFERENTIAL PULSE ANODIC STRIPPING VOLTAMMETRY METHOD WITH A HANGING MERCURY ELECTRODE FOR THALLIUM (I) DETERMINATION IN THE PRESENCE OF LEAD (II) AND COPPER (II) FOR APPLICATION IN CONTAMINATED SOILS. *Revista Internacional De Contaminacion Ambiental* **2019,** *35* (2), 481-494.

88. Arancibia, V.; Nagles, E.; Garcia-Beltran, O.; Hurtado, J., Adsorptive Stripping Voltammetric Determination of Lead and Cadmium in Natural Waters in the Presence of Rutin Using a Nafion-Mercury Coated Film Electrode. *International Journal of Electrochemical Science* **2018,** *13* (9), 8711-8722.

89. Vollset, M.; Iszatt, N.; Enger, O.; Gjengedal, E. L. F.; Eggesbo, M., Concentration of mercury, cadmium, and lead in breast milk from Norwegian mothers: Association with dietary habits, amalgam and other factors. *Science of the Total Environment* **2019,** *677,* 466-473.

90. Palisoc, S.; Sow, V. A.; Natividad, M., Fabrication of a bismuth nanoparticle/Nafion modified screen-printed graphene electrode for in situ environmental monitoring. *Analytical Methods* **2019,** *11* (12), 1591-1603.

91. Shiba, S.; Takahashi, S.; Kamata, T.; Hachiya, H.; Kato, D.; Niwa, O., Selective Au Electrodeposition on Au Nanoparticles Embedded in Carbon Film Electrode for Se(IV) Detection. *Sensors and Materials* **2019,** *31* (4), 1135-1146.

92. Palisoc, S. T.; Natividad, M. T.; De Jesus, N.; Carlos, J., Highly Sensitive AgNP/MWCNT/Nafion Modified GCE-Based Sensor for the Determination of Heavy Metals in Organic and Non-organic Vegetables. *Scientific Reports* **2018,** *8*.

93. Yakoh, A.; Chaiyo, S.; Siangproh, W.; Chailapakul, O., 3D Capillary-Driven Paper-Based Sequential Microfluidic Device for Electrochemical Sensing Applications. *ACS Sensors* **2019,** *4* (5), 1211-1221.

94. Nantaphol, S.; Kava, A. A.; Channon, R. B.; Kondo, T.; Siangproh, W.; Chailapakul, O.; Henry, C. S., Janus electrochemistry: Simultaneous electrochemical detection at multiple working conditions in a paper-based analytical device. *Analytica Chimica Acta* **2019**, *1056*, 88-95.

95. Jadon, N.; Jain, R.; Sharma, S.; Singh, K., Recent trends in electrochemical sensors for multianalyte detection - A review. *Talanta* **2016**, *161*, 894-916.

96. Qu, S.; Wang, J.; Kong, J.; Yang, P.; Chen, G., Magnetic loading of carbon nanotube/nano-Fe3O4 composite for electrochemical sensing. *Talanta* **2007,** *71* (3), 1096-1102.

97. Méndez, J. H.; Martínez, R. C.; López, M. E. G., Simultaneous determination of tin and lead by a.c. anodic stripping voltammetry at a hanging mercury drop electrode sensitized by cetyltrimethylammoniu. *Analytica Chimica Acta* **1982**, *138*, 47-54.

98. Yang, D.; Wang, L.; Chen, Z. L.; Megharaj, M.; Naidu, R., Anodic stripping voltammetric determination of traces of Pb(II) and Cd(II) using a glassy carbon electrode modified with bismuth nanoparticles. *Microchimica Acta* **2014,** *181* (11-12), 1199-1206.

99. Vittal, R.; Gomathi, H.; Kim, K.-J., Beneficial role of surfactants in electrochemistry and in the modification of electrodes. *Advances in Colloid and Interface Science* **2006,** *119* (1), 55-68.

100. Ciavatta, L.; De Tommaso, G.; Iuliano, M., A potentiometric study on oxalate and citrate complexes of tin(II). *Annali Di Chimica* **2001,** *91* (5-6), 285-293.

101. Klatt, L. N., Complex formation in lead oxalate solutions. *Analytical Chemistry* **1970,** *42* (14), 1837-1839.

102. Stadlober, M.; Kalcher, K.; Raber, G., Anodic stripping voltammetric determination of vanadium(V) using a carbon paste electrode modified in situ with cetyltrimethylammonium bromide. *Electroanalysis* **1997,** *9* (3), 225-230.

103. Tang, W. X.; Bin, J.; Fan, W.; Zhang, Z. M.; Yun, Y. H.; Liang, Y. Z., Simultaneous determination of lead and tin at the bismuth film electrode by square wave stripping voltammetry and chemometric methods. *Analytical Methods* **2016,** *8* (27), 5475-5486.

104. Chomisteková, Z.; Culková, E.; Vojtko, J.; Brescher, R.; Tomčík, P., Voltammetric behavior of I2/2I− redox system on boron-doped diamond electrode in various media and its utilization for the indirect detection of tin(II). *Journal of Electroanalytical*

Chemistry **2015,** *758*, 46-53.

105.   Pourshirband, N.; Nezamzadeh-Ejhieh, A., Experimental design on determination of Sn(II) by the modified carbon paste electrode with Fe(II)-exchanged clinoptilolite nanoparticles. *Solid State Sciences* **2020,** *99*, 106082.

106.   Hwang, J.-H.; Wang, X.; Zhao, D.; Rex, M. M.; Cho, H. J.; Lee, W. H., A novel nanoporous bismuth electrode sensor for in situ heavy metal detection. *Electrochimica Acta* **2019,** *298*, 440-448.

107.   Niu, P.; Fernández-Sánchez, C.; Gich, M.; Navarro-Hernández, C.; Fanjul-Bolado, P.; Roig, A., Screen-printed electrodes made of a bismuth nanoparticle porous carbon nanocomposite applied to the determination of heavy metal ions. *Microchimica Acta* **2016,** *183* (2), 617-623.

108.   Jeong, H.-S.; Park, M.-J.; Kwon, S.-H.; Joo, H.-J.; Kwon, H.-I., Highly sensitive and selective room-temperature NO2 gas-sensing characteristics of SnOX-based p-type thin-film transistor. *Sensors and Actuators B: Chemical* **2019,** *288*, 625-633.

109.   Song, Y.; Chen, F.; Zhang, Y.; Zhang, S.; Liu, F.; Sun, P.; Yan, X.; Lu, G., Fabrication of highly sensitive and selective room-temperature nitrogen dioxide sensors based on the ZnO nanoflowers. *Sensors and Actuators B: Chemical* **2019,** *287*, 191-198.

110.   Izumi, K.; Utiyama, M.; Maruo, Y. Y., Colorimetric NOx sensor based on a porous glass-based NO2 sensing chip and a permanganate oxidizer. *Sensors and Actuators B: Chemical* **2015,** *216*, 128-133.

111.   Allen, C.; Carrico, C. M.; Gomez, S. L.; Andersen, P. C.; Turnipseed, A. A.; Williford, C. J.; Birks, J. W.; Salisbury, D.; Carrion, R.; Gates, D.; Macias, F.; Rahn, T.; Aiken, A. C.; Dubey, M. K., NOx instrument intercomparison for laboratory biomass burning source studies and urban ambient measurements in Albuquerque, New Mexico. *Journal of the Air & Waste Management Association* **2018,** *68* (11), 1175-1189.

112.   Hoa, N. D.; El-Safty, S. A., Synthesis of Mesoporous NiO Nanosheets for the Detection of Toxic NO2 Gas. *Chemistry – A European Journal* **2011,** *17* (46), 12896-12901.

113.   Passaretti Filho, J.; da Silveira Petruci, J. F.; Cardoso, A. A., Development of a simple method for determination of NO2 in air using digital scanner images. *Talanta* **2015,** *140*, 73-80.

114. Jung, J.; Lee, J.; Kim, B.; Oh, S., Seasonal variations in the NO2 artifact from chemiluminescence measurements with a molybdenum converter at a suburban site in Korea (downwind of the Asian continental outflow) during 2015–2016. *Atmospheric Environment* **2017,** *165*, 290-300.

115. Thornton, J. A.; Wooldridge, P. J.; Cohen, R. C., Atmospheric NO2: In Situ Laser-Induced Fluorescence Detection at Parts per Trillion Mixing Ratios. *Analytical Chemistry* **2000,** *72* (3), 528-539.

116. Rajesh, N.; Kannan, J. C.; Leonardi, S. G.; Neri, G.; Krishnakumar, T., Investigation of CdO nanostructures synthesized by microwave assisted irradiation technique for NO2 gas detection. *Journal of Alloys and Compounds* **2014,** *607*, 54-60.

117. Deng, S.; Tjoa, V.; Fan, H. M.; Tan, H. R.; Sayle, D. C.; Olivo, M.; Mhaisalkar, S.; Wei, J.; Sow, C. H., Reduced Graphene Oxide Conjugated Cu2O Nanowire Mesocrystals for High-Performance NO2 Gas Sensor. *Journal of the American Chemical Society* **2012,** *134* (10), 4905-4917.

118. Gomes, F. O.; Maia, L. B.; Loureiro, J. A.; Pereira, M. C.; Delerue-Matos, C.; Moura, I.; Moura, J. J. G.; Morais, S., Biosensor for direct bioelectrocatalysis detection of nitric oxide using nitric oxide reductase incorporated in carboxylated single-walled carbon nanotubes/lipidic 3 bilayer nanocomposite. *Bioelectrochemistry* **2019,** *127*, 76-86.

119. Lu, L., Highly sensitive detection of nitrite at a novel electrochemical sensor based on mutually stabilized Pt nanoclusters doped CoO nanohybrid. *Sensors and Actuators B: Chemical* **2019,** *281*, 182-190.

120. Dumitrescu, E.; Wallace, K. N.; Andreescu, S., Real time electrochemical investigation of the release, distribution and modulation of nitric oxide in the intestine of individual zebrafish embryos. *Nitric Oxide* **2018,** *74*, 32-38.

121. Brown, M. D.; Schoenfisch, M. H., Catalytic selectivity of metallophthalocyanines for electrochemical nitric oxide sensing. *Electrochimica Acta* **2018,** *273*, 98-104.

122. Dungchai, W.; Chailapakul, O.; Henry, C. S., Electrochemical Detection for Paper-Based Microfluidics. *Analytical Chemistry* **2009,** *81* (14), 5821-5826.

123. Chaiyo, S.; Mehmeti, E.; Siangproh, W.; Hoang, T. L.; Nguyen, H. P.;

Chailapakul, O.; Kalcher, K., Non-enzymatic electrochemical detection of glucose with a disposable paper-based sensor using a cobalt phthalocyanine–ionic liquid–graphene composite. *Biosensors and Bioelectronics* **2018,** *102,* 113-120.

124.   Arduini, F.; Cinti, S.; Caratelli, V.; Amendola, L.; Palleschi, G.; Moscone, D., Origami multiple paper-based electrochemical biosensors for pesticide detection. *Biosensors and Bioelectronics* **2019,** *126,* 346-354.

125.   Rattanarat, P.; Dungchai, W.; Cate, D.; Volckens, J.; Chailapakul, O.; Henry, C. S., Multilayer Paper-Based Device for Colorimetric and Electrochemical Quantification of Metals. *Analytical Chemistry* **2014,** *86* (7), 3555-3562.

126.   Ma, C.; Li, W.; Kong, Q.; Yang, H.; Bian, Z.; Song, X.; Yu, J.; Yan, M., 3D origami electrochemical immunodevice for sensitive point-of-care testing based on dual-signal amplification strategy. *Biosensors and Bioelectronics* **2015,** *63,* 7-13.

127.   Sun, X.; Li, B.; Tian, C.; Yu, F.; Zhou, N.; Zhan, Y.; Chen, L., Rotational paper-based electrochemiluminescence immunodevices for sensitive and multiplexed detection of cancer biomarkers. *Analytica Chimica Acta* **2018,** *1007,* 33-39.

128.   Moreira, C. M.; Pereira, S. V.; Raba, J.; Bertolino, F. A.; Messina, G. A., Paper-based enzymatic platform coupled to screen printed graphene-modified electrode for the fast neonatal screening of phenylketonuria. *Clinica Chimica Acta* **2018,** *486,* 59-65.

129.   Panraksa, Y.; Siangproh, W.; Khampieng, T.; Chailapakul, O.; Apilux, A., Paper-based amperometric sensor for determination of acetylcholinesterase using screen-printed graphene electrode. *Talanta* **2018,** *178,* 1017-1023.

130.   Manoj, D.; Saravanan, R.; Santhanalakshmi, J.; Agarwal, S.; Gupta, V. K.; Boukherroub, R., Towards green synthesis of monodisperse Cu nanoparticles: An efficient and high sensitive electrochemical nitrite sensor. *Sensors and Actuators B: Chemical* **2018,** *266,* 873-882.

131.   Zhang, J.; Ma, J.; Zhang, S.; Wang, W.; Chen, Z., A highly sensitive nonenzymatic glucose sensor based on CuO nanoparticles decorated carbon spheres. *Sensors and Actuators B: Chemical* **2015,** *211,* 385-391.

132.   Prakash, S.; Rajesh, S.; Singh, S. K.; Bhargava, K.; Ilavazhagan, G.; Vasu, V.; Karunakaran, C., Copper nanoparticles entrapped in SWCNT-PPy nanocomposite on Pt electrode as NOx electrochemical sensor. *Talanta* **2011,** *85* (2), 964-969.

133.   Ghouma, I.; Jeguirim, M.; Dorge, S.; Limousy, L.; Matei Ghimbeu, C.; Ouederni, A., Activated carbon prepared by physical activation of olive stones for the removal of NO2 at ambient temperature. *Comptes Rendus Chimie* **2015,** *18* (1), 63-74.

134.   Belhachemi, M.; Jeguirim, M.; Limousy, L.; Addoun, F., Comparison of NO2 removal using date pits activated carbon and modified commercialized activated carbon via different preparation methods: Effect of porosity and surface chemistry. *Chemical Engineering Journal* **2014,** *253*, 121-129.

135.   Suryaraman, M. G.; Viswanathan, A., Preparation of nitric oxide: some laboratory methods. *Journal of Chemical Education* **1949,** *26* (11), 594.

136.   Lee, Y.-W.; Kim, H.-J.; Park, J.-W.; Choi, B.-U.; Choi, D.-K.; Park, J.-W., Adsorption and reaction behavior for the simultaneous adsorption of NO–NO2 and SO2 on activated carbon impregnated with KOH. *Carbon* **2003,** *41* (10), 1881-1888.

137.   Kuang, P.; Natsui, K.; Einaga, Y., Comparison of performance between boron-doped diamond and copper electrodes for selective nitrogen gas formation by the electrochemical reduction of nitrate. *Chemosphere* **2018,** *210*, 524-530.

138.   Jafari, M. T.; Javaheri, M., Selective Method Based on Negative Electrospray Ionization Ion Mobility Spectrometry for Direct Analysis of Salivary Thiocyanate. *Analytical Chemistry* **2010,** *82* (15), 6721-6725.

139.   Wang, Z.; Zhang, J.; Tian, Z.; Wang, Z.; Li, Y.; Liang, S.; Cui, L.; Zhang, L.; Zhang, H.; Yang, B., Organic–inorganic hybrid photonic hydrogels as a colorful platform for visual detection of SCN−. *Chemical Communications* **2010,** *46* (45), 8636-8638.

140.   Lv, J.; Chen, D.; Du, Y.; Wang, T.; Zhang, X.; Li, Y.; Zhang, L.; Wang, Y.; Jordan, R.; Fu, Y., Visual Detection of Thiocyanate Based on Fabry–Perot Etalons with a Responsive Polymer Brush as the Transducer. *ACS Sensors* **2020,** *5* (2), 303-307.

141.   Laurberg, P.; Pedersen, I. B.; Carlé, A.; Andersen, S.; Knudsen, N.; Karmisholt, J., Chapter 28 - The Relationship between Thiocyanate and Iodine. In *Comprehensive Handbook of Iodine*, Preedy, V. R.; Burrow, G. N.; Watson, R., Eds. Academic Press: San Diego, 2009; pp 275-281.

142.   Madiyal, A.; Ajila, V.; Babu, S. G.; Hegde, S.; Kumari, S.; Madi, M.; Achalli, S.; Alva, P.; Ullal, H., Status of thiocyanate levels in the serum and saliva of non-smokers, ex-smokers and smokers. *Afr Health Sci* **2018,** *18* (3), 727-736.

143.   Pienpinijtham, P.; Han, X. X.; Ekgasit, S.; Ozaki, Y., Highly Sensitive and Selective Determination of Iodide and Thiocyanate Concentrations Using Surface-Enhanced Raman Scattering of Starch-Reduced Gold Nanoparticles. *Analytical Chemistry* **2011,** *83* (10), 3655-3662.

144.   Gavrilenko, N. A.; Volgina, T. N.; Urazov, E. V.; Gavrilenko, M. A., Transparent polymer sensor for visual and photometrical detection of thiocyanate in oilfield water. *Journal of Petroleum Science and Engineering* **2019,** *172*, 960-963.

145.   Hussain, A.; Pu, H.; Sun, D.-W., SERS detection of sodium thiocyanate and benzoic acid preservatives in liquid milk using cysteamine functionalized core-shelled nanoparticles. *Spectrochimica Acta Part A: Molecular and Biomolecular Spectroscopy* **2020,** *229*, 117994.

146.   Ma, Y.-J.; Li, M.; Yu, H.; Li, R.-S., Fast analysis of thiocyanate by ion-pair chromatography with direct conductivity detection on a monolithic column. *Chinese Chemical Letters* **2013,** *24* (12), 1067-1069.

147.   Peng, C.-F.; Pan, N.; Zhi-Juan, Q.; Wei, X.-L.; Shao, G., Colorimetric detection of thiocyanate based on inhibiting the catalytic activity of cystine-capped core-shell Au@Pt nanocatalysts. *Talanta* **2017,** *175*, 114-120.

148.   He, Y.; Niu, X.; Li, L.; Li, X.; Zhang, W.; Zhao, H.; Lan, M.; Pan, J.; Zhang, X., Microwave-Assisted Fabrication of Bimetallic PdCu Nanocorals with Enhanced Peroxidase-Like Activity and Efficiency for Thiocyanate Sensing. *ACS Applied Nano Materials* **2018,** *1* (5), 2397-2405.

149.   Cate, D. M.; Adkins, J. A.; Mettakoonpitak, J.; Henry, C. S., Recent Developments in Paper-Based Microfluidic Devices. *Analytical Chemistry* **2015,** *87* (1), 19-41.

150.   Yamada, K.; Takaki, S.; Komuro, N.; Suzuki, K.; Citterio, D., An antibody-free microfluidic paper-based analytical device for the determination of tear fluid lactoferrin by fluorescence sensitization of Tb3+. *Analyst* **2014,** *139* (7), 1637-1643.

151.   Qiu, Z.; Shu, J.; Tang, D., Bioresponsive Release System for Visual Fluorescence Detection of Carcinoembryonic Antigen from Mesoporous Silica Nanocontainers Mediated Optical Color on Quantum Dot-Enzyme-Impregnated Paper. *Analytical Chemistry* **2017,** *89* (9), 5152-5160.

152.   Jokerst, J. C.; Adkins, J. A.; Bisha, B.; Mentele, M. M.; Goodridge, L. D.; Henry,

C. S., Development of a Paper-Based Analytical Device for Colorimetric Detection of Select Foodborne Pathogens. *Analytical Chemistry* **2012,** *84* (6), 2900-2907.

153.   Srisa-Art, M.; Boehle, K. E.; Geiss, B. J.; Henry, C. S., Highly Sensitive Detection of Salmonella typhimurium Using a Colorimetric Paper-Based Analytical Device Coupled with Immunomagnetic Separation. *Analytical Chemistry* **2018,** *90* (1), 1035-1043.

154.   Apilux, A.; Dungchai, W.; Siangproh, W.; Praphairaksit, N.; Henry, C. S.; Chailapakul, O., Lab-on-Paper with Dual Electrochemical/Colorimetric Detection for Simultaneous Determination of Gold and Iron. *Analytical Chemistry* **2010,** *82* (5), 1727-1732.

155.   Wang, C.-C.; Hennek, J. W.; Ainla, A.; Kumar, A. A.; Lan, W.-J.; Im, J.; Smith, B. S.; Zhao, M.; Whitesides, G. M., A Paper-Based "Pop-up" Electrochemical Device for Analysis of Beta-Hydroxybutyrate. *Analytical Chemistry* **2016,** *88* (12), 6326-6333.

156.   Pena-Pereira, F.; Lavilla, I.; Bendicho, C., Paper-based analytical device for instrumental-free detection of thiocyanate in saliva as a biomarker of tobacco smoke exposure. *Talanta* **2016,** *147,* 390-396.

157.   Ponnaiah, S. K.; Prakash, P.; Vellaichamy, B.; Paulmony, T.; Selvanathan, R., Picomolar-level electrochemical detection of thiocyanate in the saliva samples of smokers and non-smokers of tobacco using carbon dots doped Fe3O4 nanocomposite embedded on g-C3N4 nanosheets. *Electrochimica Acta* **2018,** *283*, 914-921.

158.   Ozoemena, K. I.; Nyokong, T., Surface electrochemistry of iron phthalocyanine axially ligated to 4-mercaptopyridine self-assembled monolayers at gold electrode: Applications to electrocatalytic oxidation and detection of thiocyanate. *Journal of Electroanalytical Chemistry* **2005,** *579* (2), 283-289.

159.   Song, J.; Huang, P.-C.; Wan, Y.-Q.; Wu, F.-Y., Colorimetric detection of thiocyanate based on anti-aggregation of gold nanoparticles in the presence of cetyltrimethyl ammonium bromide. *Sensors and Actuators B: Chemical* **2016,** *222*, 790-796.

160.   Deng, H.-H.; Wu, C.-L.; Liu, A.-L.; Li, G.-W.; Chen, W.; Lin, X.-H., Colorimetric sensor for thiocyanate based on anti-aggregation of citrate-capped gold nanoparticles. *Sensors and Actuators B: Chemical* **2014,** *191*, 479-484.

161.   Noiphung, J.; Nguyen, M. P.; Punyadeera, C.; Wan, Y.; Laiwattanapaisal, W.;

Henry, C. S., Development of Paper-Based Analytical Devices for Minimizing the Viscosity Effect in Human Saliva. *Theranostics* **2018,** *8* (14), 3797-3807.

162.   Schipper, R. G.; Silletti, E.; Vingerhoeds, M. H., Saliva as research material: Biochemical, physicochemical and practical aspects. *Archives of Oral Biology* **2007,** *52* (12), 1114-1135.

163.   Devices to Drool For. *Analytical Chemistry* **2006,** *78* (13), 4255-4259.

164.   Shangguan, J.-W.; Liu, Y.; Wang, S.; Hou, Y.-X.; Xu, B.-Y.; Xu, J.-J.; Chen, H.-Y., Paper Capillary Enables Effective Sampling for Microfluidic Paper Analytical Devices. *ACS Sensors* **2018,** *3* (7), 1416-1423.

165.   Adams, P. E., Determining Iron Content in Foods by Spectrophotometry. *Journal of Chemical Education* **1995,** *72* (7), 649.

166.   Park, M.-S.; Kim, Y.-J., Viscosity and wettability of carboxymethylcellulose (CMC) solutions and artificial saliva. *Journal of Oral Medicine and Pain* **2007,** *32* (4), 365-373.

167.   Yamasaki, M.; Kume, K.; Yoshikawa, I.; Otsuki, M., A novel method of endoscopic submucosal dissection with blunt abrasion by submucosal injection of sodium carboxymethylcellulose: an animal preliminary study. *Gastrointestinal Endoscopy* **2006,** *64* (6), 958-965.

168.   Park, M. S.; Chung, J. W.; Kim, Y. K.; Chung, S. C.; Kho, H. S., Viscosity and wettability of animal mucin solutions and human saliva. *Oral Diseases* **2007,** *13* (2), 181-186.

169.   Zagal, J. H.; Griveau, S.; Silva, J. F.; Nyokong, T.; Bedioui, F., Metallophthalocyanine-based molecular materials as catalysts for electrochemical reactions. *Coordination Chemistry Reviews* **2010,** *254* (23), 2755-2791.

170.   Zhao, D.; Chen, C.; Lu, L.; Yang, F.; Yang, X., A dual-mode colorimetric and fluorometric "light on" sensor for thiocyanate based on fluorescent carbon dots and unmodified gold nanoparticles. *Analyst* **2015,** *140* (24), 8157-8164.

171.   Wu, L.; Wang, Z.; Zong, S.; Cui, Y., Rapid and reproducible analysis of thiocyanate in real human serum and saliva using a droplet SERS-microfluidic chip. *Biosensors and Bioelectronics* **2014,** *62*, 13-18.

172.   Lin, C.-Y.; Liu, C.-H.; Tseng, W.-L., Fluorescein isothiocyanate-capped gold nanoparticles for fluorescent detection of reactive oxygen species based on thiol

oxidation and their application for sensing glucose in serum. *Analytical Methods* **2010,** *2* (11), 1810-1815.

VITA

NAME	Kingkan Pungjunun
DATE OF BIRTH	30 November 1992
PLACE OF BIRTH	Saraburi
INSTITUTIONS ATTENDED	Chulalongkorn University
HOME ADDRESS	9/2 M.7 Soi Tharua-Thalan 3, Jumpa, Tharua, Phra Nakhon Si Ayutthaya 13130

PUBLICATION

1. Kingkan Pungjunun, Sudkate Chaiyo, Issarapong Jantrahong, Siriwan Nantaphol, Weena Siangproh, Orawon Chailapakul "Anodic stripping voltammetric determination of total arsenic using a gold nanoparticle-modified boron-doped diamond electrode on a paper-based device" Microchimica Acta, 2018, 158, 324.

2. Kingkan Pungjunun, Sudkate Chaiyo, Narong Praphairaksit, Weena Siangproh, Astrid Ortner, Kurt Kalcher, Orawon Chailapakula, Eda Mehmeti "Electrochemical detection of NOx gas based on disposable paper-based analytical device using a copper nanoparticles-modified screen-printed graphene electrode" Biosensors and Bioelectronics, 2019,143, 111606.

3. Kingkan Pungjunun, Siriwan Nantaphol, Narong Praphairaksit, Weena Siangproh, Sudkate Chaiyo, Orawon Chailapakul "Enhanced sensitivity and separation for simultaneous determination of tin and lead using paper-based sensors combined with a portable potentiostat" Sensors and Actuators B: Chemical, 2020, 318, 128241.

AWARD RECEIVED

1. รางวัลการเขียนข้อเสนอโครงการระดับดี และรางวัลผลงานนวัตกรรมระดับดีเด่น "การรวมทุกขั้นตอนในอุปกรณ์ฐานกระดาษ

เพียงชิ้นเดียวสำหรับการวิเคราะห์สารหนูในข้าว" การประกวดผลงาน
นวัตกรรมสายอุดมศึกษา ประจำปี 2562

2. The best oral presentation award "Portable Paper-based
Electrochemical Sensor for Simultaneous Determination of
Tin and Lead Using Bismuth Nanoparticles Modified
Electrode" The First Materials Research Society of Thailand
International Conference (MRS-Thailand 2017)